# **В**існик
# **Х**арківського
# **Н**аціонального
# **У**ніверситету
## імені В. Н. Каразіна

# СЕРІЯ «ХІМІЯ»
# Вип. 33 (56)

Заснований 1935 року як
“Труди інституту хемії при Харківському державному університеті”

Харків 2019

Вісник містить статті, присвячені різним аспектам теоретичної хімії, хімічного аналізу, органічної хімії, спектроскопії, фізико-хімії розчинів та поверхневих явищ, електрохімії, хімічного матеріалознавства.

Для науковців і фахівців. Видання є фаховим в галузі хімічних наук. (наказ МОН України № 1328 від 21 грудня 2015 р.)

*Затверджено до друку рішенням Вченої ради Харківського національного університету імені В.Н. Каразіна (протокол № 11 від 23 грудня 2019 р.)*

Адреса редакційної колегії: Україна, 61022, Харків, майдан Свободи, 4, ХНУ імені В.Н. Каразіна, хімічний факультет; тел.: +38 057 707 51 29. E-mail: chembull@karazin.ua a.korobov@karazin.ua

Статті пройшли внутрішнє та зовнішнє рецензування.

*Свідоцтво про державну реєстрацію КВ № 21563-11463Р від 27.07.2015.*

# ЗМІСТ

# CONTENTS

# СОДЕРЖАНИЕ

УДК 544.7773.3 + 546.55/59

# MECHANISM OF ENHANCED OXIDATION ABILITY OF DILUTE NITRIC ACID AND DISSOLUTION OF PURE GOLD IN SEAWATER WITH NITRIC ACID

## M. Hojo

*Department of Chemistry, Faculty of Science, Kochi University, Kochi, 780-8520, Japan*

✉ *mhojo@kochi-u.ac.jp*          ⓘ *https://orcid.org/0000-0001-7936-8104*

It has been discovered that dilute nitric acid in reversed micelle systems can oxidize the $Br^-$ ion to $Br_2$ and we have proposed that the nitryl (or nitronium) ion $NO_2^+$ should be the active species in the oxidation process. Nitration of phenol in reversed micelle systems with dilute nitric acid, $CHCl_3/CTAC/H_2O$ (2.0 mol dm$^{-3}$ $HNO_3$ in the 1.0% (v/v) $H_2O$ phase), has been performed at 35 ºC to obtain 2- and 4-nitrophenols, where CTAC represents cetyltrimethylammonium chloride. In aqueous 2.0 mol dm$^{-3}$ $HNO_3$ solution accompanied by 4.0 mol dm$^{-3}$ LiCl (and a small amount of LiBr as the bromide resource), trans-1,4-dibromo-2-butene was successfully brominated to 1,2,3,4-tetrabromobutane. This result is good evidence that the $Br^-$ ion can be oxidized to $Br_2$ in dilute nitric acid (2.0 mol dm$^{-3}$) providing it contains concentrated salts. For chloride salts, the cation effects increased as $Et_4N^+ << Na^+ < Li^+ < Ca^{2+} < Mg^{2+}$. Even the evolution of $Cl_2$ has been demonstrated from < 2.0 mol dm$^{-3}$ $HNO_3$ solution containing concentrated LiCl, $MgCl_2$, and $CaCl_2$ as well as $AlCl_3$. The dissolution of precious metals (Au, Pt, and Pd), especially, of gold has been demonstrated in 0.1 - 2 mol dm$^{-3}$ $HNO_3$ accompanied by alkali metal, alkaline earth metal, and aluminum chlorides. The complete dissolution time of pure gold plate (20±2 mg, 0.1 mm thickness) in 2.0 mol dm$^{-3}$ $HNO_3$ accompanied by 1.0 mol dm$^{-3}$ $AlCl_3$ has been shortened remarkably with temperature increase from 15 to 80 ºC. The dissolution rate constants, log (k /s$^{-1}$), of a piece of gold wire (19.7±0.5 mg) in 20 mL of 2.0 mol dm$^{-3}$ $HNO_3$ accompanied by the metal chlorides, in general, increase with increasing salt concentrations at 40 and 60 ºC. The gold can be dissolved in the solution of <1.0 mol dm$^{-3}$ $HNO_3$ and <1.0 mol dm$^{-3}$ HCl, i.e. a "dilute aqua regia." We have achieved a total dissolution of five pieces of the gold wire (totally 0.10 g) in 100 mL of the 1:1 mixture between seawater and 2.0 mol dm$^{-3}$ $HNO_3$ at ca. 100 ºC.

**Keywords:** nitryl or nitronium ion, CTAC, evolution of chlorine, oxidation of bromide, salt effect, bulk water structure, dilute aqua regia, tetrachloroaurate, concentrated salt, Raman spectrum.

## Introduction

Nitric acid has two different functions, a strong acid and a strong oxidizing agent in diluted and in concentrate conditions, respectively, and is one of the best known and most widely applied oxidizing agents in chemistry. Although the oxidation ability of $HNO_3$ depends on its concentration in solution, it is common knowledge that dilute nitric acid has no oxidation ability. Airborne sea salt particles wet or dry can react with various gases, in particular various oxides of nitrogen, potentially contributing to the chemistry of the troposphere [1]. Cotton and Wilkinson [2] have described that nitric acid of 0.1 mol dm$^{-3}$ dissociates about 93% and that nitric acid of less than 2.0 mol dm$^{-3}$ has virtually no oxidation ability. The dissociation constants of $HNO_3$ at different concentration ranges in aqueous solution have been determined [3].

In a previous paper [4], however, we have reported that the $Br^-$ ion of the surfactant, CTAB, is oxidized to $Br_2$ (or $Br_3^-$) in the $CHCl_3/CTAB/H_2O$ reversed micelle system of W = 1.0 - 4.0 with dilute nitric acid (0.25 - 2.5 mol dm$^{-3}$ in the 1.0% (v/v) $H_2O$ phase) at 15 – 40 °C where CTAB stands for cetyltrimethylammonium bromide and the W value is the ratio of $[H_2O]/[surfactant]$. We proposed that the $NO_2^+$ ion should be the active species in this oxidation process. Unfortunately, our proposal for the active species may not be recognized so much, regardless of our supplying reasonable evidence in the study. The changes in the hydrogen-bonding conditions of the water droplets in reversed micelle systems have been discussed on the basis of $^1H$ NMR chemical shifts [4]. The influence of salts, acids, and phenols on the hydrogen-bond structure of water-ethanol mixtures has been examined also by $^1H$ NMR spectroscopy [5].

For more than thirty years, we [6] have tried to demonstrate that alkali metal ($M^+$) and alkaline earth metal ($M^{2+}$) ions have potentially the ability to coordinate with simple anions, such as $Cl^-$, $NO_3^-$, $RSO_3^-$, $RCO_2^-$, etc. Such minor interactions between $M^+$ or $M^{2+}$ and simple anions could not be observed normally in dilute aqueous solution because of strong hydration toward both the metal cations

and the anions. In poor solvating media such as acetonitrile, however, the chemical as well as Coulombic interaction between $M^+$ or $M^{2+}$ and simple anions has been demonstrated by careful examination with electrochemical and spectroscopic techniques. Rather strong chemical interactions between alkaline earth metal ions and the benzoate ion in acetonitrile were found by UV-visible and NMR spectroscopy [7].

We have also proposed [6] that the properties of bulk water are based on the hydrogen-bond network among a huge number of $H_2O$ molecules (e.g., $n_w > \sim 10^7$). Water can lose its property as bulk water (H-O-H) to get that of a non-aqueous solvent, such as an alcohol (R-O-H) or even an ether (R-O-R) if the highly "self-assembled structure" of bulk water is destroyed in the following cases: (a) the residual water ($c(H_2O) \sim 10^{-3}$ mol dm$^{-3}$) in organic solvents; (b) aqueous solutions or organic solvent-water mixtures containing highly concentrated salts; (c) nanoscale water droplets in nano-tubes or reversed micelle systems; (d) water on metal electrodes, ion-exchange resins, proteins, organic solvents as the solvent extraction, and glass vessels; (e) water under supercritical conditions. Such waters can be "reduced" to the authentic singular $H_2O$ molecules (also called "dihydrogen ether", (H)-O-(H)) [8]. Reichardt et al. [9] have concisely interpreted "dihydrogen ether" that, at high salt concentrations ($c$(salt) > 5 mol dm$^{-3}$), region C, according to the solvation model of Frank and Wen [10], can be abolished and only regions A and B survive, resulting in an aqueous solvent called "dihydrogen ether".

Now, we would like to point out that hydrogen-bond dynamics of both water in highly concentrated NaBr solutions and in reversed micelle systems show a similar behavior [11]. In addition, Park et al. [11] have described that the water dynamics in 4 nm nano-pools in reversed micelle systems of both ionic and non-ionic surfactants is almost identical: confinement by an interface to form a nanoscopic water pool is the primary factor governing the dynamics of nanoscopic water rather than the presence of charged groups at the interface. Spectroscopic studies of the structure of surface water as it is affected by added salts, acids, and ammonia have been presented in a review article by Gopalakrishnan et al. [12]. The OH stretch of nitric acid in $CCl_4$ has provided definitive proof of molecular nitric acid rather than $NO_3^-$ [13].

With the assistance of above-mentioned two ideas, i.e., (1) chemical interaction between the metal cations and simple anions, (2) the change of water properties with the addition of concentrated salts and/or organic solvents, we have successfully explained the concentrated salt effects on solvolysis reactions of organic haloalkanes and related compounds without resorting to different types of ion pairs [8].

It is widely accepted that the $NO_2^+$ ion is the active species in nitration reactions. March [14] has described in his textbook: "there is a great deal of evidence that $NO_2^+$ is present in most nitration reactions and that it is the attacking entity".

In Part 1 of the present paper, a few examples for the nitration of phenols with dilute nitric acid (2.0 mol dm$^{-3}$) in various reversed micelle systems are reported. After that, we examine the oxidation of Br$^-$ to $Br_2$ by dilute nitric acid in aqueous bulk solution containing concentrated salts in order to recognize that the $NO_2^+$ ion can be produced within nanoscale water droplets in reversed micelle systems. In the course of our experiments, even the evolution of $Cl_2$ as well as the oxidation of Br$^-$ to $Br_2$ has been observed in dilute nitric acid in aqueous bulk solution containing concentrated salts. Finally, the distortion of bulk water structure is fully discussed for aqueous solutions containing concentrated salts, such as LiCl and NaCl, based on experimental data observed with Raman and $^1$H NMR spectroscopy.

In Part 2, pure gold dissolution in seawater mixed with aqueous nitric acid is demonstrated.

## Results and Discussion

### Part 1 Formation of $NO_2^+$ as the Intermediate in Reversed Micelle Systems and Bulk Aqueous Media from Dilute HNO$_3$

*1.1. Nitration of phenol with dilute nitric acid in CHCl$_3$/CTAC reversed micelle*

First of all, we would like to characterize the reaction field in reversed micelle systems. Fig. 1 shows the change with time in the $^1$H NMR chemical shift ($\delta$) values of OH in water droplets (1.0% $H_2O$ phase containing 2.0 mol dm$^{-3}$ HNO$_3$) of reversed micelle systems, CHCl$_3$/CTAB/$H_2O$ (W = [$H_2O$]/[surfactant] = 2.0) and CHCl$_3$/CTAC/$H_2O$ (W = 4.0) at 25 ºC. The $\delta$($^1$H) value of the CTAB micelle system decreased after two hours with changing of the color from colorless to yellow,

whereas that of the CTAC micelle system remained constant during five hours and even after 7 days. In the previous study [4], we have established that the oxidation of $Br^-$ ions to $Br_2$ (or $Br_3^-$) occurs with $0.25 - 2.0$ mol $dm^{-3}$ $HNO_3$ (in the 1.0% $H_2O$ phase) of the $CHCl_3/CTAB/H_2O$ (W = 2.0) reversed micelle system at 25 ºC. We have also suggested that the oxidizing species should be the $NO_2^+$ ion which is formed from the dilute nitric acid in the micelle system.

The decrease of the $\delta(^1H)$ value in the CTAB micelle system has been attributed to the decrease in the nitric acid concentration, which should accompany the oxidation of $Br^-$ ions of the surfactant, CTAB. Contrastingly, it is obvious that 2.0 mol $dm^{-3}$ $HNO_3$ in the $CHCl_3/CTAC/H_2O$ (W = 4.0) micelle system could not oxidize the $Cl^-$ ions (of the surfactant, CTAC) into $Cl_2$, thus, no decrease in the $HNO_3$ concentration was observed. In brief conclusion, Eq. 1 can take place but not Eq. 2 in the two reversed micelle systems.

$$2Br^- + NO_2^+ \rightarrow Br_2 + NO_2^- \tag{1}$$

$$2Cl^- + NO_2^+ \rightarrow Cl_2 + NO_2^- \tag{2}$$
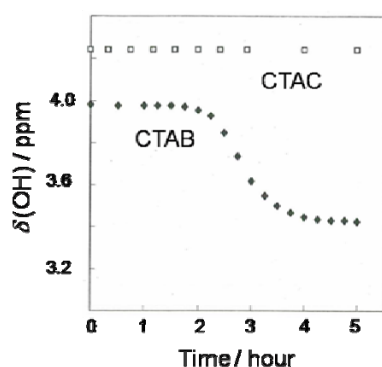


**Figure 1.** Time-dependent chemical shifts of $\delta(OH)$ in reversed micelle systems, $CHCl_3/CTAB/H_2O$ (W = 2.0) and $CHCl_3/CTAC/H_2O$ (W = 4.0), containing 2.0 mol $dm^{-3}$ $HNO_3$ (in the 1.0% $H_2O$ phase) at 25 ºC.
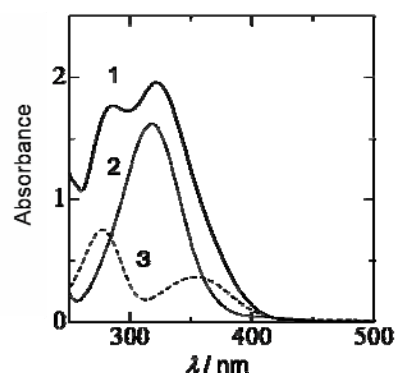


**Figure 2.** UV absorption spectra (0.1 cm path-length) of the products from $2.5 \times 10^{-3}$ mol $dm^{-3}$ phenol formed in the reversed micelle system $CHCl_3/CTAC/H_2O$ (W = 4.0), containing 2.0 mol $dm^{-3}$ $HNO_3$ (in the 1.0% $H_2O$ phase) at 35 ºC and the candidate compounds in the reversed micelle system: (1) products formed after four days; (2) $1.0 \times 10^{-3}$ mol $dm^{-3}$ 2-nitrophenol; (3) $1.0 \times 10^{-3}$ mol $dm^{-3}$ 4-nitrophenol.

Fig. 2 shows the UV spectrum based on the reaction products from $2.5 \times 10^{-3}$ mol $dm^{-3}$ phenol in the reversed micelle ($CHCl_3/CTAC/H_2O$) at W = 4.0 containing 2.0 mol $dm^{-3}$ $HNO_3$ (in the 1.0 % $H_2O$ phase) after four days at 35 ºC. Two bands at $\lambda_{max} = 285$ and 323 nm were observed. The UV spectrum of the reaction products was able to be fit with $1.6 \times 10^{-3}$ mol $dm^{-3}$ 2-nitrophenol and $1.4 \times 10^{-3}$ mol $dm^{-3}$ 4-nitrophenol, that is, the ratio of (1.14):(1.00) for 2- and 4-nitrophenols with a reaction yield of 80 % from phenol. This result seems to be reasonable since the OH-group of phenol has an ortho- and para-orientation tendency [15]. The production of 3-nitrophenol and 2,4-dinitrophenol was excluded based on their UV absorption spectra: reaction conditions are so gentle that 3-nitro- and dinitro-derivatives were not produced.

*1.2. Nitration of 4-methylphenol with dilute nitric acid in CTAC and AOT reversed micelle systems*

Nitration of 4-methylphenol with dilute nitric acid was examined in the $CDCl_3/CTAC/H_2O$ reversed micelle system at 35 ºC. Fig. 3(a) shows the $^1H$ NMR spectrum of 0.010 mol $dm^{-3}$ 4-methylphenol in the reversed micelle ($CDCl_3/CTAC/H_2O$) at W = 8.0 containing 2.0 mol $dm^{-3}$ $HNO_3$ (in the 1.0 % $H_2O$ phase) just after solution preparation. Two doublet signals characterize the reactant 4-methylphenol. The $^1H$ NMR spectrum (for $\delta(^1H) = 5 - 10$ ppm) of 4-methylphenol in the $CDCl_3/CTAC/H_2O$ reversed micelle system was almost identical with that of a commercial compound in $CDCl_3$ solution. After completion of the reaction (two days later), the $^1H$ NMR signals shifted to the down-field direction; one singlet (3H) and two doublet signals (5H and 6H), shown in Fig. 3(b), indicated the formation of 2-nitro-4-methylphenol and the absence of the reactant 4-methylphenol.
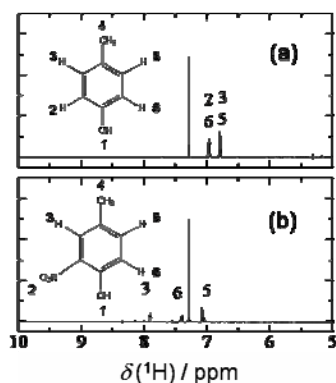
**Figure 3.** $^1$H NMR spectra of (a) 0.01 mol dm$^{-3}$ 4-methylphenol in CDCl$_3$/CTAC/H$_2$O (W= 4.0) reversed micelle in the presence of 2.0 x 10$^{-3}$ mol dm$^{-3}$ HNO$_3$ (in the 1.0% H$_2$O phase) just after solution preparation and (b) the product formed from 0.01 mol dm$^{-3}$ 4-methylphenol in the reversed micelle system after reaction completion (two days later at 35 ºC).
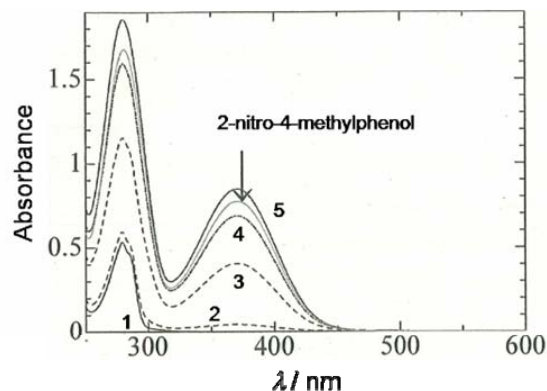


**Figure 4.** Changes of UV and visible spectra (0.1 cm path-length) from 2.5 x 10$^{-3}$ mol dm$^{-3}$ 4-methylphenol to 2-nitro-4-methylphenol with time in reversed micelle, CHCl$_3$/AOT/H$_2$O (W = 2.0), containing 2.0 mol dm$^{-3}$ HNO$_3$ (in the1.0% water phase) at 35 ºC: (1) 0; (2) 2.0; (3) 4.0; (4) 5.0; (5) 6.0 h later. Commercially obtained 2-nitro-4-methylphenol of 2.0 x 10$^{-3}$ mol dm$^{-3}$ is also displayed.

The reaction yield was evaluated by means of UV spectroscopy of 2-nitro-4-methylphenol from 2.5 x 10$^{-3}$ mol dm$^{-3}$ 4-methylphenol in the CHCl$_3$/CTAC/H$_2$O reversed micelle system. The yield of the product increased with increasing W value, e.g. 88.5, 91.7, and 95.7 % for W = 1.2, 2.0, and 8.0, respectively, and the reaction time (for completion) was prolonged by smaller W values: 2, 3, and 5 days for W = 2 - 8, 1.5, and 1.2, respectively. One can expect some superiority in the yields and reaction rates for the smaller W values because of more remarkable distortion of the water structure. However, the experimental data indicates the opposite tendency. Similar opposite tendency have been reported for the oxidation of Br$^-$ in CTAB reversed micelle system [4].

The cationic surfactant, CATC, was then replaced by an anionic surfactant, AOT. Fig. 4 shows the formation of 2-nitro-4-methylphenol from 2.5 x 10$^{-3}$ mol dm$^{-3}$ 4-methylphenol in the reversed micelle (CHCl$_3$/AOT/H$_2$O) at W = 2.0 containing 2.0 mol dm$^{-3}$ HNO$_3$ (in the 1.0 % H$_2$O phase) at 35 ºC. Two hours later, a reaction to some extent could be observed with a slight increase of absorbance at around λ = 280 and 370 nm. The reaction was completed after six hours to give a UV spectrum with two bands at λ = 281 and 371 nm for 2-nitro-4-methylphenol with a reaction yield of 93.2 %. The influence of the W value on reaction time and yield was examined only for W = 1.0 – 3.0, since the reversed micelle system was unstable for W = 4.0 or more. Smaller W values caused slightly lower yields and longer reaction times: 92.1 % (8 h) and 94.0 % (6 h) for W = 1.0 and 3.0, respectively.

For the AOT system at W = 2.0, the replacement of CHCl$_3$ with heptane as the organic phase caused the reaction rate of the nitration of 4-methylphenol to be much faster. The nitration reaction was completed in two hours with a yield of 98 %. At various W values (W = 1.0 – 8.0), the yield and reaction time were obtained for 2-nitro-4-methylphenol from 2.5 x 10$^{-3}$ mol dm$^{-3}$ 4-methylphenol in the reversed micelle (heptane/AOT/H$_2$O) containing 2.0 mol dm$^{-3}$ HNO$_3$ (in the 1.0 % H$_2$O phase) at 35 ºC. The reaction or completion time was always 2 h, except for W = 1.0 (3.5 h), and the yields were within 93 – 98 %. However, the insolubility of the CTAC surfactant in heptane prevented us from examining the reaction in a heptane/CTAC/H$_2$O reversed micelle system.

Onori and Santucci [16] have investigated water structure in CCl$_4$/AOT/H$_2$O reversed micelle systems. They have stated that the IR spectra can be expressed as sum of the contributions from interfacial and bulk-like water. Without doubt, the conditions in the nanoscale water droplets are quite different from that of intrinsic bulk water.

In 10 mL of heptane without surfactants, the nitration of 2.5 x 10$^{-3}$ mol dm$^{-3}$ 4-methylphenol with 2.0 mol dm$^{-3}$ HNO$_3$ (0.1 mL) was examined at 35 ºC. Turbidity was observed in heptane when sonication was performed for several minutes in order to mix the solvent and the small amount of dilute nitric acid. After one day at 35 ºC, however, the solution became clear and the UV spectrum of the solution indicated the formation of 2-nitro-4-methylphenol of 93 % yield. In this case, nitration took place in the absence of surfactants. In the review article of Gopalakrishnan et al. [12] they commented that

infrared spectra of saturated solutions of water in CCl$_4$ at room temperature can be assigned to water monomers or dimers. The water molecules mixed into heptane, including the turbidity particles, may exist in a variety of forms from the monomer to hydrogen-bonded oligomers, (H$_2$O)$_n$.

In 10 mL of CHCl$_3$, on the other hand, 4-methylphenol could not be nitrated by 2.0 mol dm$^{-3}$ HNO$_3$ (0.1 mL) even after two weeks. Now, we would like to discuss briefly the reactivity (formation of NO$_2^+$ as intermediate) in both solvents: the most obvious difference between two organic solvents must be in their acceptor numbers: ~ 0 and 23.1 for heptane and CHCl$_3$, respectively [17], whereas the donor numbers of both solvents should be quite small (~0). Chloroform with the larger acceptor number (i.e., the larger basicity) can accept the hydrogen bond from the H-atoms of nitric acid, which might cause a lower tendency to produce the NO$_2^+$ ion.

Now, we wonder what kind of function surfactants may have for the reaction in reversed micelle systems. Additionally, the question is where the NO$_2^+$ ion is generated, either within the aqueous phase or in the organic phase. In order to solve these problems, we examined the oxidation ability of dilute nitric acid in bulk water containing concentrated salts, as described in the following sections.

### 1.3. Oxidation of Br$^-$ to Br$_2$ with dilute nitric acid in aqueous bulk solution containing abundant salts

Fig. 5 shows the UV-visible absorption spectra of a 2.0 mol dm$^{-3}$ HNO$_3$ aqueous solution, after addition of 4.0 mol dm$^{-3}$ LiCl and 0.010 mol dm$^{-3}$ LiBr at 35 ℃. Note that the concentration of nitric acid is less than 2.0 mol dm$^{-3}$ (actually found to be 1.83 mol dm$^{-3}$) because a substantial part of the volumetric flask is occupied by a large amount of the salt, LiCl, and only 2.0 mol dm$^{-3}$ HNO$_3$ was handled for preparation of the solution. The solution turned soon from colorless to yellow. In the UV-visible spectra, a band of at around 371 nm developed gradually with time until 30 min passed. Commercially available Br$_2$ gave UV absorption band at around 371 nm (absorptivity, e /cm$^{-1}$ mol$^{-1}$ dm$^3$ = ca. 200) in 4.0 mol dm$^{-3}$ LiCl aqueous solution, cf., $\varepsilon$ = ca. 180 at $\lambda$ = 390 nm in 2 mol dm$^{-3}$ HClO$_4$ [18]. Based on the absorptivity of Br$_2$, the oxidation of the Br$^-$ ion (LiBr) is suggested to be completed after 30 min. The presence of Br$_2$ in the concentrated salt solution (e.g., 4.0 or 5.0 mol dm$^{-3}$ LiCl) after the reaction was detected by the Rosaniline method [19]; the appearance of a red color (l = ca. 570 nm) proved the formation of Br$_2$.
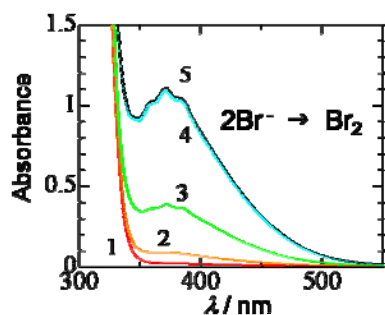


**Figure 5.** Formation of Br$_2$ (1.0 cm path-length) from 0.010 mol dm$^{-3}$ LiBr in 2.0 mol dm$^{-3}$ HNO$_3$ solution, accompanied by 4.0 mol dm$^{-3}$ LiCl at 35 ℃: (1) 0; (2) 5; (3) 10; (4) 25; (5) 30 min later.
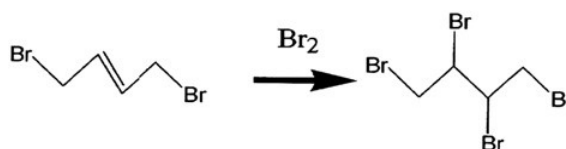
Scheme 1. The bromination of a butene to the butane.

The formation of Br$_2$ from LiBr with 2.0 mol dm$^{-3}$ HNO$_3$ accompanied by 4.0 mol dm$^{-3}$ LiCl (and 0.010 mol dm$^{-3}$ LiBr) was confirmed also by means of $^1$H NMR as follows: before and after the reaction, each solution of 10 mL in the presence of trans-1,4-dibromo-2-butene (0.010 mol dm$^{-3}$) was extracted with 2 mL of CDCl$_3$. After the completion of reaction, the formation of 1,2,3,4-tetrabromobutane was demonstrated by the disappearance of a signal at $\delta$($^1$H) = ca. 6.0 ppm stemming from trans-1,4-dibromo-2-butene as well as the appearance of signals between $\delta$($^1$H) = 3.5 – 5.0 ppm. The formation of 1,2,3,4-tetrabromobutane from trans-1,4-dibromo-2-butene (cf. Scheme 1) is a good evidence for the oxidation of Br$^-$ with dilute nitric acid in the presence of LiCl. It is true that the lithium ion has an advantage for getting good oxidation ability with dilute nitric acid, however, we would like to stress that Li$^+$ is not the essential ion component. At 35 ℃, a solution of 2.0 mol dm$^{-3}$ HNO$_3$ accompanied by sodium chloride (3.0 mol dm$^{-3}$) and bromide (0.010 mol dm$^{-3}$),

which contains no lithium ions, produced also $Br_2$, though the reaction rate and the yield of $Br_2$ (ca. 25 %) was low.

At various temperatures, examined were the time-dependent changes of absorbance at $l$ = ca. 371 nm of $Br_2$ in 2.0 mol $dm^{-3}$ $HNO_3$ accompanied by 4.0 mol $dm^{-3}$ LiCl (and 0.010 mol $dm^{-3}$ LiBr). With increasing temperature, the reaction rate increases. The activation energy for 20 – 35 ºC was evaluated to be 67.2 kJ $mol^{-1}$ for the 4.0 mol $dm^{-3}$ LiCl solution. With decreasing salt concentration, however, the reaction rate decreased remarkably; the activation energies were evaluated to be 58.6 and 45.0 kJ $mol^{-1}$ for 3.7 and 3.5 mol $dm^{-3}$ LiCl. Naturally, with increasing LiCl concentration, the reaction rate increased. In 2.0 mol $dm^{-3}$ $HNO_3$ accompanied by 5.0 mol $dm^{-3}$ LiCl (and 0.010 mol $dm^{-3}$ LiBr), the oxidation reaction proceeded too fast to evaluate the rate constant precisely, therefore, nitric acid of 1.0 mol $dm^{-3}$ was used for 5.0 mol $dm^{-3}$ LiCl to obtain log $(k/s^{-1})$ = -3.87 at 25 ºC.

In the case of 9.0 mol $dm^{-3}$ LiCl, at last, the nitric acid concentration was decreased down to 0.1 mol $dm^{-3}$ to get reasonable experimental conditions. In Table 1 are listed the apparent oxidation-reaction rate constants, log $(k/s^{-1})$, for 0.10 – 2.0 mol $dm^{-3}$ nitric acid accompanied by LiCl in high concentrations (3.5 – 9.0 mol $dm^{-3}$). It should be mentioned that the rate constants are not very precise values because the apparent molarity concentrations of nitric acid are always reduced by the volumes of a large amount of salts (vide supra); the actual molarity values are also listed in the table.

Table 1. The apparent rate constants, log $(k/s^{-1})$,[a] of formation of $Br_2$ from dilute nitric acid (and 0.010 mol $dm^{-3}$ LiBr as the $Br^-$ resource) solution containing alkali metal and alkaline earth metal chlorides at 20 – 40 ºC.

| salt/mol $dm^{-3}$ | $HNO_3$/ mol $dm^{-3}$ | 40ºC | 35ºC | 30ºC | 25ºC | 20ºC |
|---|---|---|---|---|---|---|
| LiCl, 4.0 | 2.0[b] (1.83)[c] | | -2.57 | -2.76 | -2.96 | -3.24 |
| LiCl, 5.0 | 1.0 (0.894) | | -3.23 | -3.63 | -3.87 | -4.13 |
| LiCl, 6.5 | 0.5 (0.431) | | -3.36 | -3.72 | -3.94 | -4.22 |
| LiCl, 8.0 | 0.2 (0.167) | -3.70 | -3.80 | -4.03 | | |
| LiCl, 9.0 | 0.1 (0.081) | -3.87 | -3.97 | -4.20 | | |
| NaCl, 3.5 | 2.0 (1.84) | | -4.81 | -5.19 | -5.43 | |
| $MgCl_2$, 1.7 | 2.0 (1.60) | | | -2.51 | -3.14 | -3.49 |
| $CaCl_2$, 2.5 | 2.0 (1.83) | | -2.68 | -2.93 | -3.47 | -3.51 |

[a] Evaluated from the slope of ln $(A_\infty - A_t)$ vs. t, where $A_\infty$ and $A_t$ represent the absorbance at reaction completion and at each time, respectively.
[b] The concentration of $HNO_3$ solution, with which the salt was dissolved.
[c] The actual $HNO_3$ concentration in the reaction flask, evaluated by the weight and the total volume values.

All the log $(k/s^{-1})$ values observed are between ca. -4.0 to ca. -2.5 at 25 – 35 ºC, in other words, the reaction rates were adjusted by controlling the concentrations of both $HNO_3$ and LiCl for obtaining appropriate experimental data. In the case of sodium chloride, 3.5 and not 4.0 mol $dm^{-3}$ salt solution was utilized because of the smaller solubility of NaCl in 2.0 mol $dm^{-3}$ $HNO_3$. A 2.0 mol $dm^{-3}$ $HNO_3$ aqueous solution accompanied by 3.5 mol $dm^{-3}$ NaCl (and 0.010 mol $dm^{-3}$ LiBr) at 25 ºC gave the log $(k/s^{-1})$ value of -5.43 and this value is much smaller than that (-3.75) for 3.5 mol $dm^{-3}$ LiCl. Note that the actual concentration of "2.0 mol $dm^{-3}$ $HNO_3$", accompanied by 3.5 mol $dm^{-3}$ LiCl or NaCl were found to be each 1.84 mol $dm^{-3}$. The large difference in the log $(k/s^{-1})$ values between LiCl and NaCl is probably caused not only by some interaction between $M^+$ and $NO_3^-$ but also by the change of the water structure through hydrogen bonding in the presence of these salts. In the final section of Part 1, the water structure through hydrogen bonding will be discussed based on the Raman and $^1H$ NMR spectral data of $D_2O$ or $H_2O$ containing LiCl, NaCl, and other salts.

As for non-metallic salts, a 2.0 mol $dm^{-3}$ $HNO_3$ solution accompanied by 3.5 mol $dm^{-3}$ $Et_4NCl$ (and 0.010 mol $dm^{-3}$ LiBr) at 30 and 35 ºC gave no $Br_2$ even 50 h later, although we have observed the production of $Br_3^-$ salts (brown-color) on $Et_4NBr$ crystals from a 2.0 mol $dm^{-3}$ $HNO_3$ solution, saturated with $Et_4NBr$ after several days at room temperature. It is obvious that the metal ions play an important role in the oxidation process with dilute nitric acid. Magnesium and calcium chlorides promoted remarkably the oxidation reaction with dilute nitric acid: it was necessary for us to employ lower concentrations for these salts to obtain appropriate experimental data. The log $(k/s^{-1})$ values for $MgCl_2$ and $CaCl_2$ are also listed in Table 1. The effects by alkali metal and alkaline earth metal chlorides were

classified as $Et_4NCl \ll NaCl < LiCl < CaCl_2 < MgCl_2$. This order of cations is just similar to that of the cation effect on solvolysis reaction rates of $S_N1$ substrates [8].

After examining the heterogeneous reactions of oxides of nitrogen with NaCl as a model for sea salt particles, Langer et al. [1] inferred that NaCl may not be the component of sea salt which is most reactive with $HNO_3$. Rossi [20] has summarized the study by Langer et al. [1] in a review article, "this study indicates that $HNO_3$ and $NO_2$ appear to react preferentially with hydrate salts such as $MgCl_2 \cdot 6H_2O$, which is one of the constituents of natural sea salt". Admitting that they studied in heterogeneous phases, our observation is consistent with the result obtained by them [1].

*1.4. Evolution of $Cl_2$ in concentrated chloride salt solutions and mechanism of the oxidation of the $Br^-$ ion*

In 2.0 mol dm$^{-3}$ $HNO_3$ accompanied by 1.0 mol dm$^{-3}$ $AlCl_3$ (and 0.010 mol dm$^{-3}$ LiBr) at 20 – 35 ºC, the reaction proceeded quickly to give $Br_2$ but yields were not so high. In addition, we noticed that $Cl_2$ gas seemed to be produced from the solution. Therefore, the $Cl_2$ formation was examined by the o-tolidine method [21] for 2.0 mol dm$^{-3}$ $HNO_3$ accompanied by 1.0 mol dm$^{-3}$ $AlCl_3$ at room temperature. Chlorine was detected by the absorption band at $\lambda = 437.5$ nm in the test solutions, sampled from the vapor phase as well as from the condense phase (the $HNO_3$ solution). By the same method, the formation of $Cl_2$ was demonstrated in 2.0 mol dm$^{-3}$ $HNO_3$ accompanied by LiCl, $MgCl_2$, and $CaCl_2$ of 4.0, 1.7, and 2.5 mol dm$^{-3}$, respectively. Although we failed to determine $Cl_2$ from 2.0 mol dm$^{-3}$ $HNO_3$ accompanied by 3.5 mol dm$^{-3}$ NaCl in a preliminary experiment, we believe that the formation of $Cl_2$ is possible from all the (dilute) nitric acid solutions containing concentrated chloride salts which we have examined.

The standard redox potentials, $E^o$, of $NO_2^+/NO_2^\cdot$ and $NO_2^+/N_2O_4$ are reported to be 1.35 and 1.50 V [22], respectively, cf. $E^o = 1.396$ V for $Cl_2(aq) + 2e^- \rightarrow 2Cl^-(aq)$ [23]. Olah [24] has described that the reversible potential for reduction of $NO_2^+$ in acetonitrile is 1.45 V (vs. NHE), citing an electrochemical paper [25]. The oxidation of $Cl^-$ to $Cl_2$ with $NO_2^+$ must be possible according to the redox potentials of $NO_2^+$ and $Cl_2$.

Behnke et al. [26] have stated that $NO_2^+$ reacts with water to form $2H^+$ and $NO_3^-$ or with $Cl^-$ to produce nitryl chloride ($ClNO_2$) in their atmospheric chemical experiment of $N_2O_5$ on liquid NaCl aerosols or bulk NaCl solution at 291 K. However, it is known that [27] nitryl chloride is soluble in water and it decomposes to nitric and hydrochloric acids. The mixture (aqua regia) of concentrate $HNO_3$ and HCl is ready to evolve $Cl_2$ and nitrosyl chloride (NOCl) [28]. Coincidentally, nitration of a calixarene compound by anhydrous $AlCl_3$ and $KNO_3$ in $CH_2Cl_2$ has been reported [29]. Another aluminum salt, $Al(H_2PO_4)_3$, serves as an efficient solid acid catalyst of nitration of a variety of organic substances with 70 % nitric acid [30].

Having the evolution of $Cl_2$ is demonstrated, the oxidation mechanism of the $Br^-$ to $Br_2$ should be reconsidered. The oxidation of the $Br^-$ ion of LiBr in concentrated LiCl solution can occur not only directly by $NO_2^+$ but also indirectly through $Cl_2$, as expressed by Eqs. 2 and 3:

$$2Br^- + Cl_2 \rightarrow Br_2 + 2Cl^- \qquad (3)$$

The reaction given in Eq. 3 was inferred from the formation profile of $Br_2$ in the dilute nitric acid containing chloride salts, that is, the absorbance of $Br_2$ increased gradually from the beginning of reaction time. On the other hand, the formation profile of $Br_2$ in dilute nitric acid containing non-chloride salts is completely different from that of chloride salts. Fig. 6 shows the change of $Br_2$ concentration with time in 2.0 mol dm$^{-3}$ $HNO_3$ (and 0.010 mol dm$^{-3}$ LiBr) accompanied by lithium trifluoromethanesulfonate, perchlorate, and nitrate salts. The absorbance of $Br_2$ increased not from the initial time but after an induction period for each salt. The oxidation reaction of other non-chloride lithium and sodium salts, such as $CH_3SO_3Na$ or $NaHSO_4$, also need a long induction period before the formation of $Br_2$ starts. The details of the influence of cation and anion components on the generation of $NO_2^+$ as the active species from dilute nitric acid will be reported later. We just mention that the basicities of anions from salts in higher concentrations may influence on the generation of $NO_2^+$ from dilute $HNO_3$. Kinetics and mechanism of the autocatalytic oxidation with nitric acid have been reviewed by Bazsa [31].

*1.5. Distortion of bulk water structure in the presence of concentrated LiCl and NaCl*

According to Frank and Wen [10], $Li^+$ and $Cs^+$ ions in aqueous solution are regarded to be structure making and breaking, respectively. This classification for cations or salts is widely accepted in solu-

tion chemistry. However, we would like to point out that this argument must be limited to lower salt concentrations in solution. In the presence of salts in high concentrations (e.g., 5 mol dm$^{-3}$), bulk water molecules are consumed for hydrating the ions, therefore, the bulk water part (properly structured with an enormous number of water molecules) in solution is reduced or even disappears and only isolated water molecules should be left for solvating foreign chemical species [6].
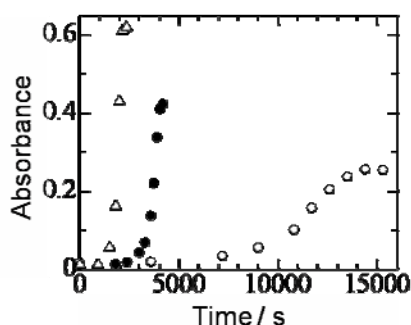


**Figure 6.** Time-dependent absorbance (1.0 cm path-length) at around l = 371 nm of a 2.0 mol dm$^{-3}$ HNO$_3$ solution, accompanied by 3.5 mol dm$^{-3}$ lithium salts (and 0.010 mol dm$^{-3}$ LiBr) at 35 °C: (△) CF$_3$SO$_3$Li; (●) LiClO$_4$; (○) LiNO$_3$.
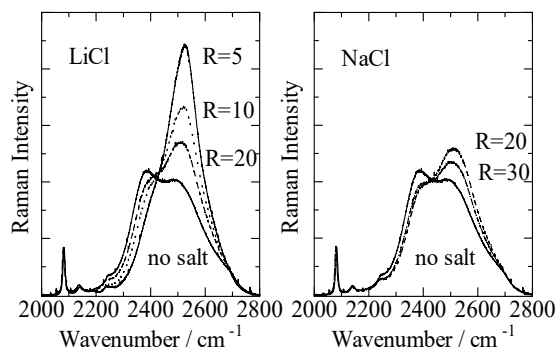
**Figure 7.** The changes of Raman spectra of D$_2$O with changing R values of LiCl and NaCl, where R = [D$_2$O] / [salt].

Fig. 7 shows the changes of Raman spectra of D$_2$O with changing R values of LiCl and NaCl where R = [D$_2$O] / [salt]. Excitation for the Raman spectroscopy was provided by a 514.5 nm argon laser. The two peaks at ca. 2390 and 2500 cm$^{-1}$ of D$_2$O in the absence of salts can be attributed to O-D stretching bands of strongly and weakly hydrogen-bonded D$_2$O molecules, respectively [8c-8e,32]. With decreasing R values (i.e., with increasing salt concentration), the intensity of the band of weakly hydrogen-bonded water increases at the expense of that of strongly hydrogen-bonded water for both LiCl and NaCl solutions. The Raman spectra obviously indicate that the water structure through hydrogen-bonding is much destroyed in concentrated LiCl as well as NaCl solution. Furthermore, examining the distortion of the water structure, we found, LiCl has a stronger impact than NaCl. At R = 20, for instance, the ratio of Raman intensities ($I_2/I_1$) is 0.64 and 0.72 for LiCl and NaCl, respectively, where $I_1$ and $I_2$ represent Raman intensities at ca. 2500 and 2390 cm$^{-1}$. The smaller Raman ratio for the D$_2$O solution of LiCl, as compared with that of NaCl, indicates that the water structure is more distorted by LiCl, rather than NaCl of the same molality concentration: R value of 20 corresponds to 2.5 mol kg$^{-1}$.

Coincidently, Pastroczak et al. [33] have demonstrated how the intensity ratio of two main band components of H$_2$O (around 3200 and 3400 cm$^{-1}$) depends on the excitation laser wavelength in the visible range. Note that the ratio ($I_2/I_1$) is 1.08 for pure D$_2$O and that D$_2$O is somewhat more structured than H$_2$O ($I_2/I_1$ = 0.90 for 3250 and 3400 cm$^{-1}$, laser excitation at 514.5 cm$^{-1}$). Gordon [34] has already mentioned that D$_2$O is a more structured liquid than H$_2$O.

### 1.6. Integration of apparent contradiction between NMR and Raman spectroscopy

Now, we have to declare that $^1$H NMR chemical shifts of H$_2$O containing the salts were found to be apparently controversy to the Raman results. Fig. 8 shows the $\Delta\delta$ values changed by various cations or anions of 1.0 mol dm$^{-3}$ in 2.0 % (v/v) EtOH-H$_2$O solution. We have found that these $\Delta\delta$ values observed in 2.0% are not so much different from those observed in 20% (v/v) EtOH-H$_2$O solution, previously reported [5]. We can notice that the difference of the $\Delta\delta$ values between Mg$^{2+}$ and Ca$^{2+}$ are definitely smaller than that observed in 20% (v/v) EtOH-H$_2$O solution, though.

The separation of the effects by the anion and cation components in a salt was performed according to Hindman's method [35] ($\Delta\delta$ (NH$_4^+$) = 0): the details of the procedure have been described previously [5]. Magnesium, calcium, and lithium ions having smaller ionic sizes (r/z) gave positive $\Delta\delta$ values while Na$^+$, K$^+$, Rb$^+$, and Cs$^+$ gave negative values; where r and z are the crystal ion radius and the

number of charges, respectively. Positive and negative $\Delta\delta$ values should be correspondent to structure making and breaking, respectively. Based on the ^{1}H NMR data, $Li^+$ is structure making while $Na^+$ and $Cl^-$ are structure braking. Thus, the ^{1}H NMR data for these ions are in good accordance with the model of Frank and Wen [10].
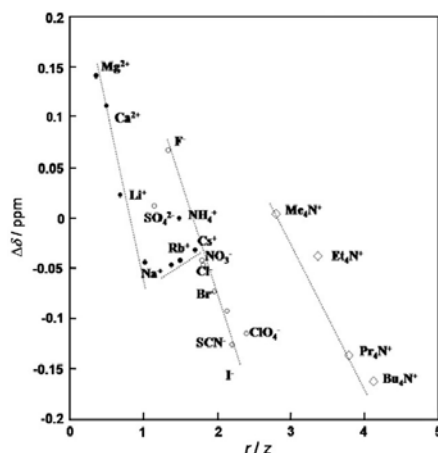


**Figure 8.** The $\Delta\delta$ values vs. r/z for various cations and anions at 1.0 mol dm$^{-3}$ in 2.0 % (v/v) EtOH-H$_2$O solution, where r and z are the crystal ion radius and the number of charge, respectively. The signal of the methyl group in EtOH served as the internal standard for the chemical shift.

As discussed above, however, the Raman spectra supply us with the information that the water structure is more distorted by higher concentration of LiCl than of NaCl. Such an apparent contradiction between Raman and NMR data has been one of the most difficult points to clear in solution chemistry. Now we suppose that ^{1}H NMR system may reflect the ion hydration (neighboring part of ions) even though the bulk water is almost lost in the presence of salts in higher concentrations, whereas Raman spectroscopy seems to be able to evaluate the degree how much an aqueous solution is changed from the initial bulk water as the result of adding salts. Note that the condition of water structure around a metal ion (e.g., $Li^+$ or $Fe^{2+}$), developed by its ionic field or coordination ability, must be quite different from that of the bulk water. Raman spectra may distinguish the difference between hydration and bulk water molecules but NMR spectra may not. As mentioned above, we have proposed of change in the properties of bulk water into those of "dihydrogen ether" [8] in the presence of highly concentrated salts. It is, indeed, necessary for us to arrange slightly the idea of Frank and Wen [10] (structure-making or breaking ions) in order to account for the controversy feature between Raman and ^{1}H NMR spectroscopy.

The influence of MgCl$_2$ and CaCl$_2$ on the water structure has been examined by means of $^{17}O$ NMR and Raman spectroscopy [36]. Changes in Raman spectra indicated the break of the fully hydrogen bonded water structure with increasing concentration of MgCl$_2$ and CaCl$_2$. However, the $\delta(^{17}OH_2)$ values increased (down-field shift) with increasing concentration of MgCl$_2$ and CaCl$_2$. The authors have described that results from $^{17}O$ NMR and Raman measurements are "compatible" with each other. Obviously, in the truth, they have had encountered the contradiction just similar to ours. However, they evaded the difficult situation by describing, "though CaCl$_2$ and MgCl$_2$ destroy four hydrogen-bonded water structures, they promote the water structure in the mass".

Yonehama et al. [37] reported the O-D stretching frequency in aqueous electrolyte solutions. Although they paid their precise attention only to the frequency changes but not to the intensities in Raman spectra, they cast a most important comment as follows: the term "structure-making and structure-breaking" is a confusing expression in that incorporation of small ions in water invites a new structure (hydration structure) formation different from the intrinsic water structure.

**Part 2 Pure gold dissolution in seawater mixed with aqueous nitric acid**

In an editorial article [38] is written that "many people have the impression that gold occurs as nuggets in streambeds and being a noble metal is only dissolved by aqua regia, mixture of concentrated hydrochloric and nitric acids". Beckham et al. [39] described that Geber, an Arabian chemist, mentioned aqua regia in the eighth century. In the metallurgy of gold, many leaching (dissolution in

liquids) methods were known [40]. Chlorine-Chloride leaching was applied commercially in the 19th century, but its use diminished following the introduction of the cyanide process in 1887.

The redox potentials [23] for gold species are as follows:

$$Au^+ + e^- \rightarrow Au, \; E^0 = 1.83 \, V \; \text{ and } \; Au^{3+} + 3e^- \rightarrow Au, \; E^0 = 1.52 \, V$$

$$AuCl_2^- + e^- \rightarrow Au + 2Cl^-, \; E^0 = 1.154 \, V \tag{4}$$

$$AuCl_4^- + 3e^- \rightarrow Au + 4Cl^-, \; E^0 = 1.002 \, V \tag{5}$$
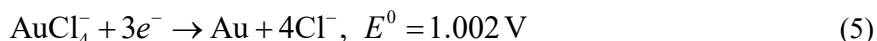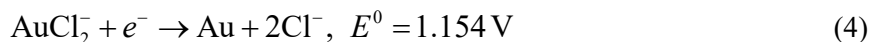
The comparison between Eqs. 4 and 5 indicates that the Au(III) complex is more stable than the Au(I) species by 0.15 V. Oxidation will occur only above approximately, 1.2 V, and therefore a strong oxidant, such as $Cl_2$ or $O_3$, is required to dissolve gold at a reasonable rate [41]. The redox potential of $Cl_2$ (g) to $Cl^-$ (aq) is reported to be 1.358 V [41] and that of $O_3$ to $O_2$ to be 2.075 V or 1.246 V in acidic or basic solution, respectively [41].

We have recognized that the nitronium ion ($NO_2^+$), the active species for nitration or oxidation, can be generated not only in the water phase of reversed micellar systems but also in bulk water containing salts in higher concentrations. Eq. 6 is the common reaction scheme to produce $NO_2^+$ in concentrate nitric acid and we have assumed that the same scheme can be applied to even the diluted nitric acid in reversed-micellar water droplets [4] as well as in bulk water containing higher concentrations of salts.

$$2HNO_3 \rightarrow NO_2^+ + NO_3^- + H_2O \tag{6}$$
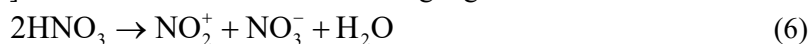
With an intimate examination of Eq. 6, we may notice that enhanced formation of $HNO_3$ in its molecular state and not dissociated ($H^+ + NO_3^-$) is essential for a favorite $NO_2^+$ generation. In bulk aqueous solution, however, many people may be suspicious that diluted nitric acid is apt to dissociate completely. How could we keep the nitric acid molecules from dissociating to protons and nitrate ions? Reducing the solvent's permittivity (e.g. $\varepsilon_r < 10$) may be an excellent way for that purpose. However, the permittivity of bulk aqueous solutions cannot be reduced so well. Then, our idea, the alternation of $H_2O$ into "dihydrogen ether"[8], could resolve some of the problems. Both the "strong" acidity and basicity of water are lost at once when the water molecules in the huge network are broken into isolated molecules by some of the causes already mentioned, such as, the abundant addition of salts and increased temperature. For solutions with very high salt concentrations, we may not rely so much on the Debye-Hückel [42] and Pitzer [43] theories, even though being highly developed, because such new or extraordinary phenomena have not been predicted in advance by calculations making use of these theories, at least at the moment. We have already mentioned that the redox potential of $NO_2^+$ generated in diluted nitric acid should be high enough to oxidize $Cl^-$ into $Cl_2$.

The present adventure, that is, dissolving gold in aqueous nitric acid, has been initiated not by any coincidence but by our reasoned deduction. As described above, dilute nitric acid in bulk water, provided it contains salts in high concentrations, can oxidize the $Cl^-$ ion to $Cl_2$. Therefore, it is an inevitable theory that the evolved $Cl_2$ should oxidize $Au^0$ into $Au^{3+}$, which is, at the same time, coordinated by the abundant $Cl^-$ ions, when the aqueous nitric acid is accompanied by sufficient amounts of chloride salts.

In Part 2, we would like to demonstrate the dissolution of precious metals (Au, Pt, and Pd), and to give detailed reports on gold dissolution in aqueous nitric acid (< 2 mol dm$^{-3}$) containing alkali metal, alkaline earth metal, and aluminum chlorides at 15 – 100 °C.

*2.1. Total dissolution of pure gold in 2 mol dm$^{-3}$ aqueous HNO$_3$ solution containing concentrated salts*

The gold dissolution has been examined with gold plate. Fig. 9 shows the period (time in hour) needed for the complete dissolution of a piece of gold plate (20±2 mg, the thickness of 0.1 mm) in a 20 mL solution of 2.0 mol dm$^{-3}$ HNO$_3$, accompanied by 1.0 mol dm$^{-3}$ AlCl$_3$, at various temperatures. It takes a long time, ca. 35 hours at 15 °C, however, the dissolution period was shortened with increasing temperature, e.g. less than 30 minutes at 70 or 80 °C. The aqueous HNO$_3$ solution acquires the increased dissolution ability with the temperature increase.

Next, the gold dissolution into the aqueous HNO$_3$ solution has been examined with the gold wire instead of the gold plate. Fig. 10 shows the time for complete dissolution of a piece of gold wire (19.7±0.5 mg, diameter of 0.25 mm) in a 20 mL solution of 2.0 mol dm$^{-3}$ HNO$_3$, accompanied by various chloride salts, at 60 °C. With increasing salt concentrations (from 1.0 mol dm$^{-3}$), generally speaking, the complete dissolution time is shortened. However, an interesting reversal trend is observed for

more than 5.0 mol dm$^{-3}$ LiCl: the gold dissolution in a 2 mol dm$^{-3}$ HNO$_3$ solution needs longer time in the presence of 7.0 or 9.0 than 5.0 mol dm$^{-3}$ LiCl. The most remarkable reversal effect is exhibited by CaCl$_2$. The dissolution time reaches its minimum at around 2.5 mol dm$^{-3}$ CaCl$_2$ and get longer again after reaching a concentration of 3.0 mol of the salt.
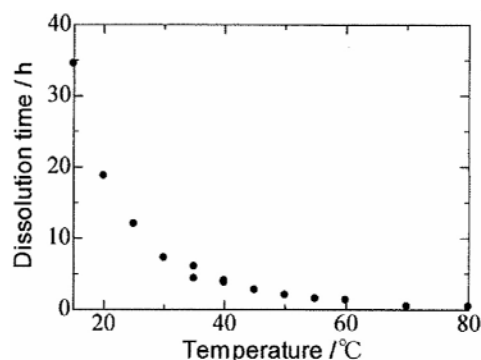


**Figure 9.** Time for the complete dissolution of gold plate (20 ± 2 mg) in 2.0 mol dm$^{-3}$ HNO$_3$, accompanied by 1.0 mol dm$^{-3}$ AlCl$_3$ at various temperatures.
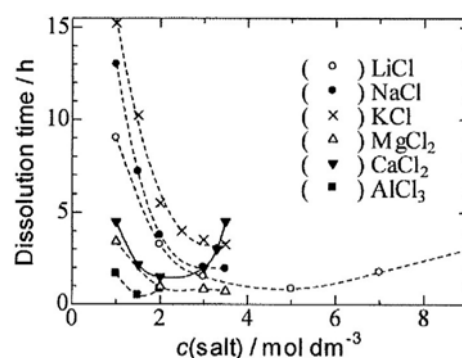
**Figure 10.** Time for the complete dissolution of gold wire (19.7 ± 0.5 mg) in 2.0 mol dm$^{-3}$ HNO$_3$, accompanied by various chloride salts at 60 °C.

As to dissolving gold, MgCl$_2$ is more effective than CaCl$_2$. The influence of metal chlorides (at 1.0 mol dm$^{-3}$) for the rate of gold dissolution increases in the order KCl < NaCl < LiCl < CaCl$_2$ < MgCl$_2$ < AlCl$_3$. At a lower temperature, 40 °C, much longer time is needed for complete dissolution of the gold wire in a 20 mL solution of 2.0 mol dm$^{-3}$ HNO$_3$ than at 60 °C. For instance, it takes 13 hours for the solution with 3.0 mol dm$^{-3}$ NaCl at 40 °C, but only 2 hours at 60 °C. In any case, all the results obtained with the metal chlorides at 40 °C were very similar to those observed at 60 °C. We would like to mention that the complete dissolution experiments of the gold wire in the solutions of much lower HNO$_3$ (down to 0.1 mol dm$^{-3}$) concentrations containing the chloride salts have been also successfully performed at 60 °C.

The dissolution capacity for Au has been examined as follows: a 2 mL solution of 2.0 mol dm$^{-3}$ HNO$_3$ is poured to 0.57 g of MgCl$_2$ (ca. 3 mol dm$^{-3}$) in a small beaker, and gold wire of 0.10 g is put in the solution. The beaker is placed on a hot-plate at ca. 80 °C, the gold wire dissolved completely in 40 minutes: the capacity can be estimated to be 50 g Au/L of 2 mol dm$^{-3}$ HNO$_3$, accompanied by 3 mol dm$^{-3}$ MgCl$_2$. On the other hand, it takes several days for a 0.040 g Pt wire (0.1 mm diameter) to be dissolved in 10 mL of 2 mol dm$^{-3}$ HNO$_3$, accompanied by 3 mol dm$^{-3}$ MgCl$_2$ at 80 °C, giving a Pt capacity of at least 4 g Pt/L. We will also note that Pd can be dissolved in a 1:1 mixture between 2.0 mol dm$^{-3}$ HNO$_3$ and seawater (vide infra).

For other precious metals, Ir and Ru, dissolution experiments have been performed. However, these metals (in powder) are not dissolved in 2 mol dm$^{-3}$ HNO$_3$, accompanied by 3 mol dm$^{-3}$ MgCl$_2$. It is well known that both Ir and Ru are not dissolved even in proper aqua regia [44]. Our method for dissolving precious metals (such as Au, Pt, or Pd) has a similar but weaker function than normal aqua regia. However, we would like to stress that our method has a higher efficiency of chemicals, without useless evolution of NO and Cl$_2$ during gold dissolution in regular aqua regia.

### 2.2. Dissolution rate constants and cation effects

The UV-visible spectroscopy has been employed to identify the dissolved species formed from the gold wire. Fig. 11 shows the changes with time in the absorption spectra (in 0.1 cm path-length) of a 2.0 mol dm$^{-3}$ HNO$_3$ solution containing a piece of gold wire (ca. 19.7 mg) in the presence of 3.5 mol dm$^{-3}$ NaCl. A band appears and increases with time, which is accompanied by a peak at λ ~ 306 nm and a shoulder around 400 nm, while the initial HNO$_3$ gives a band at λ ~ 300 nm. The spectrum observed after 12 hours in a 0.05 cm cuvette is consistent to that of 5.0 x 10$^{-3}$ mol dm$^{-3}$ NaAuCl$_4$ dissolved in a 2.0 mol dm$^{-3}$ HNO$_3$ solution. Therefore, we can safely conclude that the species dissolved in the 2 mol dm$^{-3}$ HNO$_3$ and 3.5 mol dm$^{-3}$ NaCl solution is definitely the AuCl$_4^-$ ion. Jones et al. [45] have reported the single crystal X-ray structure of Mg[Au(OH)$_4$]$_2$ and Ca[Au(OH)$_4$]$_2$, which have been obtained from reactions between HAuCl$_4$ and Ca(OH)$_2$.

Beckham et al.[39] noted that, when nitric acid is mixed with solid sodium chloride, there are formed sodium nitride, chlorine, and nitrosyl chloride: $3\,NaCl + 4\,HNO_3 \rightarrow 3NaNO_3 + Cl_2 + NOCl + 2\,H_2O$. They mentioned that "the system is similar to aqua regia." Concentrated NOCl in solution, such as aqua regia, should give a more dark orange or reddish color. The UV-visible absorption cross-sections of NOCl have been reported [46].
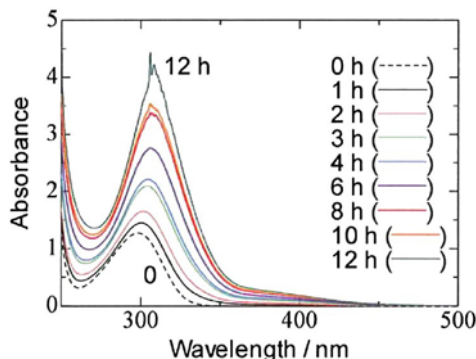


**Figure 11.** Changes in the UV–vis absorption spectra with time of $AuCl_4^-$ in 2.0 mol $dm^{-3}$ $HNO_3$ containing 3.5 mol $dm^{-3}$ NaCl at 40 °C.

The dissolution reaction rate constants (the first-order reaction) have been evaluated with the changes in the solid gold mass as well as the absorbance at $\lambda \sim 375$ nm, for avoiding the rather large $HNO_3$ absorbance (at $\lambda \sim 300$ nm). We have adopted the linear part of the plots of ln [S] vs. t, since the plots tend to deviate from the linearity downward (i.e., reaction accelerated) after the half-life period. It should be mentioned that the rate constant is for the initial dissolution process and that effects of the surface area on the reaction rate can be minimized by taking the values obtained with the initial part of each experiment.

**Table 2.** The gold dissolution rate constant, log $(k/s^{-1})$, measured in 2.0 mol $dm^{-3}$ $HNO_3$, accompanied by various added chloride salts at 40 °C.

| c(salt)/mol $dm^{-3}$ | LiCl | NaCl | MgCl$_2$ | CaCl$_2$ | AlCl$_3$ |
|---|---|---|---|---|---|
| 0.5 | | | | | −4.67[a] |
| | | | | | −4.63[b] |
| 1.0 | | | −4.49 | −4.59 | −4.00 |
| | | | −4.48 | −4.57 | −3.97 |
| 1.5 | | | −4.09 | | −3.61 |
| | | | −4.07 | | −3.60 |
| 2.0 | −4.39 | −4.62 | −3.82 | −4.09 | |
| | −4.37 | −4.69 | | −4.06 | |
| 3.0 | −4.10 | −4.29 | −3.51 | −3.99 | |
| | −4.03 | −4.27 | | | |
| 3.5 | | −4.21 | | | |
| | | −4.27 | −3.54 | −4.26 | |
| 4.0 | −3.84 | | | | |
| | −3.84 | | | | |
| 5.0 | −3.59 | | | | |
| 6.0 | −3.62 | | | | |

[a] The $(k/s^{-1})$ values in the upper rows are evaluated from the loss of the gold mass, ln $(M_t/M_0)$ vs. t/s where $M_0$ and $M_t$ are the gold masses at the initial and a certain time, respectively.
[b] The $(k/s^{-1})$ values in the lower rows are evaluated from the absorbance values at 375 nm, ln $(A_\infty - A_t)$ vs. t/s where $A_\infty$ and $A_t$ are absorbance values after the complete gold dissolution and at a certain time, respectively.

In general, rate constants obtained by the different two ways are consistent to each other (cf. Table 2). However, the results from the absorbance method can be fluctuated, especially, when the concentrations of the chloride ion are quite high; in such cases, the solution turns already to a yellow color

before placing gold. For its simplicity, we may take the rate constants obtained by the loss of the gold mass, except for some cases in which the mass method could not be appropriately applied. In the present paper, the rate constants evaluated by the mass method are given, unless otherwise noted.

*2.3 Gold dissolution into seawater and the seawater assisted by added chloride salts*

Seawater is an electrolyte solution. Its chemistry is dominated by the presence of six ions ($Na^+$, $K^+$, $Mg^{2+}$, $Ca^{2+}$, $Cl^-$, $SO_4^{2-}$) which constitute more than 99.5% of the dissolved constituents [47]. The concentrations of the main components have been reported to be 0.468, 0.010, 0.053, 0.010, 0.545, and 0.028 mol $kg^{-1}$, respectively, for the 35‰ seawater [48]. Taking into account its density (d = 1.025 as the average)[49], we can regard the seawater as a 0.55 ~ 0.56 mol $dm^{-3}$ chloride solution with mainly sodium and partly magnesium cations.

All experimental results in the present work strongly suggest that pure gold should dissolve in seawater if it is mixed with aqueous nitric acid and then heated. We have utilized "Muroto Deep Seawater" as a standard sample of seawater. The main components in the seawater are well consistent with the typical 35‰ seawater. By mixing 50 mL seawater with 50 mL of 2.0 mol $dm^{-3}$ $HNO_3$, we have a 100 mL solution of 1.0 mol $dm^{-3}$ $HNO_3$ containing 0.278 mol $dm^{-3}$ $Cl^-$, 0.225 mol $dm^{-3}$ $Na^+$, 0.026 mol $dm^{-3}$ $Mg^{2+}$ (0.014 mol $dm^{-3}$ $SO_4^{2-}$) and other ions. The mixed solution is heated up to ca. 100 ºC in a flask, equipped with a condenser. When boiling starts, then five pieces of gold wire (totally 0.10 g) are placed into the solution. Occasionally, samplings are carried out from the boiling solution and the pieces of gold wire are dissolved completely within 17 hours. The absorbance values at l = 375 nm are utilized for evaluating the dissolution rate constant to give log (k /$s^{-1}$) = -4.52. Another Pacific seawater off Hawaii (1,000 m depth) gives a value (-4.54) similar to that of "Muroto Deep Seawater". Although ten pieces of gold wire (totally ca. 0.20 g) have appeared to dissolve completely in the 100 mL (seawater and nitric acid mixture) solution, after cooling down, some residue is noticed on the solution surface. Therefore, we keep five pieces (0.10 g) of gold wire as the limit for the seawater experiments. Incidentally, platinum is too tough to be dissolved in the seawater and 2.0 mol $dm^{-3}$ $HNO_3$ (1:1) mixture even after 10 days at ca. 100 ºC. However, within 24 hours, a piece of Pd wire (0.04 g, 0.25 mm diameter, 99.9%) has dissolved in a 50 mL mixed (1:1) solution between the seawater and 2.0 mol $dm^{-3}$ $HNO_3$ at ca. 100 ºC.

Fig. 12 shows the increasing dissolution rate constant with increasing NaCl added to the seawater. The solution preparation procedure is as follows: The seawater is poured to 11.69 g NaCl crystals up to 50 mL in a volumetric flask to prepare an additional 4.0 mol $dm^{-3}$ NaCl seawater solution. Mixing between 50 mL of 2.0 mol $dm^{-3}$ $HNO_3$ and 50 mL of the additional 4.0 mol $dm^{-3}$ NaCl seawater solution gives 100 mL of 1.0 mol $dm^{-3}$ $HNO_3$ containing additional 2.0 mol $dm^{-3}$ NaCl seawater solution (totally ca. 2.23 mol $dm^{-3}$ $Na^+$ and ca. 2.28 mol $dm^{-3}$ $Cl^-$).

The log (k /$s^{-1}$) value increases remarkably from -4.52 to -3.71 with additional 0.5 mol $dm^{-3}$ NaCl and it remains almost a constant value up to 2.0 mol $dm^{-3}$ NaCl. As for platinum, however, a 2.8 mg Pt mass has been left without dissolving out of ca. 20 mg platinum wire (0.1 mm diameter) in 100 mL of the 1.0 mol $dm^{-3}$ $HNO_3$ and 0.5 mol $dm^{-3}$ NaCl added seawater after six days. Without the support by additional salts, however, no Pt can be dissolved in the 1:1 mixture between seawater and 2.0 mol $dm^{-3}$ $HNO_3$ (vide supra).

We just mention that the "excellent" dissolution ability of seawater mixed with 2.0 mol $dm^{-3}$ $HNO_3$ for gold has been successfully applied to collecting of gold from waste electronic devises, just mechanically tipped. The ICP-atomic emission spectrometry has demonstrated the dissolution of Au out of the waste electronic devices, as well as Cu, Ni, Al, Si, Zn, and B. Recovery of gold from secondary sources has been widely reviewed by S. Syed [50].

*2.4 "Dilute aqua regia" of various $HNO_3$ and HCl concentrations*

In the CRC book [51] the preparation procedure of aqua regia is described as follows: "Mix 1 part concentrated $HNO_3$ with 3 parts of concentrated HCl. This formula should include one volume of water if the aqua regia is to be stored for any length of time. Without water, objectionable quantities of chlorine and other gases are evolved". According to this description, it has been well known that dilution with water is essential for the long term storage of active aqua regia. Assuming 16 mol $dm^{-3}$ $HNO_3$ (70%) and 12 mol $dm^{-3}$ HCl, the original aqua regia is composed of 4 mol $dm^{-3}$ $HNO_3$ and

9 mol dm$^{-3}$ HCl, while the water added solution is calculated to contain still 3.2 mol dm$^{-3}$ HNO$_3$ and 7.2 mol dm$^{-3}$ HCl.
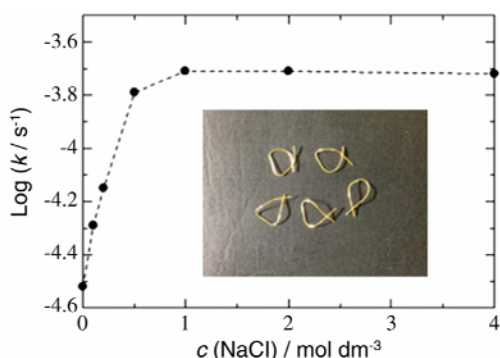


**Figure 12.** The increase of the dissolution rate constant of gold wire with increasing added NaCl concentration in the 1.0 mol dm$^{-3}$ HNO$_3$ and seawater (a half-concentration) solution at ca. 100 °C. The rate constants have been evaluated by means of spectroscopy.
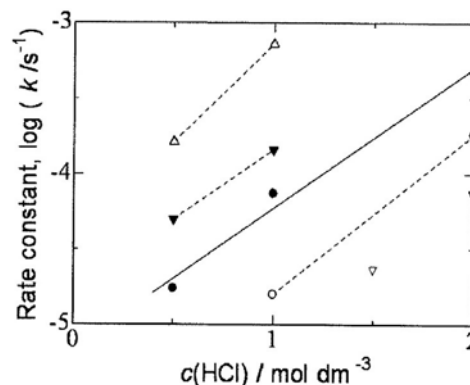


**Figure 13.** The dissolution rate constants of gold wire (19.7 ± 0.5 mg) in various concentrations of "dilute aqua regia" at 60 and ca. 100 °C: (▽) 0.5 mol dm$^{-3}$ HNO$_3$ 60 °C; (○) 1.0 mol dm$^{-3}$ HNO$_3$ 60 °C; (●) 2.0 mol dm$^{-3}$ HNO$_3$ 60 °C; (▼) 0.5 mol dm$^{-3}$ HNO$_3$ 100 °C; (△) 1.0 mol dm$^{-3}$ HNO$_3$ 100 °C. The rate constants at 60 and ca. 100 °C have been evaluated by the mass and spectroscopy, respectively.

The gold dissolution in "dilute aqua regia" has been examined with different HNO$_3$ and HCl combinations in various concentrations: 0.5, 1.0, and 2.0 mol dm$^{-3}$ HNO$_3$; 0.5, 1.0, (1.5), and 2.0 mol dm$^{-3}$ HCl at 60 ºC (cf. Fig. 13). The [1.0, 1.0] "dilute aqua regia" (of 1.0 mol dm$^{-3}$ HNO$_3$ and 1.0 mol dm$^{-3}$ HCl) gives a dissolution rate constant of log (k /s$^{-1}$) = -4.80 at 60 ºC. With increased HCl concentration, i.e., of 2.0 mol dm$^{-3}$, the rate constant increases: the [1.0, 2.0] "dilute aqua regia" gives -3.74. The [2.0, 0.5], [2.0, 1.0], and [2.0, 2.0] solutions give a linear relation between log (k /s$^{-1}$) and c(HCl) values, to be -4.76, -4.13, and -3.33. Comparing the [0.5, 2.0] with the [2.0, 0.5] solution, we have noticed that the [0.5, 2.0] (-4.13) is faster than the [2.0, 0.5] (-4.76), probably because the ratio between c(HNO$_3$) and c(HCl) in the [0.5, 2.0] may be more favorable than that of the [2.0, 0.5] as the "dilute aqua regia" medium. Similarly, the [1.0, 2.0] (-3.74) is faster than the [2.0, 1.0] (-4.13) at 60 ºC. At 100 ºC, the rate constant of "dilute aqua regia" increases remarkably, e.g. the [1.0, 1.0] (-3.14) at ca. 100 ºC is 46 times faster than the [1.0, 1.0] (-4.80) at 60 ºC. In a very "dilute aqua regia," it takes a very long time to dissolve gold wire (ca. 19.7 mg) completely: 8 days in both the [0.5, 1.0] and the [1.0, 0.5] solutions at 60 ºC.

## Conclusion

Nitration of phenols was performed by dilute nitric acid (2.0 mol dm$^{-3}$) in reversed micelle systems at 35 ºC. Even dilute nitric acid in bulk water system, provided it contains salts in high concentrations, can oxidize the Cl$^-$ ion to Cl$_2$ as well as Br$^-$ to Br$_2$. The nitronium ion (NO$_2^+$), the active species for nitration or oxidation, can be generated not only in water phase of reversed micelle systems but also in bulk water containing salts in high concentrations. Just as the water structure of nanoscale water droplets in reversed micelle systems is distorted, that of "bulk" aqueous solution can be also distorted by salts in high concentrations and, consequently, "bulk" aqueous solutions should lose the properties of the bulk water.

Although aqueous nitric acid (< 2 mol dm$^{-3}$) itself exhibits no oxidation ability, it acquires the strong oxidation ability to oxidize Cl$^-$ to Cl$_2$ in the presence of chloride salts. The chlorine (Cl$_2$)–chloride (Cl$^-$) systems provided by aqueous nitric acid containing enough amounts of chloride salts, have been found to be excellent media for dissolving precious metals, especially, pure gold. In general, the increasing concentrations of chloride salts cause the advanced ability for gold dissolution. At higher temperatures, such as 60 or 100 ºC, gold can easily be dissolved into the mixed solution between diluted aqueous HNO$_3$ and HCl, i.e. "dilute aqua regia", which can be applied to prepare a 1000 ppm gold stock solution easily. The "excellent" gold dissolution ability of the mixture of sea-

water with aqueous nitric acid can be applied to the recovery of gold from waste electronic devices. In electrochemical operation, the Au or Pt electrodes can be dissolved naturally in concentrated halides salt solutions.

The present paper is composed of the rearrangement of J. Mol. Liquids 2011, 163, 161-169 and J. Mol. Liquids 2014, 194, 68-76.

## References

1. Langer, S.; Pemberton, R.S.; Finlayson-Pitts, B.J. J. Phys. Chem. A 1997, 101, 1277.
2. Cotton, F.A.; Wilkinson, G. Advanced Inorganic Chemistry: A Comprehensive Text; 4th Ed; Wiley: New York, 1980; Chap. 6.
3. Petkovic, D.M. J. Chem. Soc. Dalton Trans. 1982, 2425.
4. Hojo, M.; Ueda, T.; Daike, C.; Takezaki, F.; Furuya, Y.; Miyamoto, K.; Narutaki, A.; Kato, R. Bull. Chem. Soc. Jpn. 2006, 79, 1215.
5. Nose, A.; Hojo, M.; Ueda, T. J. Phys. Chem. B 2004, 108, 798.
6. Hojo, M. Pure Appl. Chem. 2008, 80, 1539; and therein.
7. Hojo, M.; Ueda, T.; Ike, M.; Kobayashi, M.; Nakai, H. J. Mol. Liquids 2009, 145, 152.
8. (a) Manege, L. C.; Ueda, T.; Hojo, M. Bull. Chem. Soc. Jpn. 1998, 71, 589. (b) Manege, L. C.; Ueda, T.; Hojo, M.; Fujio, M. J. Chem. Soc. Perkin Trans. 2 1998, 1961. (c) Hojo, M.; Ueda, T.; Inoue, S.; Kawahara, Y. J. Chem. Soc. Perkin Trans. 2 2000, 1735. (d) Hojo, M.; Ueda, T.; Ueno, E.; Hamasaki, T.; Fujimura, D. Bull. Chem. Soc. Jpn. 2006, 79, 751. (e) Hojo, M.; Ueda, T.; Ueno, T.; Hamasaki, T.; Nakano, T. Bull. Chem. Soc. Jpn. 2010, 83, 401. (f) Hojo, M.; Aoki, S. Bull. Chem. Soc. Jpn. 2012, 85, 1023.
9. Reichardt, C.; Che, D.; Heckenkemper, G.; Schaefer, G. Eur. J. Org. Chem. 2001, 2343.
10. Frank, H.S.; Wen, W.-Y.; Discuss. Faraday Soc. 1957, 24, 133.
11. Park, S.; Molianen, D.E.; Fayer, M.D. J. Phys. Chem. B 2008, 112, 5279.
12. Gopalakrishnan, S.; Liu, D.; Allen, H.C.; Kuo, M.; Shultz, M.J. Chem. Rev. 2006, 106, 1155.
13. Kuo, David, M.H.; A.; Kamelamela, N.; White, M.; Shultz, M.J. J. Phys. Chem. C 2007, 111, 8827.
14. Smith, M.B.; March, J. March's Advanced Organic Chemistry Reactions, Mechanisms, and Structure; 6th Ed; Wiley-Interscience: Hoboken, NJ, USA, 2007; p. 689.
15. Smith, M.B.; March, J. March's Advanced Organic Chemistry Reactions, Mechanisms, and Structure; 6th Ed; Wiley-Interscience: Hoboken, NJ, USA, 2007; p. 665.
16. Onori, G.; Santucci, A. J. Phys. Chem. 1993, 97, 5430.
17. Gutmann, V. The Donor-Acceptor Approach to Molecular Interactions; Plenum: New York; 1978.
18. Grove, J. R.; Raphael, L. J. Inorg. Nucl. Chem. 1963, 25, 130.
19. Wright, E.R.; Smith, R.A.; Messick, B.G. In Colorimetric Determination of Nonmetals. Boltz, D.F.; Howell J.A., Eds. Wiley: New York, 1978; Chap. 2, p. 47.
20. Rossi, M.J. Chem. Rev. 2003, 103, 4823.
21. Boltz, D.F.; Holland, W.J.; Howell, J.A. In Colorimetric Determination of Nonmetals. Boltz, D.F.; Howell J.A., Eds. Wiley: New York, 1978; Chap. 4, p. 88.
22. Boughriet, A.; Wartel, M.; Fischer, J.C. J. Electroanal. Chem. 1985, 190, 103.
23. Bard, A.J.; Parsons, R.; Jordan J., Eds. Standard Potentials in Aqueous Solution; Marcel Dekker: New York, 1985.
24. Olah, G.A.; Malhotra, R.; Narang, S.C. Nitration: Methods and Mechanisms; VCH: New York, 1989; p. 192.
25. Bontempelli, G.; Mozzocchin, G.-A.; Magno, F. J. Electroanal. Chem. 1974, 55, 91.
26. Behnke, W.; George, C.; Scheer, V.; Zetzsch, C. J. Geophys. Res. 1997, 102, 3795.
27. Oki, M.; Ohsawa, T.; Tanaka, M.; Chihara H., Eds. Encyclopedic Dictionary of Chemistry; Tokyo Kagaku Dozin: Tokyo, 1989; p. 322 (in Japanese).
28. Moeller, T.; Bailar, J.C. Jr.; Kleinberg, J.; Guss, C.O.; Castellion, M.E.; Metz, C. Chemistry with Inorganic Qualitative Analysis; Academic Press: New York, 1980; p. 670.

29. Kumar, S.; Varadarajan, R.; Chawla, H.M.; Hundal, G.; Hundal, M.S. Tetrahedron 2004, 60, 1001.

30. Bharadwaj, S.K.; Hussain, S.; Kar, M.; Chaudhuri, M.K. Catalysis Commun. 2008, 9, 919.

31. Bazsa, G. Comments Inorg. Chem. 1986, 5, 57.

32. Scherer, J.R.; Go, M.K.; Kint, S. J. Phys. Chem. 1974, 78, 1304. Irish, D.E.; Brooker, M.H. In Advances in Infrared and Raman Spectroscopy. Clark, R.J.H.; Hester R.E., Eds. Heyden: London, 1976; Vol. 2, Chap. 6, p. 239.

33. Pastorczak, M.; Kozanecki, M.; Ulanski, J. J. Phys. Chem. A 2008, 112, 10705.

34. Gordon, J.E. The Organic Chemistry of Electrolyte Solutions; Wiley: New York, 1975; p. 167.

35. Hindman, J.C. J. Chem. Phys. 1962, 36, 1000.

36. Li, R.; Jiang, Z.; Shi, S.; Yang, H. J. Mol. Struct. 2003, 645, 69.

37. Yonehama, K.; Yoshimura, Y.; Takekiyo, T.; Kanno, H. Bull. Chem. Soc. Jpn. 2009, 82, 563.

38. Abelson, P.H. Science 1986, 233, 141.

39. Beckham, L.J.; Fessler, W.A.; Kise, M. A. Chem. Rev. 1951, 48, 319.

40. Marsden, J.O.; House, C.I. The Chemistry of Gold Extraction; 2nd Ed; Society for Mining, Metallurgy, and Exploration (SME), Inc.: Littleton, Colorado, 2006; p. 233.

41. Marsden, J.O.; House, C.I. The Chemistry of Gold Extraction; 2nd Ed; Society for Mining, Metallurgy, and Exploration (SME), Inc.: Littleton, Colorado, 2006; p. 272.

42. (a) Debye, P.; Hückel, E. Phys. Z. 1923, 24, 185, 305. (b) Fraenkel, D. J. Phys. Chem. B, 2011, 115, 14634.

43. Pitzer, K.S. Activity Coefficients in Electrolyte Solutions; 2nd Ed; CRC: Boca Raton, Florida, 1991.

44. Nakahara, M. Dictionary of Inorganic Compounds and Complexes; Kodansha Scientific: Tokyo, 1997 (in Japanese).

45. Jones, P.G.; Schelbach, R.; Schwarzmann, E. Z. Naturforsch. B 1987, 42, 522.

46. Roehl, C.M.; Orlando, J.J.; Calvert, J.G. J. Photochem. Photobiol. A: Chem. 1992, 69, 1.

47. Whitfield, M. Sea Water as an Electrolyte Solution. In Chemical Oceanography. Riley, J. P.; Skirrow G., Eds.; Vol. 1; 2nd Ed; Academic Press: London, 1975; Chap. 2.

48. Holland, H.D. The Chemistry of the Atmosphere and Ocean; Wiley: New York, 1978; Chap. 5.

49. http://en.wikipedia.org/wiki/Seawater.

50. Sayd, S. Hydrometallurgy 2012, 115-116, 30.

51. Weast, R. C. Handbook of Chemistry and Physics; 70th Ed; CRC: Boca Raton, Florida, 1989; D-130.

М. Ходжо. Механизм повышенной окисляющей способности разбавленной азотной кислоты и растворение металлического золота в азотной кислоте, разбавленной морской водой.

Департамент химии, факультет науки, Университет г. Кочи, Кочи, 780-8520, Япония

Обнаружено, что разбавленная азотная кислота в обращённых мицеллах может окислять ион $Br^-$ до $Br_2$, и предложено использовать нитроний, $NO_2^+$, как активный реагент в окислительном процессе. Нитрование фенола разбавленной азотной кислотой в водной дисперсной фазе обращённой мицеллярной системы $CHCl_3$/хлорид цетилтриметиламмония/$H_2O$ (2.0 моль дм$^{-3}$ $HNO_3$ при содержании воды 1.0 % (v/v), проведённое при 35 ºC, привело к образованию 2- и 4-нитрофенолов. В водном растворе $HNO_3$ с концентрацией 2.0 моль дм$^{-3}$ в присутствии 4.0 моль дм$^{-3}$ LiCl и небольшого количества LiBr как источника бромида *транс*-1,4-дибром-2-бутен успешно бромируется до 1,2,3,4-тетрабромбутана. Этот результат является хорошим подтверждением возможности окисления иона $Br^-$ до $Br_2$ в разбавленной до 2.0 моль дм$^{-3}$ азотной кислоте в присутствии концентрированных солей. Для серии хлоридов эффект катиона возрастает в ряду: $Et_4N^+$ << $Na^+$ < $Li^+$ < $Ca^{2+}$ < $Mg^{2+}$. Наблюдалось даже выделение $Cl_2$ из раствора $HNO_3$ с концентрацией < 2.0 моль дм$^{-3}$, содержащего высокие концентрации $LiCl$, $MgCl_2$ и $CaCl_2$, а также $AlCl_3$. Показано растворение благородных металлов (Au, Pt, and Pd) и особенно золота в 0.1 - 2 моль дм$^{-3}$ $HNO_3$ в присутствии хлоридов щелочных и щелочноземельных металлов, а также хлорида алюминия. Время полного растворения пластины из металлического золота массой 20±2 мг и толщиной 0.1 мм в 2.0 моль дм$^{-3}$ $HNO_3$ в присутствии 1.0 моль дм$^{-3}$ $AlCl_3$ заметно сокращается при повышении температуры от 15 до 80 ºC. Скорость растворения кусочка золотой проволоки массой 19.7±0.5 мг в 20 мл раствора $HNO_3$ концентрации 2.0 моль дм$^{-3}$ в

присутствии хлоридов металлов в целом возрастает при увеличении концентрации солей при 40 и 60 ºC. Золото может растворяться при концентрациях $HNO_3$ и $HCl$ менее 1.0 моль дм$^{-3}$, т.е. в "разбавленной царской водке". Нами достигнуто полное растворение пяти кусочков золотой проволоки суммарной массой 0.10 г в 100 мл смеси морской воды с 2.0 моль дм$^{-3}$ $HNO_3$ в соотношении 1: 1 при ≈ 100 ºC.

**Ключевые слова:** нитроний ион, хлорид цетилтриметиламмония, выделение хлора, окисление бромида, солевой эффект, структура объёмной воды, разбавленная царская водка, тетрахлораурат, концентрированная соль, Рамановский спектр.

М. Ходжо. Механізм підвищеної окислюючої здатності розведеної нітратної кислоти і розчинення металевого золота в нітратній кислоті, розведеній морською водою.

Департамент хімії, факультет науки, Університет м. Кочі, Кочі, 780-8520, Японія

Знайдено, що розведена нітратна кислота в обернених міцелах може окислювати іон $Br^-$ до $Br_2$, та запропоновано використовувати нітроній, $NO_2^+$, як активний реагент в окислювальному процесі. Нітрування фенолу розведеною нітратною кислотою в водній дисперсній фазі оберненої міцелярної системи $CHCl_3$/хлорид цетилтриметиламонію/$H_2O$ (2.0 моль дм$^{-3}$ $HNO_3$ при вмісті води 1.0 % (v/v), проведене при 35 ºC, привело до створення 2- та 4-нітрофенолів. У водному розчині $HNO_3$ з концентрацією 2.0 моль дм$^{-3}$ в присутності 4.0 моль дм$^{-3}$ $LiCl$ і невеликої кількості $LiBr$ як джерела броміду *транс*-1,4-дибром-2-бутен успішно хромується до 1,2,3,4-тетрабромбутану. Цей результат є добрим підтвердженням можливості окислення іону $Br^-$ до $Br_2$ в розведеній до 2.0 моль дм$^{-3}$ нітратній кислоті у присутності концентрованих солей. Для серії хлоридів ефект катіону зростає у послідовності: $Et_4N^+ << Na^+ < Li^+ < Ca^{2+} < Mg^{2+}$. Спостерігалося також виділення $Cl_2$ з розчину $HNO_3$ з концентрацією < 2.0 моль дм$^{-3}$, який містить високі концентрації $LiCl$, $MgCl_2$ и $CaCl_2$, а також $AlCl_3$. Показано повне розчинення благородних металів (Au, Pt, and Pd) і особливо золота в 0.1 - 2 моль дм$^{-3}$ $HNO_3$ в присутності хлоридів лужних та лужноземельних металів, а також хлориду алюминию. Час повного розчинення пластини з металевого золота масою 20±2 мг і товщиною 0.1 мм в 2.0 моль дм$^{-3}$ $HNO_3$ в присутності 1.0 моль дм$^{-3}$ $AlCl_3$ помітно зменшується при підвищенні температури від от 15 до 80 ºC. Швидкість розчинення шматочка золотого дроту масою 19.7±0.5 мг в 20 мл розчину $HNO_3$ з концентрацією 2.0 моль дм$^{-3}$ в присутності хлоридів металів в цілому зростає при підвищенні концентрації солей при 40 і 60 ºC. Золото може розчинятися при концентраціях $HNO_3$ і $HCl$ менших ніж 1.0 моль дм$^{-3}$, тобто в «розведеній царській водці». Нами досягнуте повне розчинення п'яти шматочків золотого дроту сумарною масою 0.10 г в 100 мл суміші морської води з 2.0 моль дм$^{-3}$ $HNO_3$ у співвідношенні 1:1 при ≈ 100 ºC.

**Ключові слова:** нітроній іон, хлорид цетилтриметиламонію, виділення хлору, окислення броміду, сольовий ефект, структура об'ємної води, розведена царська водка, тетрахлораурат, концентрована сіль, Рамановський спектр.

УДК 541.135

# ELECTRICAL CONDUCTIVITY, ION-MOLECULAR AND INTERIONIC INTERACTIONS IN SOLUTIONS OF SOME TETRAALKYLAMMONIUM SALTS IN ACETONITRILE: THE INFLUENCE OF THE ION AND TEMPERATURE

## O.N. Kalugin [a], E.V. Lukinova [b], D.O. Novikov [c]

*V.N. Karazin Kharkiv National University, School of Chemistry, Department of Inorganic Chemistry 4 Svobody sqr., 61022 Kharkiv, Ukraine*

a) ✉ *onkalugin @gmail.com*      https://orcid.org/0000-0003-3273-9259
b) ✉ *elena.v.lukinova @gmail.com*      https://orcid.org/0000-0002-8016-0439
c) ✉ *dmitrynovikovs @gmail.com*      https://orcid.org/0000-0003-3584-4521

Conductance data for $Et_4NBr$, $Et_4NBF_4$, $Bu_4NBr$, $Bu_4NBF_4$ in acetonitrile for the molar concentration range of $2 \cdot 10^{-4}$–$1 \cdot 10^{-2}$ $mol \cdot dm^{-3}$ over the temperature range from 5 to 55 °C are reported. Limiting molar conductivities and ion association constants were determined by using the Lee-Wheaton equation for the symmetrical electrolytes. On the basis of the preliminary conductometric data analysis it was established that the closest approach parameter is almost independent from the temperature for all studied acetonitrile solutions. Therefore, the closest approach parameter was adopted as a sum of cation and anion radii for further conductometric data treatment.

The limiting conductivities of $Br^-$, $BF_4^-$, $Et_4N^+$ and $Bu_4N^+$ ions and the structure-dynamic parameter of ion-molecular interaction obtained from the experimental data on limiting molar conductivities were evaluated in the framework of the approach proposed by authors [Kalugin O. N., Vjunnik I. N. Limiting ion conductance and dynamic structure of the solvent in electrolyte solution. *Zh. Khim. Fiz. (Rus.)* **1991,** *10* 708-714]. Elongation of the alkyl radical of the tetraalkylammonium cation from $Et_4N^+$ to $Bu_4N^+$ leads to a significant increase in the structure-dynamic parameter, which indicates the dynamic structuring of the solvent near the tetrabutylammonium ion and increased solvophobic solvation of the $Bu_4N^+$ compared to $Et_4N^+$.

Ion association constants are discussed in terms of competition between Coulomb and non-Coulomb forces in terms of short-range square-mound potential. An increase in the ion association constants in the sequence $Bu_4NBF_4 < Et_4NBF_4 < Bu_4NBr < Et_4NBr$ was explained by the increase in the contribution of short-range ion-molecular interactions to the interionic attraction in addition to the electrostatic component. An increase in temperature enhances the ionic association due to both the electrostatic and short-range components.

**Keywords:** tetraethylammonium bromide, tetrabutylammonium bromide, tetraethylammonium tetrafluoroborate, tetrabutylammonium tetrafluoroborate, acetonitrile, electrical conductivity, ion association constant, limiting molar conductivity, square-mound interionic potential, ion solvation microdynamics.

## Introduction

Non-aqueous electrolyte solutions are widely used in electrochemical energy storage devices, such as supercapacitors (SCs) with porous nano-carbon electrodes [1]. Non-aqueous solutions of tetraalkylammonium salt-based electrolytes were used to test samples of porous carbon electrodes in SCs [2]. On one hand, non-aqueous solutions of tetraalkylammonium salts have a broader operating current range [3] and a wider operating temperature range, compared to water electrolyte solutions [4-5]. On the other hand, non-aqueous solutions of tetraalkylammonium salts have even greater ionic conductivity than ionic liquids [6-7]. It was also shown that electrical conductivity of symmetrical tetraalkylammonium salts in acetonitrile is greater compared to the corresponding solutions in propylene carbonate, γ-butyrolactone and dimethylformamide [8]. Moreover, a unique combination of dielectric permittivity, viscosity and solubility in acetonitrile of both solid and liquid electrolytes and ionic liquids (ILs) have caused an extensive use of acetonitrile in electrochemical practice.

Electrolytes for SCs have to satisfy a set of requirements that determine technical and operational characteristics of the electrochemical device: a broad temperature interval of the liquid state, high electrochemical stability and non-hygroscopicity [9]. However, high electrical conductivity of solvent-electrolyte system still remains the property of paramount importance.

A literature review shows that the data on electrical conductivity adequately cover many 1-1 electrolytes in acetonitrile, including tetraalkylammonium salts [10-13]. Unfortunately, in most of them either only data at 298.15 K is given, or is interpreted not deep enough. In the same time, conductome-

try, as a method of analysis, allows to obtain precious information about ion-ion and ion-molecular environment, electrolyte association constant and quantitative characteristics of ionic solvation. As a result, using conductometry it becomes possible to investigate regularities in the influence of composition and nature of electrolyte solution components on its macroscopic properties.

Giving the fact that solutions of $Et_4NBF_4$ are considered as model electrolyte solutions for SCs [14], within this research we focused on studying the influence of the temperature on the electrical conductivity of tetraalkylammonium salts $R_4NX$ (R = Bu, Et; X = $BF_4$, Br) in acetonitrile. Exceptional attention was paid to quantitative characteristics of ion-ion and ion-molecular interactions when interpreting obtained conductometric data. This data is important not only for systematization of already available data but also to formulate new approaches to optimize properties of electrolyte solutions for SCs.

## Experimental Section

*Materials*. Tetrabutylammonium tetrafluoroborate was synthesized by the reaction:

$$Bu_4NOH + HBF_4 \rightarrow Bu_4NBF_4 + H_2O$$
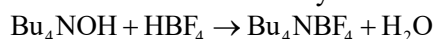
An excess of tetrafluoroboric acid (up to pH=5) was added to the water solution of tetrabutylammonium hydroxide ($\omega$=40%). Precipitated needle crystals were filtered on a glass filter and rinsed by double-distilled water until the filtrate had pH=7. Obtained salt was recrystallized 2 times from benzene with the addition of octane.

Tetrabutylammonium bromide (Sigma-Aldrich, 99% purity) and tetraethylammonium tetrafluoroborate (Sigma-Aldrich, 98% purity) were recrystallized 2 times from benzene with the addition of hexane and acetone respectively. Tetraethylammonium bromide was recrystallized 3 times from the waterless ethanol.

Purified salts were dried under vacuum at room temperature for 24h. Needle crystals were then ground down in the agate mortar and re-dried under vacuum at 55-65°C to the constant weight ($\delta$m<0.005%). Dried salts were stored in the glass weighting bottles in the desiccator dehydrated with $P_2O_5$.

*Acetonitrile*, previously withstood over dry potassium permanganate, was distilled, collecting the $2^{nd}$ fraction of the solvent. Collected acetonitrile was distilled 4 more times over $P_4O_{10}$ in order to remove remaining water [15]. In order to remove polyphosphoric acids acetonitrile was boiled with calcined potassium carbonate for 90 minutes. Trace quantities of water were removed by storing acetonitrile over calcium hydride for 12h followed by the distillation. The purity of acetonitrile was controlled by specific electrical conductivity (1.1-2.5·$10^{-8}$ S cm$^{-1}$ at 25°C).

*Measurements*. Initial concentrated solutions for conductometric study were prepared from the solid salt. The rest of the solutions were prepared by diluting the concentrated solution by mass taking into account Archimedes force correction. Molar concentrations of solutions prepared were calculated by the equation (1).

$$c_i = \tilde{m}_i \cdot d_i(T) \tag{1}$$

where $d_i(T)$ is the density of a solution at a given temperature, $\tilde{m}$ is the concentration of a solution, expressed in moles per kg of the solution (malonity). $d_i(T)$ was found by the equation (2)

$$d(T) = d_0(T) + B\tilde{m} \tag{2}$$

where $d_0$ is the density of a pure solvent, $B$ is the density concentration coefficient.

Experimental densities of the solutions of $Bu_4NBF_4$, $Bu_4NBr$ and $Et_4NBF_4$ in acetonitrile were obtained for the concentration range of 0-1 mol kg$^{-1}$ and fitted by equation (2).

The permanence of $B$ coefficient was observed for all solutions studied in the temperature range of 25-55°C. Therefore, 0.072, 0.084 and 0.066 kg (mol dm$^3$)$^{-1}$ values of $B$ coefficient were used for $Bu_4NBF_4$, $Bu_4NBr$ and $Et_4NBF_4$ respectively. The value of $B$ = 0.070 kg (mol dm$^3$)$^{-1}$ for $Et_4NBr$ in acetonitrile was taken from the literature [16].

The electrical resistance of solutions was measured at 5, 15, 25, 35, 45 and 55 °C in four double-electrode conductometric cells using P5083 and Gwinstek LCR-821 AC bridges. Conductometric cells were previously calibrated against potassium chloride solutions. When measuring the resistance of solutions, conductometric cells were thermostated with the accuracy of ±0.02°C for 20 minutes before taking the measurements.

Obtained values of the solutions' resistance were used to derive specific ($\kappa$, S cm$^{-1}$) and molar ($\Lambda$, S cm$^2$ mol$^{-1}$) electrical conductivities. Specific and molar electrical conductivities were calculated taking into account the conductivity of a pure acetonitrile. Obtained primary data is given in Appendix A.

### Data Treatment

A joint approach of conductometric data treatment was used to process experimental data [17]. The approach is based on the application of non-linear least squares method to solve the overfilled system of the equations: concentration dependence of electrical conductivity ($\Lambda^{theor}$) (3), the mass action law (4), mass balance equation (5) and expression for mean ionic activity coefficient (6) for a set of $k$ experimental points:

$$\Lambda^{theor} = \frac{c_{\pm}}{c} f\left(c; \Lambda_0; R\right) \tag{3}$$

$$K_A = c_0 \big/ \left(c_{\pm} \cdot y_{\pm}\right)^2 \tag{4}$$

$$c = c_0 + c_{\pm} \tag{5}$$

$$y_{\pm} = \varphi\left(c_{\pm}; R\right) \tag{6}$$

where $c_{\pm}$, $c_0$ and $c$ are equilibrium concentration of ions, ionic pairs and stoichiometric concentration of electrolyte respectively, $\Lambda_0$ is the limiting molar electrical conductivity, $R$ is the closest approach parameter, $K_A$ is the ionic association constant, $f$ and $\varphi$ are theoretical analytical concentration dependencies of $\Lambda$ and $y_{\pm}$ respectively.

Solving the overfilled system of equations $X\left(\Lambda_0, K_A, R\right)$ comes down to minimization of the sum of squared deviations of experimental electrical conductance ($\Lambda^{exp}$) from respective theoretical values ($\Lambda^{theor}$):

$$Q = \sum_{j=1}^{k} \left[\Lambda_j^{exp} - \Lambda_j^{theor}\left(c_j; X\right)\right]^2 \Rightarrow \min \tag{7}$$

The Debye−Hückel equation was used for the concentration function of activity coefficients:

$$\ln y_{\pm} = -\frac{1}{2}\frac{\beta \kappa_D}{\left(1 + \kappa_D R\right)} \tag{8}$$

The Pethybridge modification [18] of Lee-Wheaton equation [19-21] was used for the concentration dependence of electrical conductance of diluted solutions:

$$\Lambda = \alpha\left\{\Lambda_0\left[1 + C_1 \cdot \left(\beta \kappa_D\right) + C_2 \cdot \left(\beta \kappa_D\right)^2 + C_3 \cdot \left(\beta \kappa_D\right)^3\right] - \right.$$
$$\left. -\frac{\rho \kappa_D}{1 + \kappa_D R}\left[1 + C_4 \cdot \left(\beta \kappa_D\right) + C_5 \cdot \left(\beta \kappa_D\right)^2 + \frac{\kappa_D R}{12}\right]\right\} \tag{9}$$

where $\beta = e^2 \big/ \left(4\pi\varepsilon\varepsilon_0 k_B T\right)$, $\kappa_D^2 = 2N_A e^2 c / 1000\varepsilon_r\varepsilon_0 k_B T$, $\rho = Fe/299.7925 \cdot 3\pi\eta$, $e$ is the elementary charge, $\varepsilon$ and $\eta$ are dielectric permittivity and viscosity of a pure solvent respectively, $\varepsilon_0$ is the vacuum permittivity, $F$ and $N_A$ are Faraday's and Avogadro's constants respectively, $k_B$ is the Boltzmann constant, $T$ is the temperature, $R$ is the closest approach parameter, $c$ is the electrolyte concentration, $C_1 - C_5$ are terms that characterize electrophoretic and relaxation effects [18].

All required density ($d_0$, g cm$^{-3}$), viscosity ($\eta$, mPa s) and dielectric permittivity ($\varepsilon$) values of pure acetonitrile were calculated using equations (10-12) [22]

$$1/d_0 = 1.24446 + 1.6458 \cdot 10^{-3}\left(T - 273.15\right) + 2.92 \cdot 10^{-6}\left(T - 273.15\right)^2 \tag{10}$$

$$\ln\eta = -3.5164 + 620 \cdot T^{-1} + 32500 \cdot T^{-2} \tag{11}$$

$$\varepsilon = -21.06 + 20230 \cdot T^{-1} - 963000 \cdot T^{-2} \tag{12}$$

## Results and Discussion

Processing of experimental conductometric data for solutions of tetraalkylammonium salts in acetonitrile was done with regards to three parameters: limiting molar electrical conductivity ($\Lambda_0$), logarithm of association constant ($\lg K_A$) and the closest approach parameter ($R$). The results are presented in Tables 1 and 2 (option I). Concentration functions of molar electrical conductance of tetraalkylammonium salts in acetonitrile are shown in Figure 1.
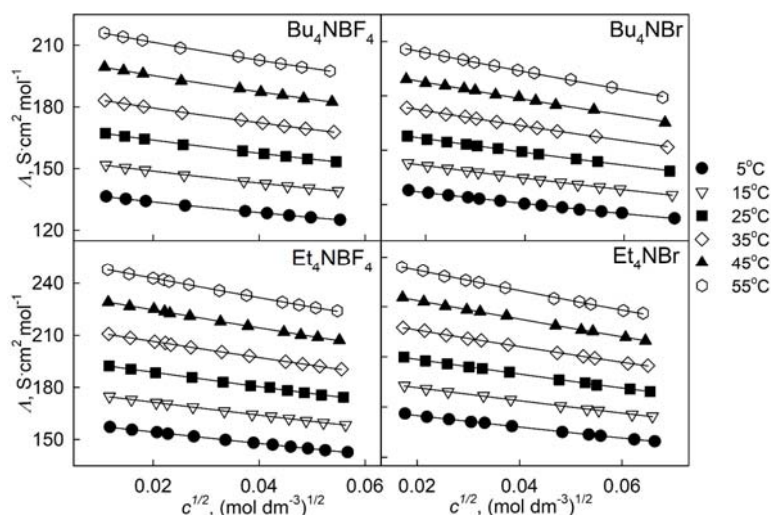


**Figure 1.** Concentration functions of molar electrical conductivity of tetraalkylammonium salts in acetonitrile at different temperatures. Lines on the figure represent theoretical function of electrical conductance, obtained by the f Lee-Wheaton equation.

**Table 1.** Results of conductometric data processing for Bu$_4$NBF$_4$ and Bu$_4$NBr in acetonitrile. $\sigma_\Lambda$ is a dispersion of approximation.

| $t$, °C | Option | $\Lambda_0$, S·cm$^2$·mol$^{-1}$ | $\lg K_A$ | $R$, nm | $\sigma_\Lambda$, S·cm$^2$·mol$^{-1}$ |
|---|---|---|---|---|---|
| | | Bu$_4$NBF$_4$ | | | |
| 5 | I | 139.65±0.08 | 0.3±0.4 | 0.3±0.2 | 0.095 |
| | **II** | **139.57±0.06** | **0.76±0.03** | **0.726** | **0.097** |
| 15 | I | 155.3±0.1 | 0.4±0.5 | 0.4±0.3 | 0.13 |
| | **II** | **155.26±0.08** | **0.77±0.03** | **0.726** | **0.13** |
| 25 | I | 171.1±0.2 | 0.7±0.6 | 0.6±0.7 | 0.18 |
| | **II** | **171.1±0.1** | **0.75±0.04** | **0.726** | **0.16** |
| 35 | I | 187.4±0.2 | 0.7±0.5 | 0.6±0.6 | 0.20 |
| | **II** | **187.4±0.1** | **0.80±0.04** | **0.726** | **0.18** |
| 45 | I | 204.1±0.2 | 0.7±0.5 | 0.5±0.5 | 0.21 |
| | **II** | **204.0±0.1** | **0.84±0.04** | **0.726** | **0.20** |
| 55 | I | 221.1±0.2 | 0.8±0.5 | 0.6±0.7 | 0.25 |
| | **II** | **221.1±0.1** | **0.88±0.04** | **0.726** | **0.24** |
| | | Bu$_4$NBr | | | |
| 5 | I | 131.5±0.2 | 1.54±0.02 | 6.53±0.02 | 0.24 |
| | **II** | **132.55±0.09** | **1.18±0.02** | **0.690** | **0.16** |
| 15 | I | 148.42±0.05 | 1.17±0.01 | 0.4±0.6 | 0.06 |
| | **II** | **148.27±0.05** | **1.222±0.006** | **0.690** | **0.08** |
| 25 | I | 163.5±0.1 | 1.35±0.04 | 1.7±0.4 | 0.12 |
| | **II** | **163.9±0.1** | **1.20±0.01** | **0.690** | **0.16** |
| 35 | I | 179.9±0.02 | 1.36±0.05 | 1.4±0.5 | 0.18 |
| | **II** | **180.2±0.1** | **1.25±0.01** | **0.690** | **0.20** |
| 45 | I | 196.1±0.3 | 1.46±.0.04 | 2.6±0.7 | 0.30 |
| | **II** | **196.8±0.2** | **1.26±0.02** | **0.690** | **0.40** |
| 55 | I | 213.3±0.2 | 1.49±0.02 | 2.8±0.4 | 0.16 |
| | **II** | **214.2±0.2** | **1.31±0.02** | **0.690** | **0.35** |

Analysis of obtained results (Tables 1, 2 – option I) had shown that the closest approach parameter is the least sensible parameter, compared to the limiting molar electrical conductivity and the logarithm of association constant. Values of $R$ were almost independent from the temperature and ranged between 0.3 – 2.8 nm for all studied acetonitrile solutions. This is why, we chose the closest approach parameter as a sum of cation and anion radii ($r(Bu_4N^+)$ = 0.494 nm, $r(Et_4N^+)$ = 0.400 nm, $r(BF_4^-)$ = 0.232 nm, $r(Br^-)$ = 0.196 nm [22]) and to process conductometric data once again, considering the limiting molar electrical conductivity ($\Lambda_0$) and the logarithm of association constant ($\lg K_A$) only as optimized parameters. Obtained data using this approach is shown in Tables 1 and 2 (option II).

It is worth mentioning that obtained values (Table 1, 2) of limiting molar electrical conductivities and respective association constants for $Et_4NBF_4$, $Bu_4NBF_4$, $Bu_4NBr$ in acetonitrile are in good agreement with the data, previously obtained in our laboratory [23-25].

**Table 2.** Results of conductometric data processing for $Et_4NBF_4$ and $Et_4NBr$ in acetonitrile. $\sigma_\Lambda$ is a dispersion of approximation.

| $t$, °C | Option | $\Lambda_0$, S·cm²·mol⁻¹ | $\lg K_A$ | $R$, nm | $\sigma_\Lambda$, S·cm²·mol⁻¹ |
|---|---|---|---|---|---|
| | | $Et_4NBF_4$ | | | |
| 5 | I | 160.99±0.06 | 1.03±0.05 | 0.4±0.01 | 0.07 |
| | **II** | **160.92±0.04** | **1.111±0.008** | **0.632** | **0.07** |
| 15 | I | 178.9±0.1 | 1.1±0.1 | 0.5±0.3 | 0.12 |
| | **II** | **178.89±0.07** | **1.14±0.01** | **0.632** | **0.12** |
| 25 | I | 197.1±0.2 | 1.1±0.1 | 0.4±0.4 | 0.22 |
| | **II** | **197.0±0.1** | **1.15±0.02** | **0.632** | **0.21** |
| 35 | I | 215.8±0.2 | 1.10±0.06 | 0.3±0.2 | 0.18 |
| | **II** | **215.7±0.1** | **1.19±0.01** | **0.632** | **0.18** |
| 45 | I | 234.9±0.2 | 1.12±0.06 | 0.3±0.2 | 0.27 |
| | **II** | **234.8±0.1** | **1.22±0.02** | **0.632** | **0.27** |
| 55 | I | 254.2±0.2 | 1.14±0.05 | 0.3±0.2 | 0.19 |
| | **II** | **254.0±0.1** | **1.22±0.01** | **0.632** | **0.19** |
| | | $Et_4NBr$ | | | |
| 5 | I | 151.6±0.1 | 1.24±0.02 | 0.5±0.1 | 0.17 |
| | **II** | **151.55±0.09** | **1.247±0.008** | **0.596** | **0.16** |
| 15 | I | 169.2±0.2 | 1.26±0.01 | 0.5±0.1 | 0.18 |
| | **II** | **169.1±0.1** | **1.270±0.008** | **0.596** | **0.18** |
| 25 | I | 186.9±0.2 | 1.29±0.01 | 0.6±0.01 | 0.18 |
| | **II** | **186.88±0.09** | **1.291±0.007** | **0.596** | **0.17** |
| 35 | I | 205.5±0.2 | 1.29±0.01 | 0.4±0.1 | 0.23 |
| | **II** | **205.3±0.1** | **1.32±0.01** | **0.596** | **0.23** |
| 45 | I | 224.0±0.2 | 1.37±0.02 | 0.7±0.2 | 0.25 |
| | **II** | **224.1±0.1** | **1.365±0.007** | **0.596** | **0.24** |
| 55 | I | 243.5±0.3 | 1.37±0.01 | 0.5±0.1 | 0.37 |
| | **II** | **243.3±0.2** | **1.38±0.01** | **0.596** | **0.36** |

*Limiting ionic conductance and dynamic of ionic solvation*

Temperature dependences of limiting molar conductivity of $Et_4NBr$, $Et_4NBF_4$, $Bu_4NBr$, $Bu_4NBF_4$ in acetonitrile are shown in Figure 2. The increase in the limiting molar conductance of electrolyte with the increase of the temperature can be explained by the decrease of the solvent viscosity.

Limiting molar conductivities of tetraalkylammonium tetrafluoroborates are greater than limiting molar conductance of tetraalkylammonium bromides for both electrolytes at all temperatures studied. This evidence is a consequence of the fact that bromide ion has smaller radius and greater surface charge that increases solvation interactions, and, as a result, decreases the mobility of bromide ion in contrast to poorly solvated tetrafluoroborate anion.

Comparing limiting molar conductivities of electrolytes with the same anion, electrolyte with a smaller cation ($Et_4NX$) has a greater value of molar conductance.
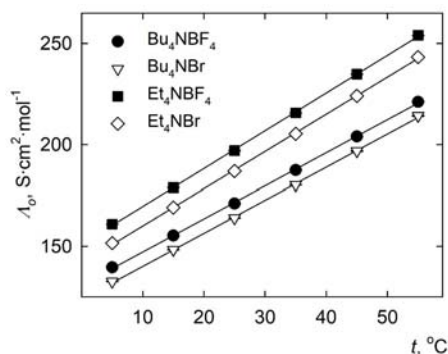
**Figure 2.** Temperature dependence of limiting molar conductivity of tetraalkylammonium salts in acetonitrile.

In order to elucidate the influence of ion on the microscopic structure of the closes molecular environment, the values of limiting ionic conductivities have been studied. The splitting of total limiting molar conductivity on the ionic constituents was done by the following scheme:

$$Bu_4NBPh_4 \begin{cases} \rightarrow BPh_4^- \\ \rightarrow Bu_4N^+ \xrightarrow{Bu_4NBr} Br^- \xrightarrow{Et_4NBr} Et_4N^+ \\ \phantom{\rightarrow Bu_4N^+} \xrightarrow{Bu_4NBF_4} BF_4^- \xrightarrow{Et_4NBF_4} \uparrow \end{cases} \qquad (13)$$
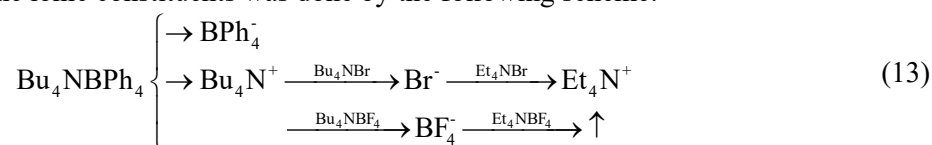
Available literature values of Walden's product for $Bu_4N^+$ and $BPh_4^-$ ions in acetonitrile at 25°C [26] were used to calculate the transference number of tetrabutylammonium cation (14):

$$t^+\left(Bu_4NBPh4\right) = \frac{\lambda_0^+ \cdot \eta}{\lambda_0^+ \cdot \eta + \lambda_0^- \cdot \eta} = \frac{0.2122}{0.2122 + 0.1993} = 0.5157 \qquad (14)$$

Values of $\lambda_0^+\left(Bu_4N^+\right)$ at other temperatures (5, 15, 35, 45 and 55 °C) were calculated by using available in the literature data on the limiting molar conductivities of $Bu_4NBPh_4$ solutions in acetonitrile [27]. The calculation was done using equations (15, 16) assuming independence of transference number $t^+(Bu_4NBPh_4)$ on temperature in non-aqueous solvents [28].

$$\lambda_0^i = t^i \cdot \Lambda_0, \qquad (15)$$

$$\Lambda_0 = \lambda_0^+ + \lambda_0^- \qquad (16)$$

On the next step according to the scheme (13), we have calculated limiting ionic conductivities of for all other ions (Table 3) by using our own experimental conductometric data of total limiting molar conductivities (Tables 1, 2).

In this work two values of limiting ionic conductance of $Et_4N^+$ were obtained: derived from limiting molar conductivity of $Et_4NBF_4$ and $Bu_4NBF_4$ (Table 1, 2). The average values of limiting ionic conductivity of $Et_4N^+$ (the last column of the Table 3) was used for further interpretation.

**Table 3.** Values of limiting molar electrical conductivities of ions in acetonitrile ( $\lambda_0$ , S·cm$^2$·mol$^{-1}$ )

| t, °C | $Bu_4N^+$ | $BPh_4^-$ | $BF_4^-$ | $Br^-$ | $Et_4N^+$ | | |
|---|---|---|---|---|---|---|---|
| | | | | | $(Br^-)$ | $(BF_4^-)$ | average |
| 5 | 50.00 49.82 [27] 49.97 [29] | 46.95 46.91 [27] 46.79 [29] | 89.57 | 82.55 81.80 [27] | 69.00 | 71.35 | 70.18 69.61 [27] 69.51 [29] |
| 15 | 55.83 55.71 [27] 55.70 [29] | 52.43 52.29 [27] 52.31 [29] | 99.43 | 92.44 90.76 [27] | 76.66 | 79.46 | 78.06 77.02 [27] 77.25 [29] |
| 25 | 61.90 61.30–62.3 [16,27,29-30] | 58.13 57.7–58.14 [16,27,29-30] | 109.20 96.8 [27] | 102.00 100.27–101.6 [16,27,29-30] | 84.88 | 87.80 | 86.34 83.7–85.9 [16,27,29-30] |
| 35 | 68.15 66.98 [27] | 64.00 64.73 [27] | 119.25 | 112.05 112.07 [27] | 93.25 | 96.45 | 94.85 91.74 [27] |
| 45 | 74.72 72.87 [27] | 70.17 71.94 [27] | 129.28 | 122.08 121.70 [27] | 102.02 | 105.52 | 103.77 100.11 [27] |
| 55 | 79.07 | 74.25 | 142.03 | 135.13 | 108.17 | 111.97 | 110.07 |

Comparison of $\lambda_0^i$ given in the Table 3 indicate a good agreement of obtained ionic conductivities with the data available in literature. Insignificant deviations might be caused by the different assumptions taken for splitting total molar conductivity on ionic constituents.

Immersion of an ion into the solvent medium leads to the change in the structure of the latter. The most significant deviations occur in the closest environment of an ion. The presence of an ion not only changes the mutual arrangement of the solvent molecules but also their kinetic parameters. The influence of the ion on the dynamic structure of the closest molecular environment can be evaluated using the approach, proposed by Kalugin with co-authors [31-34], which is a further development of the Samoilov's kinetic solvation theory for non-aqueous solutions.

Joint consideration of Hubbard–Onsager dielectric friction theory and Wolynes molecular theory allows to express Hubbard–Onsager's radius ($R_{HO}$) in the following way [31-34]:

$$R_{HO} = \left\{ \frac{(ze\mu_v)^2}{12(4\pi\varepsilon_0 k_B T)^2} \frac{(\varepsilon_\infty + 2)^2}{\varepsilon(2\varepsilon + \varepsilon_\infty)} (g_K \gamma_D)^0 \right\}^{1/4} \tag{17}$$

where $ze$ is the ion charge, $\mu_V$ is the dipole momentum of the solvent molecule in the vacuum, $\varepsilon$, $\varepsilon_\infty$ are static and infinite frequency dielectric permittivity of the solvent molecule respectively, $g_K$ and $\gamma_D$ are Kirkwood and Debye structure-sensitive factors respectively, where zero-index at $(g_K \gamma_D)^0$ refers to the pure solvent. In the expression (17) $(g_K \gamma_D)^0$ product characterizes dynamic structure of the pure solvent. When an ion is immersed in a molecular environment, $g_K \gamma_D$ must undergo significant change, which in its turn will lead to the change of theoretical Hubbard–Onsager radius [35]. Combining the deviation of the effective Hubbard–Onsager radius with the change of the $g_K \gamma_D$ product under the influence of the ion, expression (18) was derived

$$R_{HO}^{ef} = \left\{ \frac{(ze\mu_v)^2}{12(4\pi\varepsilon_0 k_B T)^2} \frac{(\varepsilon_\infty + 2)^2}{\varepsilon(2\varepsilon + \varepsilon_\infty)} (g_K \gamma_D)^{ef} \right\}^{1/4} \tag{18}$$

$(g_K \gamma_D)^{ef}$ value can be obtained from the experimental values of ionic conductivities by equations given in [31].

Therefore, the ratio of $(g_K \gamma_D)^{ef}$ to the corresponding value for the pure solvent can be used as a measure of the ion's influence on the dynamic structure of the closest molecular environment [31-34]:

$$\theta = (g_K \gamma_D)^{ef} / (g_K \gamma_D)^0 \tag{19}$$

Such an approach allows to obtain quantitative parameter ($\theta$) for the closest solvation based on the experimental data of ionic conductivities and physicochemical properties of the pure solvent.

In the framework of the abovementioned approach, we have calculated the values of structure-dynamic parameter $\theta$ for the studied ions in acetonitrile using our own experimental values of ionic conductivities in the temperature range of 5-55°C (Figure 3).
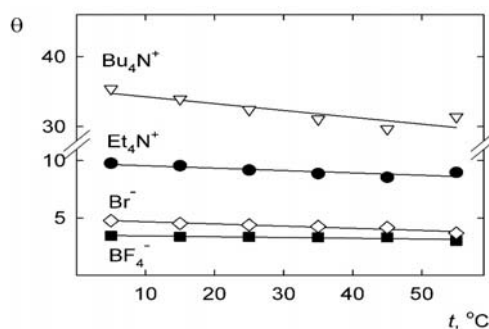


**Figure 3.** Temperature dependence of structure-dynamic parameter $\theta$ for $Bu_4N^+$, $Et_4N^+$, $Br^-$ and $BF_4^-$ in acetonitrile.

In accordance with the Samoilov's kinetic solvation theory [36], ionic solvation parameter $\theta$ is interpreted as a measure of the ion's influence on the dynamic structure of the solvent. Values of $\theta > 1$ correspond to the "structure-making" influence of the ion on the solvent in the closest environment. In the opposite case, values of $\theta < 1$ indicate that ion acts as a "structure-breaker".

Parameter $\theta$ for all investigated ions is positive that corresponds to the structure-making effect of the ion, also referred to as positive solvation. Cations facilitate the increase in vibrational stability of the solvent's structure in the greater extent than anions due to the specific interaction with the closest molecules. Elongation of the alkyl chain from $Et_4N^+$ to $Bu_4N^+$ is accompanied by the significant increase of the $\theta$ parameter, which is an evidence of the dynamic structuring of the solvent molecules around tetrabutylammonium cation and of the amplification of solvophobic solvation of $Bu_4N^+$ cation compared to the $Et_4N^+$.

$BF_4^-$ and $Br^-$ anions strengthen spatio-temporal correlations between solvent molecules in their solvation shells to the less extent when compared to cations. This is characteristic for anions in aprotic solvents due to the absence of specific interactions between solvent molecules and anions.

With the increase of the temperature, the magnitude of the $\theta$ parameter decreases, which is explained by the increase of the relative mobility of particles in the solvent layer.

Obtained results for $\theta$ parameter allow one to formulate the following recommendations regarding the electrolyte choice (both cation and anion) for SCs. Evidently, the less pronounced the effects of positive (solvophilic or solvophobic) solvation are, the higher the limiting molar electrical conductivity of the ion is. Considering values of structure-dynamic parameter $\theta$, optimal electrolytes for SCs should contain polyatomic ions whose diameter range between 0.2 to 0.4 nm.

*Ionic association of tetraalkylammonium salts in acetonitrile*

Electrolytes, studied in this work, just like overwhelming number of other tetraalkylammonium salts in acetonitrile [37], are weakly associated electrolytes (respective association constants do not exceed 20 dm$^3$mol$^{-1}$ at 25°C).

Statistical theory of ionic association states that association constant can be represented as a function of pair potential of interionic interaction $U_{\pm}(r)$ [38]:

$$K_A = \frac{4\pi N_A}{1000} \int_0^\infty r^2 \omega(r) \exp\left( -\frac{U_{\pm}(r)}{k_B T} \right) dr \qquad (20)$$

where $\omega(r)$ is a weight function of the paired state.

Equation (20) allows one to evaluate the value of association constant in terms of concept of simple electrostatic interactions between ions. Here we used Ebeling model to calculate Coulomb association constants [39]:

$$K_A^{Coul}(r) = \frac{4\pi N_A}{1000} \int_x^\infty r^2 w(r) \exp\left( -\frac{U_{\pm}^{Coul}(r)}{k_B T} \right) dr \qquad (21)$$

Coulomb association constants calculated by equation (21) as a function of temperature and experimental association constants of studied tetraalkylammonium salts in acetonitrile are shown on Figure 4.
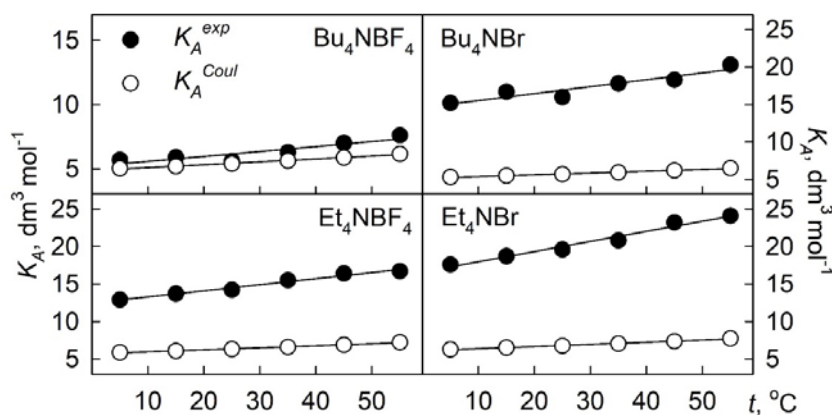


**Figure 4.** Experimental values of association constants and respective Coulomb contribution for studied tetraalkylammonium salts in acetonitrile.

Figure 4 clearly demonstrates that only association of tetrabutylammonium tetrafluoroborate is almost completely caused by the Coulomb interaction. For all other tetraalkylammonium salts in acetonitrile, solvation effects contribute to the association to the greater extent than Coulomb attraction. Solvation effects can be evaluated having reviewed the structure of paired interionic potential in more detail.

The adequate representation of the ion-ion interaction potential is a central point in the statistical description of electrolyte solutions at the McMillan-Mayer level [40]. Definite progress has been achieved in describing the long-range electrostatic interactions. Taking into account the non-electrostatic ion-ion interactions, which are manifested at short distances primarily as a consequence of the discrete structure of the solvent and strong ion-molecule interactions, is a more difficult task. One of the simplest ways used to describe non-electrostatic short-range ion-ion interactions is to add the square-mound potential $d_\pm = const$ with a radius of action from $a$ to $R'$ to the electrostatic potential $U^{Coul}$ [40]:

$$U_\pm(r) = \begin{cases} \infty, & r < a, \\ U^{Coul}(r) + d_\pm, & a < r < R', \\ U^{Coul}(r), & r > R'. \end{cases} \tag{22}$$

Here, the hard-core diameter $a = r_i + r_j$ is the sum of the ion crystallographic or structural radii. The distance $R'$ is calculated as $R' = a + nS$, where $S$ is the diameter of a solvent molecule or its functional group. $nS$ is the thickness of the first solvation shell.

Taking into account the expression (22), equation (20) can be expressed as:

$$K_A = \frac{4\pi N_A}{1000}\left\{ \exp\left(-\frac{d_\pm}{k_B T}\right)\left[ K_A^{Coul}(a) - K_A^{Coul}(R') \right] + K_A^{Coul}(R') \right\} \tag{23}$$

This equation allows one to evaluate $d_\pm$ values having experimental data on association constants and theoretical estimation for Coulomb association constants, for example by equation (21). The calculated in this way values of non-Coulomb short-range potential $d_\pm$ for tetraalkylammonium salts in acetonitrile are shown on Figure 5. The values of the radii of the ions were taken from [41]. The upper boundary of action of the non-electrostatic potential $R'$ was determined, as in the original paper by Rasaiah and Friedman [40], from the relation $R' = a + S$. The diameter of the AN molecule was calculated from the molar volume of the solvent.
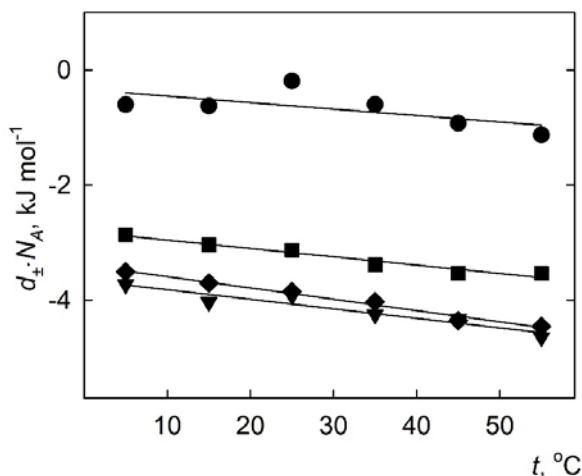


**Figure 5.** Short-range non-Coulomb potentials $d_\pm \cdot N_A$ (in molar scale) for Bu$_4$NBF$_4$(●), Bu$_4$NBr(▼), Et$_4$NBF$_4$(■), Et$_4$NBr(♦) in acetonitrile as a function of temperature.

Negative values of $d_\pm \cdot N_A$ product (Figure 5) for all studied tetraalkylammonium salts in acetonitrile testify additional attraction between ions in ionic pair due to solvation effects, which leads the equilibrium $Kt^+ + An^- \rightleftarrows \left[ Kt^+ An^- \right]$ to be shifted towards the ionic pair formation.

It is also worth mentioning that $d_{\pm} \cdot N_A$ value for Bu$_4$NBF$_4$ tends to 0 and is significantly less by the absolute value, compared to other studied electrolytes. This proves the insignificance of contribution of the solvation effects to the ionic association for tetrabutylammonium tetrafluoroborate.

Desolvation with the increase of the temperature causes the absolute value of $d_{\pm} \cdot N_A$ product to decrease for all studied electrolytes.

Considering proximity of $K_A^{Coul}$ values for all tetraalkylammonium salts in acetonitrile, an increase of experimental values of association constants in sequence Bu$_4$NBF$_4$<Et$_4$NBF$_4$<Bu$_4$NBr<Et$_4$NBr is defined by the increase of solvation interactions.

Based on the analysis of obtained experimental data about the association constants of tetraalkylammonium salts, as well as different contributions to these values, the most promising from the practical point of view combination of cation and anion for the SCs electrolyte should provide minimal value of $K_A^{Coul}$ and the absence of negative values of $d_{\pm} \cdot N_A$ product.

## Conclusions

In this study it was found that tetraalkylammonium salts in acetonitrile are weakly associated electrolytes. An increase in ion association constants in the sequence Bu$_4$NBF$_4$<Et$_4$NBF$_4$<Bu$_4$NBr<Et$_4$NBr is caused by the increase in the contribution of short-range ion-molecular interactions into interionic attraction in addition to the electrostatic constituent. An increase of the temperature amplifies the ionic association with regards to both electrostatic and short-range constituents.

The highest values of limiting ionic conductivity in acetonitrile were observed for polyatomic ions with the radius ranging from 0.2 to 0.4 nm that are not inclined to the positive solvophilic or solvophobic solvation. Analysis of structure-dynamic characteristics of ion-molecular interactions in solutions studied had shown that the increase in polyatomic ions radii leads to the decrease of the limiting ionic conductivity due to viscosity constituent and magnification of solvophobic solvation. Influence of the temperature on the limiting ionic conductivity is mainly caused by the change of the solvent's viscosity.

## Acknowledgements

## Appendix A

**Table A1.** Primary experimental data of electrical conductivity of tetraalkylammonium salts in acetonitrile

| # | $\tilde{m} \cdot 10^4$, mol kg$^{-1}$ | $\kappa \cdot 10^5$, S cm$^{-1}$ | | | | | |
|---|---|---|---|---|---|---|---|
| | | 5ºC | 15ºC | 25ºC | 35ºC | 45ºC | 55ºC |
| | | | | Bu$_4$NBF$_4$ | | | |
| 1 | 1.5634 | 1.7055 | 1.8718 | 2.0331 | 2.1966 | 2.3565 | 2.5164 |
| 2 | 2.7671 | 2.9902 | 3.2811 | 3.5651 | 3.8499 | 4.132 | 4.4114 |
| 3 | 4.3503 | 4.6626 | 5.1161 | 5.5612 | 6.0067 | 6.4451 | 6.882 |
| 4 | 6.1343 | 6.5047 | 7.1453 | 7.7661 | 8.3827 | 9.0004 | 9.6084 |
| 5 | 7.7893 | 8.282 | 9.0995 | 9.8932 | 10.682 | 11.466 | 12.238 |
| 6 | 8.4956 | 8.954 | 9.8256 | 10.674 | 11.527 | 12.363 | 13.196 |
| 7 | 10.18 | 10.734 | 11.787 | 12.805 | 13.821 | 14.83 | 15.83 |
| 8 | 12.343 | 12.923 | 14.183 | 15.412 | 16.643 | 17.856 | 19.054 |
| 9 | 17.518 | 18.083 | 19.862 | 21.596 | 23.314 | 24.999 | 26.687 |
| 10 | 21.585 | 22.114 | 24.258 | 26.379 | 28.474 | 30.523 | 32.582 |
| 11 | 26.149 | 26.564 | 29.142 | 31.684 | 34.194 | 36.677 | 39.128 |
| 12 | 31.052 | 31.311 | 34.366 | 37.332 | 40.299 | 43.182 | 46.08 |
| 13 | 38.28 | 38.244 | 41.966 | 45.619 | 49.224 | 52.764 | 56.281 |

| | | | Bu$_4$NBr | | | |
|---|---|---|---|---|---|---|
| 1 | 1.959 | 0.20333 | 0.22461 | 0.24205 | 0.26485 | 0.2832 | 0.30393 |
| 2 | 3.4194 | 0.34967 | 0.38537 | 0.41982 | 0.45494 | 0.48935 | 0.52443 |
| 3 | 5.2692 | 0.53241 | 0.58709 | 0.63903 | 0.69317 | 0.7452 | 0.79955 |
| 4 | 7.5503 | 0.75454 | 0.83225 | 0.9071 | 0.98286 | 1.06e-4 | 1.14e-4 |
| 5 | 9.3915 | 0.93532 | 1.0324 | 1.1257 | 1.2186 | 1.3136 | 1.4077 |
| 6 | 10.185 | 1.0079 | 1.1119 | 1.2136 | 1.315 | 1.4162 | 1.5167 |
| 7 | 11.882 | 1.1683 | 1.289 | 1.4064 | 1.5245 | 1.6422 | 1.7565 |
| 8 | 15.377 | 1.4979 | 1.6518 | 1.803 | 1.9508 | 2.0983 | 2.2521 |
| 9 | 19.94 | 1.9163 | 2.1151 | 2.311 | 2.5055 | 2.6999 | 2.8825 |
| 10 | 23.536 | 2.2442 | 2.4747 | 2.7041 | 2.9274 | 3.1522 | 3.3774 |
| 11 | 28.276 | 2.6725 | 2.9428 | 3.2061 | 3.4741 | 3.7376 | 4.0221 |
| 12 | 32.574 | 3.0462 | 3.3595 | 3.6727 | 3.9934 | 4.3029 | 4.5842 |
| 13 | 38.474 | 3.5678 | 3.9303 | 4.2956 | 4.6468 | 5.0074 | 5.4162 |
| 14 | 44.464 | 4.0932 | 4.4965 | 4.9457 | 5.3597 | 5.7442 | 6.1168 |
| 15 | 61.651 | 5.5303 | 6.0855 | 6.633 | 7.1706 | 7.6962 | 8.2242 |
| 16 | 84.613 | 6.3652 | 6.9969 | 7.7049 | 8.3311 | 9.0111 | 9.6258 |
| 17 | 94.926 | 6.9463 | 7.6352 | 8.4075 | 9.1062 | 9.7474 | 10.457 |

| | | | Et$_4$NBF$_4$ | | | |
|---|---|---|---|---|---|---|
| 1 | 1.7677 | 2.2222 | 2.4374 | 2.6474 | 2.8589 | 3.0638 | 3.2698 |
| 2 | 3.2196 | 4.0044 | 4.3898 | 4.768 | 5.1475 | 5.5175 | 5.8869 |
| 3 | 5.3899 | 6.6374 | 7.2713 | 7.895 | 8.5198 | 9.1659 | 9.7483 |
| 4 | 6.52 | 7.9853 | 8.7626 | – | 10.275 | 11.021 | 11.752 |
| 5 | 7.1265 | 8.6922 | 9.5307 | 10.352 | 11.173 | 11.983 | 12.788 |
| 6 | 9.6307 | 11.674 | 12.8 | 13.901 | 14.985 | 16.08 | 17.152 |
| 7 | 14.205 | 16.988 | 18.612 | 20.206 | 21.813 | 2.37 | 24.93 |
| 8 | 19.026 | 22.501 | 24.653 | 26.758 | 28.886 | 30.945 | 33.007 |
| 9 | 22.713 | 26.666 | 29.241 | 31.781 | 34.294 | 36.733 | 39.16 |
| 10 | 26.473 | 30.828 | 33.809 | 36.648 | 39.51 | 42.353 | 45.139 |
| 11 | 30.36 | 35.126 | 38.448 | 41.725 | 44.985 | 48.193 | 51.405 |
| 12 | 34.528 | 39.646 | 43.433 | 47.131 | 50.83 | 54.459 | 58.045 |
| 13 | 40.299 | 45.926 | 50.285 | 54.612 | 58.809 | 63.054 | 67.221 |

| | | | Et$_4$NBr | | | |
|---|---|---|---|---|---|---|
| 1 | 0.22467 | 0.26543 | 0.29314 | 0.31753 | 0.34454 | 0.37152 | 0.3966 |
| 2 | 0.39048 | 0.45555 | 0.50102 | 0.54601 | 0.59086 | 0.63574 | 0.68091 |
| 3 | 0.60217 | 0.6931 | 0.76272 | 0.83122 | 0.90327 | 0.96886 | 1.0388 |
| 4 | 0.86235 | 0.98217 | 1.0811 | 1.1783 | 1.2748 | 1.3701 | 1.4651 |
| 5 | 1.016 | 1.1586 | 1.2744 | 1.3885 | 1.5024 | 1.6116 | 1.727 |
| 6 | 1.1692 | 1.3171 | 1.4418 | 1.5811 | 1.7095 | 1.8377 | 1.9652 |
| 7 | 1.3816 | 1.5504 | 1.7055 | 1.8571 | 2.0093 | 2.1593 | 2.3099 |
| 8 | 1.8607 | 2.0589 | 2.2637 | 2.4708 | 2.6691 | 2.8748 | 3.0656 |
| 9 | 2.365 | 2.6108 | 2.872 | 3.1175 | 3.3797 | 3.6352 | 3.8762 |
| 10 | 2.9285 | 3.1588 | 3.4729 | 3.7825 | 4.0918 | 4.3931 | 4.6843 |
| 11 | 3.5883 | 3.8274 | 4.2029 | 4.5869 | 4.9575 | 5.3103 | 5.6885 |
| 12 | 3.906 | 4.1419 | 4.553 | 4.9534 | 5.3644 | 5.7584 | 6.1533 |
| 13 | 4.3646 | 4.6063 | 5.0654 | 5.5266 | 5.9654 | 6.3929 | 6.8319 |
| 14 | 4.8782 | 5.0903 | 5.5915 | 6.0946 | 6.5803 | 7.0623 | 7.5416 |
| 15 | 5.5218 | 5.7124 | 6.2855 | 6.8356 | 7.3954 | 7.9095 | 8.4709 |
| 16 | 7.498 | 7.5737 | 8.3183 | 9.0379 | 9.7729 | 10.451 | 11.172 |
| 17 | 9.8372 | 9.6683 | 1.0617 | 11.561 | 12.426 | 13.341 | 14.255 |

**References**

1. Kurniawan A., Ong L. K., Kurniawan F., Lin C. X., Soetaredjo F. E., Zhao X. S., Ismadji S. Easy approach to synthesize N/P/K co-doped porous carbon microfibers from cane molasses as a high performance supercapacitor electrode material. *RSC Adv.* **2014,** *4* (66), 34739-34750.

2. Laheäär A., Peikolainen A.-L., Koel M., Jänes A., Lust E. Comparison of carbon aerogel and carbide-derived carbon as electrode materials for non-aqueous supercapacitors with high performance. *J. Solid State Electrochem.* **2012,** *16*.

3. Morimoto T., Tsushima M., Suhara M., Hiratsuka K., Sanada Y., Kawasato T. Electric Double- Layer Capacitor using Organic Electrolyte. *Mat. Res. Soc. Symp. Proc.* **2011,** *496* 627.

4. Hung K., Masarapu C., Ko T., Wei B. Wide-temperature range operation supercapacitors from nanostructured activated carbon fabric. *J. Power Sources* **2009,** *193* (2), 944-949.

5. Cazorla-Amorós D., Lozano-Castelló D., Morallón E., Bleda-Martínez M. J., Linares-Solano A., Shiraishi S. Measuring cycle efficiency and capacitance of chemically activated carbons in propylene carbonate. *Carbon* **2010,** *48* (5), 1451-1456.

6. Brandt A., Pohlmann S., Varzi A., Balducci A., Passerini S. Ionic liquids in supercapacitors. *MRS Bull.* **2013,** *38* (7), 554-559.

7. Senda A., Matsumoto K., Nohira T., Hagiwara R. Effects of the cationic structures of fluorohydrogenate ionic liquid electrolytes on the electric double layer capacitance. *J. Power Sources* **2010,** *195* (13), 4414-4417.

8. Ue M. Electrochemical Properties of Organic Liquid Electrolytes Based on Quaternary Onium Salts for Electrical Double-Layer Capacitors. *J. Electrochem. Soc.* **1994,** *141* (11), 2989.

9. Wang Y., Song Y., Xia Y. Electrochemical capacitors: mechanism, materials, systems, characterization and applications. *Chem. Soc. Rev.* **2016,** *45* (21), 5925-5950.

10. Das B., Saha N., Hazra D. K. Ionic Association and Conductances of Some Symmetrical Tetraalkylammonium Salts in Methanol, Acetonitrile, and Methanol (1) + Acetonitrile (2) Mixtures at 298.15 K. *J. Chem. Eng. Data* **2000,** *45* (2), 353-357.

11. Anand H., Verma R. Solvation of Some Tetraalkylammonium Salts Investigated Conductometrically and Viscometrically in Binary Mixtures of Acetonitrile + Methanol at 298.15 K. *Z. Phys. Chem.* **2015,** *230*.

12. Patil P. P., Tiwari S. Effect of blockage ratio on wake transition for flow past square cylinder. *Fluid Dyn. Res.* **2008,** *40* (11), 753-778.

13. Wypych-Stasiewicz A., Benko J., Vollǎrovǎ O., Bald A. Conductance studies of $Et_4NIO_4$, $Et_4NClO_4$, $Bu_4NI$, $Et_4NI$ and the limiting ionic conductance in water+acetonitrile mixtures at 298.15K. *J. Mol. Liq.* **2014,** *190* 54-58.

14. Mysyk R., Gao Q., Raymundo-Piñero E., Béguin F. Microporous carbons finely-tuned by cyclic high-pressure low-temperature oxidation and their use in electrochemical capacitors. *Carbon* **2012,** *50* (9), 3367-3374.

15. Riddick J. A., Bunger W. B., Sakano T. K. *Organic solvents: physical properties and methods of purification. Fourth edition*. John Wiley and Sons,New York, NY: United States, 1986.

16. Harkness A. C., Daggett Jr H. M. The Electrical Conductivities of some tetra-n-alkylammonium salts in acetonitrile. *Can. J. Chem.* **1965,** *43* (5), 1215-1221.

17. Kalugin O. N., Vjunnik I. N. Some issues of conductometric data processing. Existing Electrolyte Options. *Russ. J. Gen. Chem.* **1989,** *59* (7), 1213-1216.

18. Pethybridge A. D., Talbot J., House W. A. Precise Conductance Measurements on Dilute Aqueous Solutions of Sodium and Potassium Hydrogenphosphate and Dihydrogenphosphate. *J. Solution Chem.* **2006,** *35* 381-393.

19. Lee W. H., Wheaton R. J. Conductance of symmetrical, unsymmetrical and mixed electrolytes. Part 1.—Relaxation terms. *J. Chem. Soc., Faraday Trans. 2* **1978,** *74* (0), 743-766.

20. Lee W. H., Wheaton R. J. Conductance of symmetrical, unsymmetrical and mixed electrolytes. Part 2.—Hydrodynamic terms and complete conductance equation. *J. Chem. Soc., Faraday Trans. 2* **1978,** *74* (0), 1456-1482.

21. Lee W. H., Wheaton R. J. Conductance of symmetrical, unsymmetrical and mixed electrolytes. Part 3. - Examination of new model and analysis of data for symmetrical electrolytes. *J. Chem. Soc., Faraday Trans. 2* **1979,** *75* 1128-1145.

22. Barthel J., Wachter R., Gores H. J. Temperature Dependence of Conductance of Electrolytes in Nonaqueous Solutions. In *Modern Aspects of Electrochemistry: No. 13*, Conway, B. E.; Bockris, J. O. M., Eds. Springer US: Boston, MA, 1979; pp 1-79.

23. Lukinova E. V., Kalugin O. N., Novikova A. J. Solutions of $Et_4NBF_4$ in acetonitrile from the standpoint of the quasilattice model: NMR and conductometry studies. *Kharkov Univ. Bull. Chem. Ser.* **2005,** *12(35)* (648), 177-180.

24. Lukinova E. V., Ivanova A. A., Kalugin O. N. Concentrated solutions of $Bu_4NBF_4$ in acetonitrile as model electrolytes for supercapacitors: problems and prospects of a theoretical description. *Sci. Bull. Chernivtsi Nat. Univ. Chem.* **2008,** *399-400* 116-118.

25. Lukinova E. V., Kalugin O. N. Electrical conductivity of solutions of $Bu_4NBr$ in acetonitrile in a wide range of concentrations. *Kharkov Univ. Bull. Chem. Ser.* **2009,** *17(40)* (870), 178-184.

26. Krumgalz B. Separation of limiting equivalent conductances into ionic contributions in non-aqueous solutions by indirect methods. *J. Chem. Soc., Faraday Trans. 1* **1983,** *79*.

27. Safonova L. P., Pasasia, B. K., Kolker, A. M. Electrical conductivity of individual ions and their association in acetonitrile at 233-318 K. *Russ. J. Phys. Chem.* **1992,** *66* (8), 2201-2208.

28. Krumgalz B., Fleisher Z. Comments on Gill's approach to the evaluation of single limiting ionic conductances in organic solvents. *J. Chem. Soc., Faraday Trans. 1* **1985,** *81*.

29. Barthel J., Iberl L., Rossmaier J., Gores H. J., Kaukal B. Conductance of 1,1-electrolytes in acetonitrile solutions from −40° to 35°C. *J. Solution Chem.* **1990,** *19* (4), 321-337.

30. Tsierkezos N. G., Philippopoulos A. I. Studies of ion solvation and ion association of n-tetrabutylammonium hexafluorophosphate and n-tetrabutylammonium tetraphenylborate in various solvents. *Fluid Phase Equilib.* **2009,** *277* (1), 20-28.

31. Kalugin O. N., Vjunnik I. N. Limiting ion conductance and dynamic structure of the solvent in electrolyte solution. *Zh. Khim. Fiz. (Rus.)* **1991,** *10* 708-714.

32. Kalugin O. N., Vjunnik I. N., Nur-Eddin I. Interparticle interactions in 1-1 electrolyte solutions in dimethylsulfoxide. II. Limiting molar conductance of ions and dynamic structure of solvent. *Russ. J. Struct. Chem.* **1992,** *33* 105-114.

33. Lebed A. V., Kalugin O. N., Vjunnik I. N. Properties of 1-1 Electrolytes Solutions in Ethylene Glycol at Temperatures from 5 to 175oC. II. Limiting ion conductances and Ion-Molecular Interactions. *J. Chem. Soc., Faraday Trans. 2* **1998,** *94* (15), 2103-2107.

34. Kalugin O. N. Dynamics of solvated ion in infinitely diluted solution: from phenomenology to microscopic description. *Kharkov Univ. Bull. Chem. Ser.* **2002,** *9* (573), 13-45.

35. Zhang H., Wang J., Chen Y., Wang Z., Wang S. Long-term cycling stability of polyaniline on graphite electrodes used for supercapacitors. *Electrochim. Acta* **2013,** *105* 69-74.

36. Samoilov O. Y. *Stucture of water solutions of electrolytes and hydration of ions*. Nauka, 1957; p 183.

37. Barthel J., Kunz W. Vapor pressure data for non-aqueous electrolyte solutions. Part 5. Tetraalkylammonium salts in acetonitrile. *J. Solution Chem.* **1988,** *17* (5), 399-415.

38. Vjunnik I. N., Kalugin O. N., Gubskiy S. M. Non-Coulombic parameters of interparticle interactions in non-aqueous solutions of 1-1 electrolytes in a wide temperature range. *Kharkov Univ. Bull. Chem. Ser.* **1993,** *377* 15-30.

39. Ebeling W. Theorie der Bjerrumschen Ionenassoziation in Elektrolyten. *Z. Phys. Chem.* **1968,** *238* (5/6), 400-408.

40. Rasaiah J. C., Friedman H. L. Charged square-well model for ionic solutions. *J. Phys. Chem.* **1968,** *72* (9), 3352-3353.

41. Barthel, J.; Gores, H. J.; Hess, P.; Kniep, R.; Rabenau, A.; Schmeer, G.; Wachter, R., *Physical and Inorganic Chemistry*. Springer-Verlag Berlin Heidelberg: 1983; Vol. 111, p VII, 196.

О.Н. Калугин, Е.В. Лукинова, Д.О. Новиков. Электрическая проводимость, ион-молекулярная ассоциация и межионные взаимодействия в растворах некоторых тетраалкиламмониевых солей в ацетонитриле: влияние иона и температуры.

Харьковский национальный университет имени В.Н. Каразина, химический факультет, кафедра неорганической химии, пл. Свободы, 4, Харьков, 61022, Украина

В работе представлены экспериментальные данные по электрической проводимости растворов $Et_4NBr$, $Et_4NBF_4$, $Bu_4NBr$, $Bu_4NBF_4$ в ацетонитриле в интервале концентраций $2 \cdot 10^{-4} – 1 \cdot 10^{-2}$ моль·дм$^{-3}$ при температурах 5 - 55 °C. Предельные молярные электропроводности и константы ионной ассоциации рассчитаны с использованием уравнения Ли-Уитона для симметричных электролитов. На основании предварительного анализа кондуктометрических данных было установлено, что параметр наибольшего сближения практически не зависит от температуры для всех исследованных ацетонитрильных растворов. Поэтому параметр наибольшего сближения был принят как сумма радиусов катионов и анионов для дальнейшей обработки кондуктометрических данных.

Значения предельных ионных проводимостей $Br^-$, $BF_4^-$, $Et_4N^+$ та $Bu_4N^+$, а также структурно-динамического параметра ион-молекулярного взаимодействия, полученные по экспериментальным предельным молярным проводимостям, были интерпретированы в рамках предложенного авторами подхода [Kalugin O. N., Vjunnik I. N. Limiting ion conductance and dynamic structure of the solvent in electrolyte solution. *Zh. Khim. Fiz. (Rus.)* **1991,** *10* 708-714]. Установлено что удлинение алкильного радикала в катионе $Bu_4N^+$ по сравнению с $Et_4N^+$ приводит к значительному увеличению структурно-динамического параметра, что свидетельствует о динамическом структурировании молекул растворителя возле иона тетрабутиламмония и увеличении сольвофобной сольватации $Bu_4N^+$ в сравнении с $Et_4N^+$.

Константы ионной ассоциации обсуждены с позиции конкуренции между электростатическими и некулоновскими силами с использованием короткодействующего некулоновского потенциала. Увеличение констант ионной ассоциации в ряду $Bu_4NBF_4 < Et_4NBF_4 < Bu_4NBr < Et_4NBr$ объясняется увеличением вклада короткодействующих ион-молекулярных взаимодействий в межионное притяжение в дополнение к электростатической составляющей. Увеличение температуры усиливает ионную ассоциацию благодаря как электростатической, так и короткодействующей составляющей.

**Ключевые слова:** бромид тетраэтиламмония, бромид тетрабутиламмония, тетрафтороборат тетраэтиламмония, тетрафтороборат тетрабутиламмония, ацетонитрил, электрическая проводимость, константа ионной ассоциации, предельная молярная электрическая проводимость, короткодействующий межионный потенциал, микродинамика ионной сольватации.

О.М. Калугін, Е.В. Лукінова, Д.О. Новіков. Електрична провідність, йон-молекулярна ассоціація та міжйонні взаємодії у розчинах деяких тетралкіламмонієвих солей в ацетонітрилі: вплив йона та температури.

Харківський національний університет імені В.Н. Каразіна, хімічний факультет, кафедра неорганічної хімії, майдан Свободи, 4, Харків, 61022, Україна

В роботі наведені експериментальні дані з електричної провідності розчинів $Et_4NBr$, $Et_4NBF_4$, $Bu_4NBr$, $Bu_4NBF_4$ в ацетонітрилі в інтервалі молярної концентрації $2 \cdot 10^{-4} – 1 \cdot 10^{-2}$ моль·дм$^{-3}$ при температурах 5 - 55 °C. Граничні молярні електропровідності та константи іонної асоціації розраховані за допомогою рівняння Лі-Вітона для симетричних елетролітів. На підставі попереднього аналізу кондуктометричних даних було встановлено, що параметр найбільшого зближення практично не залежить від температури для всіх досліджених ацетонітрильних розчинів. Тому параметр найбільшого зближення був прийнятий як сума радіусів катіонів і аніонів для подальшої обробки кондуктометричних даних.

Значення граничних іонних провідностей $Br^-$, $BF_4^-$, $Et_4N^+$ та $Bu_4N^+$, а також структурно-динамічного параметра йон-молекулярної взаємодії, що були отримані за експериментальними граничними молярними електропровідностями, були інтерпретовані в рамках підхода, запропонованого авторами [Kalugin O. N., Vjunnik I. N. Limiting ion conductance and dynamic structure of the solvent in electrolyte solution. *Zh. Khim. Fiz. (Rus.)* **1991,** *10* 708-714]. Встановлено що подовження алкільного радикалу в катіоні $Bu_4N^+$ порівняно з $Et_4N^+$ веде до значного зростанням структурно-динамічного параметра, що свідчить про динамічне структурування молекул розчинника біля йону тетрабутиламмонія та збільшенням сольвофобної сольватації $Bu_4N^+$ у порівнянні з $Et_4N^+$.

Константи іонної асоціації обговорені з позицій конкуренції між електростатичними та некулонівськими силами за допомогою короткодіючого некулонівського потенціала. Збільшення значень констант іонної асоціації у ряду $Bu_4NBF_4 < Et_4NBF_4 < Bu_4NBr < Et_4NBr$ пояснюється збільшенням внеску короткодіючих іон-молекулярних взаємодій в міжйонне притяжіння на додаток до електростатичної складової. Було встановлено, що збільшення температури посилює йонну ассоціацію завдяки як електростатичній, так і короткодіючій складовій.

**Ключові слова:** тетраетиламмоній бромід, тетрабутиламмоній бромід, тетраетиламмоній тетрафлуороборат, тетрабутиламмоній тетрафлуороборат, ацетонітрил, електрична провідність, константа йонної асоціації, гранична молярна електрична провідність, короткодіючий міжйонний потенціал, мікродинаміка йонної сольватації.

УДК 541.135

# FORCE FIELD OF TETRAFLUOROBORATE ANION
# FOR MOLECULAR DYNAMICS SIMULATION: A NEW APPROACH

## I.S. Vovchynskyi [a], O.N. Kalugin [b]

*V.N. Karazin Kharkiv National University, School of Chemistry, Department of Inorganic Chemistry, Svobody sq.,4, Kharkiv, 61022, Ukraine*

a) ✉ *vovchinsky7898@gmail.com*      ⓘ *https://orcid.org/0000-0002-3509-2385*
b) ✉ *onkalugin@gmail.com*      ⓘ *https://orcid.org/0000-0003-3273-9259*

Design of new electrical energy storage devices including supercapacitors as well as an optimization of existing ones require not only new electrolytes, but also the deep and complete understanding of the processes occurring in the electrolyte solutions. Spectral techniques and classical molecular dynamics simulation (MDS) have gained a reputation as a reliable tool for such tasks. The starting point of any MDS is a choice or development of the force fields for all simulated particles. The combination of vibrational spectroscopy and molecular dynamics technique can provide a thorough understanding of the structure and dynamics of the ionic subsystem. In this connection, the reproduction of the vibrational spectra should be added to the requirements for the force fields of the most common electrolyte components.

Many modern supercapacitors are based on organic electrolytes consisting of non-aqueous aprotic solvents such as acetonitrile, propylene carbonate and γ-butyrolactone and quaternary ammonium salts with tetrafluoroborate and hexafluorophosphate as anions.

The purpose of the current work is to develop a new force field for tetrafluoroborate anion ($BF_4^-$) able to reproduce not only translational diffusion in acetonitrile medium, but also the spectral properties of this ion in a condensed phase. Since found in the literature force fields of $BF_4^-$, cannot satisfy these requirements, there were performed intensive quantum chemical calculations of $BF_4^-$ at the M06-2X/6-311++G(d,p) level of theory to construct the potential energy surface with respect to the B-F bonds and F-B-F angles followed by evaluating corresponding intramolecular potential constants. Combining the obtained bond and angle force constants with partial charges on B and F atoms calculated at the same level of theory, and literature values of Lennard-Jones parameters, a new force field model for $BF_4^-$ anion was created. Based on the carried out MD simulations of the $BF_4^-$ ion in an infinitely diluted acetonitrile solution, it was proved that the obtained resulting model is capable to reproduce both transport and intra-ion vibrational properties of the tetrafluoroborate anion.

**Keywords:** tetrafluoroborate anion, vibrational spectrum, molecular dynamics simulation, diffusion coefficient.

## Introduction

Rapid technology increase, necessity of finding an alternative to non-renewable resources stimulated the development of new devices for storing electric energy. Supercapacitors are one of such kind devices [1-2]. Supercapacitors have several advantages such as big power density, fast charging / discharging time, long lifetime etc. In the same time they have several ways to improve its technical characteristics first of all capacitance and service voltage. Capacity and power density depends on containing electrolyte [1], therefore deep understanding of undergoing processes in electrolyte medium and interaction mechanism between solution components are the keys to successful development of new, more effective devices.

Spectral methods have proven to be a reliable tool for studying ion-molecular systems [3-6], but, like many experimental methods, for a comprehensive understanding obtained result, they need to involve computational methods, such as classical molecular dynamics simulation (MDS) [7-8]. Therefore, the development of electrolyte component force fields capable of accurately reproducing spectral properties is an important task of modern electrochemistry. Being a component of a number of electrolytes for supercapacitors [1], tetrafluoroborate anion ($BF_4^-$) can be called one of the most priority candidates for developing such a force field.

A significant part of the manufactured supercapacitors offer devices with organic solvents, mainly with propylene carbonate or acetonitrile [1]. High demand for acetonitrile (AN) as a supercapacitor component is a reason of choice this substance as a solvent of investigated systems.

Based on the foregoing, the goal of this work was to create a model of the tetrafluoroborate anion force field, able to reproduces the spectral and dynamic properties of this ion in acetonitrile.

To achieve this goal, first we reviewed existing approaches to modeling tetrafluoroborate anion as a component of an electrolyte solution (Section 1). Since classical MD simulation requires an information about the equilibrium structure and atomic partial charges for any multiatomic particle, the corresponding parameters were obtained by quantum chemical calculations as well as the vibrational spectrum of $BF_4^-$ in vacuum (section 2). In the Section 3 the details of the MD simulations are described along with the results of simulation of $BF_4^-$ vibrational spectra for the most common models in the literature. Section 4 presents the results of the potential energy surface (PES) scanning of B-F bonds and the angles of F-B-F followed by evaluation of the corresponding intramolecular potential constants. Finally, in the section 5 the validation of the developed force field of tetrafluoroborate anion is presented based on the anion diffusion coefficient in the infinitely diluted acetonitrile solution.

## 1. Various approaches to modeling $BF_4^-$ in classical molecular dynamics modeling

Several approaches of modeling tetrafluoroborate anion were found in the literature: "coarse grain" (CG) models [9-11], polarizable models [9, 12], rigid models [13-16], all-atom soft models [17-26].

CG anion of tetrafluoroborate is one particle with a total mass of five atoms and the corresponding charge. The advantage of such models is a significant saving computational resources, which allows to compute larger systems and longer phase trajectories. On the other hand, within the framework of CG approach a detailed study of ionic subsystem structure on atomic level is impossible.

Polarizable models allow one to take into account various effects of electrostatic interaction, but the existence of several ways [12] of implementation does not give complete confidence in the use of this approach.

Rigid full-atomic models save computational resources due to fixed bond lengths and angle values and provide "atomic resolution" of the ionic subsystem study. In the same time, it is impossible to obtain vibrational spectra of tetrafluoroborate anion with restricted intraionic structure.

Based on the foregoing, within current investigation, we decided to use full-atom soft force field models of tetrafluoroborate as an approach able to completely solve the problems posed to us. As a result of our literature review, models ABS [25], Liu / Wu [23-24] and CL&P [26] identified as the most popular tetrafluoroborate force fields.

## 2. Quantum-chemical calculations of the optimal geometry, partial atomic charges, and the vibrational spectrum of $BF_4^-$ in a vacuum

All quantum chemical calculations were carried out using the Gaussian 09 [27] software package were performed at the M062X/6-311++G(d,p) level. The specific charges on the atoms were calculated by the Breneman ChelpG method [28].

As a result of quantum-chemical calculations of the tetrafluoroborate anion in vacuum, following equilibrium geometry parameters were obtained: the B-F bond length equal to 1.4092033966 Å, and the F-B-F angle equal to 109.47122063°. The correct tetrahedral form of the ion was set as the initial requirement for the results of quantum-chemical calculations. For boron and fluorine atoms the partial charges of +1.188568 and -0.5471420.4569 were evaluated.

The obtained vibrational modes, their expected intensities in the IR spectrum, as well as a description of the oscillations are given in table 1.

The data presented in table 1 are in good agreement with the literature [6].

## 3. Vibrational spectra for the most common models in the literature

Based on conducted literature review, next three force field models of the tetrafluoroborate anion were selected for spectral properties efficiency testing:
1) model of Andrade (Jones de Andrade), Boes (Elvis S. Böes) and Stassen (Hubert Stassen) [25], hereinafter referred to as ABS;
2) the Liu / Wu model, first proposed by Liu [23], and then refined by Wu in [24];
3) the model of Lopez (José N. Canongia Lopes) and Padua (Agílio A. H. Pádua) [26] hereinafter referred to as CL&P.

**Table 1.** $BF_4^-$ vibrational modes obtained from quantum-chemical calculations at the level of M062X / 6-311 ++ G (d, p).

| Order number | Oscillation frequency, $cm^{-1}$ | Intensity in the IR spectrum, a.u. | Oscillation type | Oscillation involved atoms |
|---|---|---|---|---|
| 1 | 347.19 | 0 | Bending vibrations of the F-B-F angle, flattening the initial tetrahedral shape | The predominant participation of F-atoms |
| 2 | | | | |
| 3 | 519.06 | 4.3772 | Symmetric paired deformation vibrations of the F-B-F angle | Equal intensity of all participated atoms |
| 4 | | | Asymmetric paired deformation vibrations of the F-B-F angle | |
| 5 | | | Asymmetric pair deformation (second pair of angles) | |
| 6 | 778.86 | 0 | Symmetric stretching vibrations of all F-B bonds | Only F-atoms oscillate, B-atom is practically motionless |
| 7 | 1105.67 | 432.1875 | Oscillations of B-atom inside a tetrahedron formed by F-atoms | Only B-atom vibrates, F-atoms are practically motionless |
| 8 | | | | |
| 9 | | | | |

The ABS model is one of the very first soft full-atom tetrafluoroborate models. The purpose of discussed research was to create force fields for modeling of room temperature ionic liquids (RTIL) based on alkyl-imidazoline cations with tetrachloroaluminate and tetrafluoroborate anions as counterions. The AMBER [29] force field was used as the basis of the model, but since the AMBER force field is developed for modeling biological objects [29], it has no parameters of atoms untypical for biological field. The Lennard-Jones parameters of boron atom were taken from the more universal DREIDING force field [30], but parameters for fluorine atoms were taken AMBER [29]. Quantum chemical calculations were performed by GAMESS [31] program on the UHF / 6-31G (d) level of the theory; boron and fluorine atoms partial charges were set +0.8275 and -0.4569, respectively. Work of Andrade [25] was the first attempt to obtain interionic constants for B-F bonds and angles F-B-F of tetrafluoroborate anion using PES. This procedure was performed using the AMBER utilities. The ABS force field was used in a number of works [18-19, 22], and was even used as the basis for another model of the force field of the tetrafluoroborate anion - Liu / Wu.

The Liu / Wu model was also used in a number of studies [17, 20, 24] was first presented in [23], to improve the force fields of imidazolium based ionic liquids. The force field in the discussed article is similar to the tetrafluoroborate model of Andrade [25], namely the same forms of intramolecular and intermolecular potentials as well as AMBER [29] force field as source were used. Comparing to ABS model [25], the Liu / Wu model has different BF bond equilibrium value (it was taken from crystallographic data [32]), different level of quantum-chemical calculations (HF/6-31+G(d)), and therefore different atomic partial charge values (B +1.1504; F -0.5376). Lennard-Jones parameters, B-F bond potential constants, equilibrium value and potential constant of F-B-F were taken from ABS model [25] with rounding. Despite the author's attention mostly was attracted to the cations, the advantage of Liu's work [23] is presence of calculated vibrational spectra (using classical MD-simulation) and their comparison to experimental ones by vibrational frequencies.

Wu's work [24] is devoted to improving the developed Liu's force field [23] and investigation of various concentrations ionic liquids acetonitrile solutions. Compared to [23], the anion's force field parameters are represented with greater accuracy and closer to [25] values.

The third discussed force field of tetrafluoroborate, CL&P, is well-known for ionic liquid force field development. This force field is a combination of the OPLS-AA [33] and AMBER [29] fields with further author's modifications.

Despite the fact that in a number of works [34-36] the authors themselves directly declare the tetrafluoroborate anion as a component of the simulated system and provide links to publications devoted to the development of the ionic liquids force fields [26, 37-39], the data for tetrafluoroborate force field parameters were found in supplementary information for [26] as DL_POLY [40] force field file. The values of σ and ε are equal to σ and ε from ABS [25] with rounding to the fourth decimal place,

the partial charges on the boron and fluorine atoms equal +0.96 and -0.49, respectively. As in all previously considered models, the F-B-F angle equilibrium value is 109.5° and B-F bond equilibrium value is 1.394 Å, but CL&P intermolecular potential constant values of bonds and angles are 1.3 times and 1.5 times larger respectively.

In current work we have tested the force field models described above with respect to their ability to reproduce spectral properties of discussed anion in classical molecular dynamics simulation.

All MD-simulations were performed using the GROMACS v5.3 software package [41-43] with an integration step equal to 0.5 fs.

Intermolecular interactions were calculated as a sum of short-range ($U_{SR}$) and long-range ($U_{Coulomb}$) interactions:

$$U_{pot} = U_{SR} + U_{Coulomb} \tag{1}$$

The particle-mesh Ewald (PME) summation was used to calculate the long-range electrostatic interactions [41].

The Lennard-Jones potential (2) were used to calculate short-range interactions. It can be written both in classical and A-B form:

$$U_{LJ} = 4\varepsilon_{ij}\left[\left(\frac{\sigma_{ij}}{r_{ij}}\right)^{12} - \left(\frac{\sigma_{ij}}{r_{ij}}\right)^{6}\right] = \frac{A_{ij}}{r_{ij}^{12}} - \frac{B_{ij}}{r_{ij}^{6}}, \tag{2}$$

where $\varepsilon_{ij}$ is the depth of the energy well, and $\sigma_{ij}$ is the distance of zero interaction energy between the two particles, $A_{ij} = \sqrt{A_{ii}A_{jj}}$ and $B_{ij} = 4\varepsilon_{ij}\sigma_{ij}^{6}$. The geometric mean for $A$ and $B$ was used as the combination rules: $A_{ij} = \sqrt{A_{ii}A_{jj}}$ and $B_{ij} = \sqrt{B_{ii}B_{jj}}$.

Intramolecular potentials for bonds and angles were calculated according to formulas (3) and (4), respectively:

$$V_b(r_{ij}) = \frac{1}{2}K_{r,ij}(r_{ij} - r_{0,ij})^{2}, \tag{3}$$

where $K_r$ is the intramolecular potential constant, $r_0$ is the bond length equilibrium value.

$$V_a(\theta_{ijk}) = \frac{1}{2}K_{\theta,ijk}(\theta_{ijk} - \theta_{0,ijk})^{2}, \tag{4}$$

where $K_\theta$ is the intramolecular potential constant, $\theta_0$ is the angle equilibrium value. 1-4 interactions were disabled.

Intermolecular and intramolecular potential parameters of discussed force field models (ABS, Liu / Wu and CL&P) are given in tables 2 and 3, respectively.

The vibrational spectra were calculated in vacuum and in a solvent medium by Fourier transform (5) of the autocorrelation functions of linear atomic velocities

$$S_{vv}(\omega) = \int_{0}^{\infty} \overline{C_{vv}}(t)\cos(\omega t)dt, \tag{5}$$

where $\overline{C_{vv}}$ is normalized autocorrelation function of the linear velocity of the particle center-of-mass.

**Table 2.** Lennard-Jones parameters and partial charges of the ABS, Liu / Wu and CL&P models.

| Force field | Atom | $\sigma$, nm | $\varepsilon$, kJ/mol | $q_i$ |
|---|---|---|---|---|
| ABS | B | 0.35814 | 0.39748 | +0.8275 |
| | F | 0.31181 | 0.25522 | -0.4569 |
| Liu/Wu | B | 0.35814 | 0.3975 | +1.1504 |
| | F | 0.31181 | 0.2552 | -0.5376 |
| CL&P | B | 0.358 | 0.3975 | +0.96 |
| | F | 0.312 | 0.2552 | -0.49 |

**Table 3.** intramolecular potential parameters of the ABS, Liu / Wu and CL&P models.

| Force field | $K_r$, kJ·mol$^{-1}$·nm$^{-2}$ | $r_0$, nm | $K_\theta$, kJ·mol$^{-1}$·rad$^{-2}$ | $\theta_0$, degree |
|---|---|---|---|---|
| ABS | 242672 | 0.1393 | 418.4 | 109.5 |
| Liu/Wu | 242680 | 0.139 | 418.4 | 109.5 |
| CL&P | 323500 | 0.1394 | 669.5 | 109.5 |

All classical molecular dynamics simulations in a solvent medium were performed in *NPT* ensemble. Velocity rescaling thermostat [44] was used to maintain a constant temperature with $T = 298.15$K and the time constant value of 0.1 ps. The pressure was kept equal to of 1 atm using a Berendsen barostat [45] with the time constant of 10 ps. The simulated system consisted of one $BF_4^-$ ion and 500 AN molecules. Acetonitrile force field model of Koverga [46] was chosen for all MD simulations. Each simulated systems underwent through the following stages: energy minimization, thermodynamic equilibration (1 ns) and calculating properties (1 ns).

All molecular dynamics simulations in vacuum were performed in *NVT* ensemble with the volume of the simulated cubic cell equal to 100 nm³.

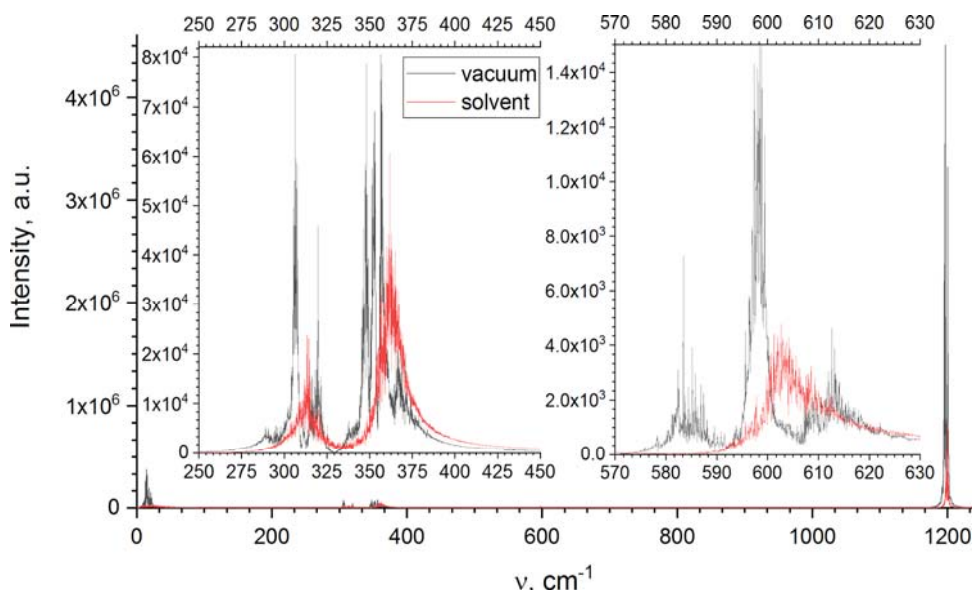Obtained vibrational spectra for the ABS, Liu / Wu, and CL&P models are shown in Figures 1, 2, and 3, respectively.



**Figure 1.** Vibrational spectra of tetrafluoroborate anion in solvent (red) and vacuum (black) medium obtained by molecular dynamics modeling for the systems contained the ABS model.
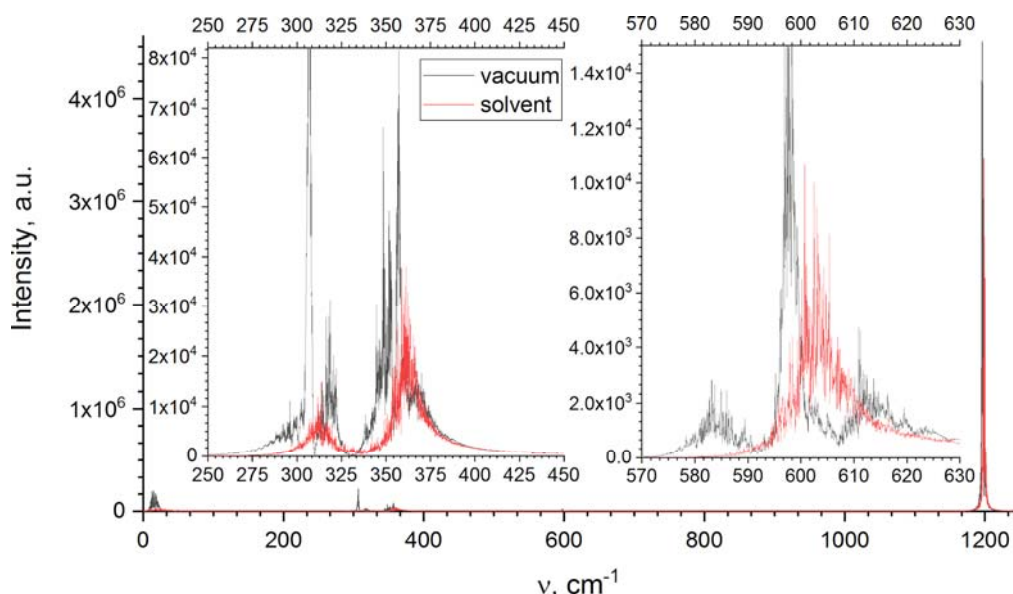


**Figure 2.** Vibrational spectra of tetrafluoroborate anion in solvent (red) and vacuum (black) medium obtained by molecular dynamics modeling for the systems contained the Liu / Wu model.

Based on the presented results (see Fig. 1-3), for all models, vibrational modes positions in vacuum and in solvent are almost the same. Placing the ion into solvent medium simplifies the vibrational spectrum, namely three distinct pics in vacuum convert into one broad peak in acetonitrile accompa-

nied by the shift of its position of $\sim$ 5-10 cm$^{-1}$ towards the long wave length range comparing to the central one in vacuum. This behavior occurs for all solvent spectra of all calculated models. Therefore for saving computational resources all further calculations of vibrational spectra by MD simulation were carried out in vacuum taking into account that the positions of triple peaks in the range of 600-700 cm$^{-1}$ were represented by one middle peak.
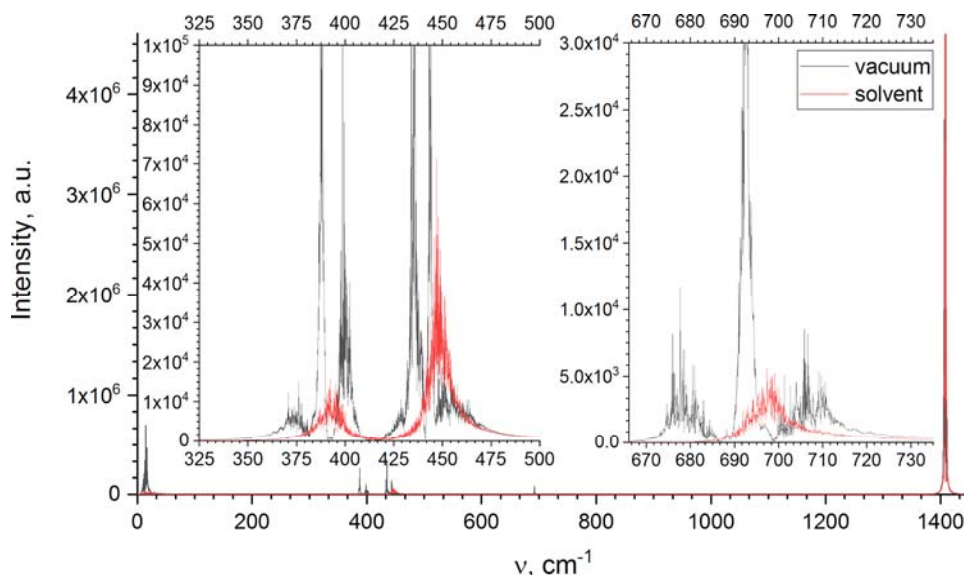


**Figure 3.** Vibrational spectra of tetrafluoroborate anion in solvent (red) and vacuum (black) medium obtained by molecular dynamics modeling for the systems contained the CL&P model.

On presented spectra (see Fig. 1-3) there are oscillations in the low-frequency region (0-100cm$^{-1}$) corresponding to inhibited translations and librations. The presence of such oscillations proves correct methodology of the molecular dynamics simulation.

The good convergence of the ABS and Liu / Wu models vibration frequencies is explained by the similarity of the intramolecular potential constant values: Liu / Wu values [23-24] were taken from [25]. This fact confirms the primary influence of intramolecular potentials over intermolecular in influence on vibrational spectra.

Both figures 1 and 2 have four modes: around 310 cm$^{-1}$, 360 cm$^{-1}$, 600 cm$^{-1}$ and 1200 cm$^{-1}$., respectively. These vibrational modes can be assigned to the modes from the table 1: 347.19 cm$^{-1}$, 519.06 cm$^{-1}$, 778.86 cm$^{-1}$ and 1105.67 cm$^{-1}$, respectively. Based on given values, all modes of the Liu/Wu and ABS models show lower frequencies comparing to results of quantum chemical calculations for all modes except the last one (1200 cm$^{-1}$). Frequency values obtained for CL&P force field model (figure 3) are closer to table 1 values: around 400 cm$^{-1}$, 450 cm$^{-1}$, 700 cm$^{-1}$ and 1200 cm$^{-1}$., respectively. Comparing to Liu/Wu and ABS models the CL&P molecular dynamics spectrum has the same value of the last frequency mode (the forth one) but higher and therefore closer to quantum spectrum (see table 1) values.

Summarizing the results mentioned above, one can conclude that the ability of literature force field models [23-26] to reproduce vibrational spectrum of tetrafluoroborate by classical molecular dynamics simulation is quite questionable. Despite CL&P model is more effective than Liu/Wu and ABS, none of chosen force field are able to fully reproduce ion spectrum.

## 4. Scanning the surface of the potential binding energy of energy of the B-F bond and F-B-F angle

As it was shown previously, intramolecular potentials make the main contribution to the vibrational spectra, and none of discussed literature force field models can fully reproduce the vibrational spectra of tetrafluoroborate, it was decided to scan the potential energy of B-F bonds and F-B-F angles to obtain intrinsic molecular potentials of their own. Three methods of scanning potential energy were selected: 1) scanning with additional optimization of geometry (hereinafter, designate them as PES-1); 2) scanning without additional optimization of geometry (hereinafter, designate them as PES-2);

3) scanning without further optimization over four B-F bonds and two vertical F-B-F angles (hereinafter, we denote them as PES-3). All the quantum chemical calculations were carried out using the same level of theory as described in the Section 2.

The last method (PES-3) was used due to two reasons. First, it was an attempt to solve the problems with a drop-down point during the bond / angle scanning for highly symmetric molecules. Second, based on the table 1 the vibration III is a symmetric vibration of all four B-F bonds and there are no single or asymmetric vibrations of the B-F bonds. In this connection, for a better representation of vibration III, it is necessary to analyze the simultaneous symmetric vibration of all four B-F bonds. Figures 4 and 5 show the results of applying PES-1, PES-2, PES-3 to scan the energy profile for the B-F bond and the F-B-F angle, respectively, as well as the results of approximating the obtained dependences by the formulas (3) and (4).

Figures 4 and 5 demonstrates that equations (3) and (4) describes well obtained PES-1, PES-2, PES-3 dependences. All three methods show similar function behavior in the region near to the optimum and geometric parameters values close to the corresponding optimal geometry as well.

The values obtained during PES-1, PES-2 and PES-3 were approximated by the next equation:

$$y = \frac{1}{2} K \left( x - x_0 \right)^2 + c, \tag{6}$$

where $c$ is a constant guaranteeing a zero value of the potential at the optimum point; $K$ is $K_r$ or $K_\theta$; $x$ is $r$ or $\theta$; $x_0$ is $r_0$ or $\theta_0$ for (3) or (4), respectively. The constants values obtained during the approximation, as well as their errors, are given in tables 5 and 6.



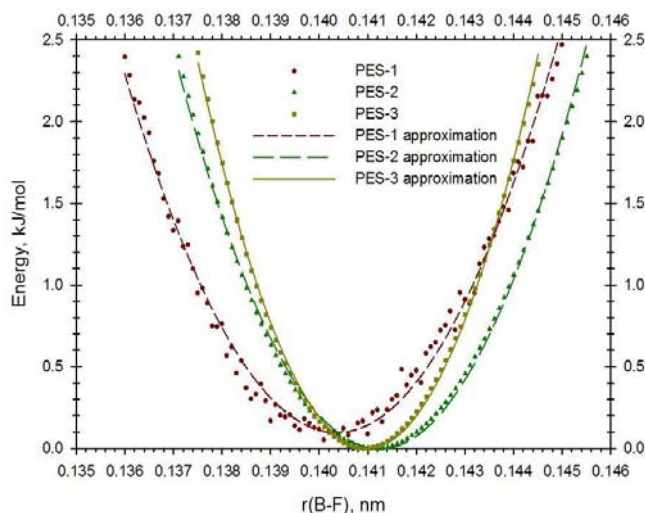**Figure 4.** Energy profile of B-F bond energy according to the PES-1, PES-2 and PES-3 methods
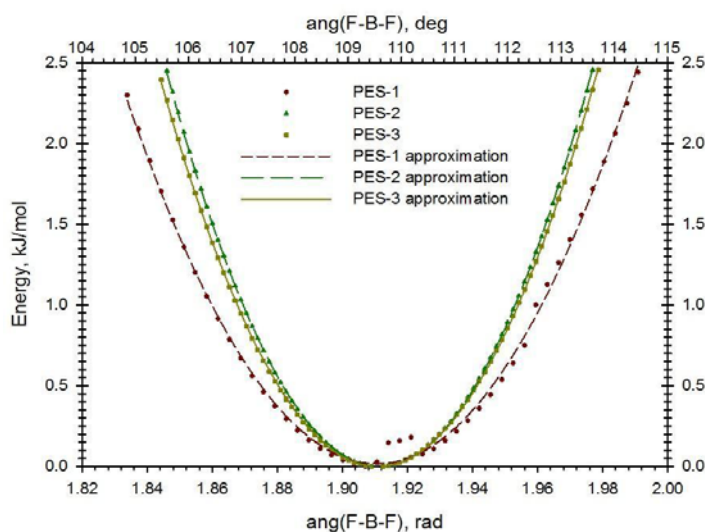


**Figure 5.** Energy profile of the F-B-F angle according to the methods PES-1, PES-2 and PES-3.

As expected the values of $C$ constants are negligible (tables 5 and 6), that indicates the methodological correctness of the applied procedure.

Obtained sets of the intramolecular potential parameters (tables 5 and 6) were used to test their effectiveness in reproducing the vibrational spectrum of the tertafluoroborate anion in MD simulation. Liu/Wu force field model was chosen for this purpose. The calculation was carried out in vacuum according to the procedure described above. The results of the MD simulation of the vibrational spectra of $BF_4^-$ anion with the intramolecular potentials based on PES-1, PES-2 and PES-3 approaches are presented in Figure 6.

**Table 5.** Approximation results of PES-1, PES-2, and PES-3 data for B-F bond of $BF_4^-$ anion.

| Parameter | PES-1 | PES-2 | PES-3 |
|---|---|---|---|
| $K_r$, kJ·mol$^{-1}$·nm$^{-2}$ | $231000 \pm 2000$ | $271000 \pm 1000$ | $389000 \pm 2000$ |
| $r_0$, nm | $0.14040 \pm 0.00001$ | $0.141200 \pm 0.000006$ | $0.141000 \pm 0.000004$ |
| $c$ | $0.10 \pm 0.01$ | $-0.003 \pm 0.006$ | $0.001 \pm 0.004$ |

**Table 6.** Approximation results of PES-1, PES-2, and PES-3 data for F-B-F angle of $BF_4^-$ anion.

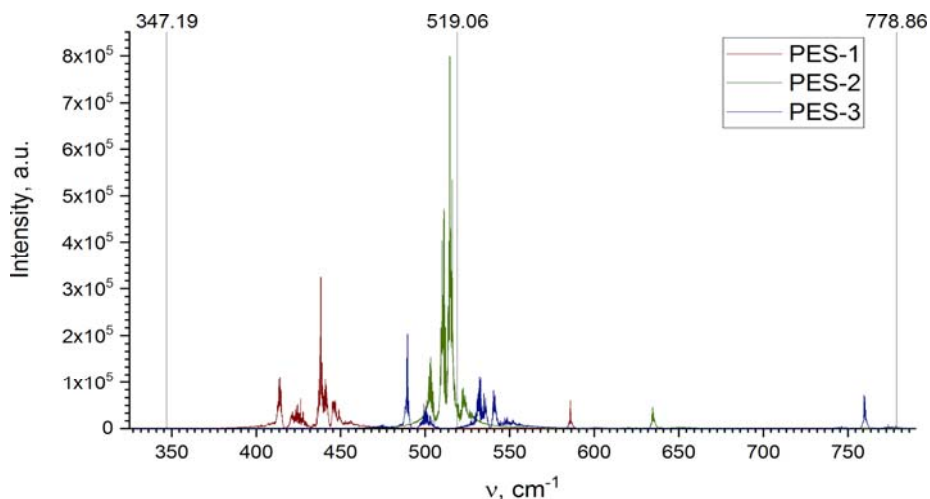| Parameter | PES-1 | PES-2 | PES-3 |
|---|---|---|---|
| $K_\theta$, kJ·mol$^{-1}$·rad$^{-2}$ | $766 \pm 7$ | $1145.2 \pm 0.9$ | $1074 \pm 1$ |
| $\theta_0$, degree | $109.47 \pm 0.01$ | $109.5095 \pm 0.0007$ | $109.4865 \pm 0.0009$ |
| $c$ | $0.02 \pm 0.01$ | $-0.0017 \pm 0.0009$ | $-0.002 \pm 0.001$ |



**Figure 6.** Molecular dynamics vibrational spectra of the $BF_4^-$ anion with intramolecular potentials based on PES-1 (red), PES-2 (blue) and PES-3 (green) and the frequencies of vibrational modes (grey vertical lines) from Table 1.

Observation of the figure 6 allows one to conclude that the PES-3 shows the best result for oscillation III (Table 1). PES-2 and PES-3 describe well oscillation II, and the results of PES-1 are equidistant from oscillations I and II. The task of reproducing vibration IV was not posed, since the tetrahedral form of $BF_4^-$ is preserved for this vibration.

Because none of the used methods can provide the intramolecular potentials parameters able to completely reproducing of the vibrational spectrum of the $BF_4^-$ anion, it was decided to use obtained values (see tables 5 and 6) as a starting point for adjusting procedure allowing to evaluate the intramolecular parameters able to show the best agreement between the vibrational spectra from molecular dynamics simulations and quantum chemical calculations. The adjusting procedure consisted of a multidimensional analysis of the intramolecular potential to determine the values of $K_r$ and $K_\theta$, which give the best possible pick locations. The values of partial atomic charges and Lennard-Jones potentials were not used in this analysis because of the insignificant effect of intermolecular interactions on the vibrational spectrum of $BF_4^-$ as compare with intramolecular potentials (see section 3). Despite the fact that the equilibrium values of bonds and angles belong to intramolecular parameters, they were also not used as tunable parameters because of the importance of keeping the equilibrium geometry of the anion equal to that obtained in quantum calculations (see section 1). As a result, the values of

$K_r = 410000$ kJ·mol$^{-1}$ nm$^{-2}$, $K_\theta = 710$ kJ·mol$^{-1}$·rad$^{-2}$ were obtained. All other parameters of the force field for of BF$_4^-$ anion were adopted as following. Equilibrium geometry parameters of the tetra-fluoroborate anion ($r$(B-F) = 0.14092033966 nm and $\theta$(F-B-F) = 109.47122063°) were calculated in section 2, as well as partial atomic charges ($q$(B) = +1.88568, $q$(F) = -0.547142). Lennard Jones parameters were taken from Liu/Wu model [23-24] ($\sigma$(B) = 0.35814 nm, $\sigma$(F) = 0.31181 nm; $\varepsilon$(B) = 0.3975 kJ·mol$^{-1}$, $\varepsilon$(F) = 0.2552 kJ·mol$^{-1}$.

The vibrational spectrum of BF$_4^-$ in vacuum obtained by MD simulation based on the final force field is shown in Figure 7.
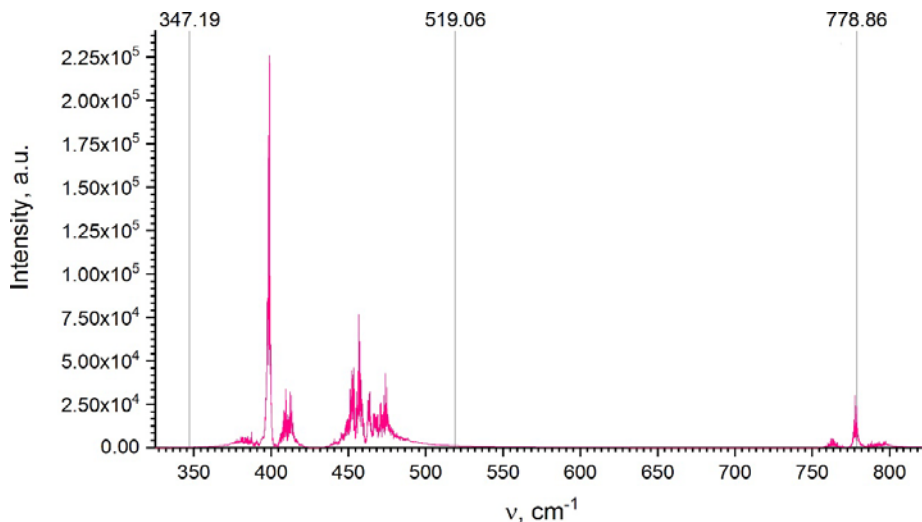


**Figure 7.** Molecular dynamics vibrational spectra of the developed force field (pink lines) and the frequencies of vibrational modes (grey vertical lines) from Table 1.

Figure 7 demonstrates that the developed force field allows to reproduce the vibrational mode III as well as to achieve the equidistant position of the vibration frequencies for modes I and II.

## 5. Validation of the developed force field by the diffusion coefficient of the tetrafluoroborate ion

Force field model of ion as a component of electrolyte solution requires not only good representation of vibrational spectra, but also good representation of dynamic properties, such as the diffusion coefficient.

In the current work, the diffusion coefficient, $D$, was calculated by two methods: via the mean square displacement $(r(0) - r(t))^2$

$$\lim_{t \to \infty} \left\langle \left( \mathbf{r}(0) - \mathbf{r}(t) \right)^2 \right\rangle = 6Dt \tag{7}$$

and the Green-Kubo formula

$$D = \frac{1}{3} \int_0^\infty C_{vv}(t)\,dt. \tag{8}$$

Validation of ionic diffusion coefficient requires previous validation of solvent diffusion coefficient because the solvent as a medium has a huge influence on the dynamic properties of containing ions [47]. For this purpose, 5 independent geometries (called "seeds") of 500 acetonitrile systems were generated using standard GROMACS utilities. Each system underwent such stages as: energy minimization, thermodynamic equilibration (1 ns) and properties calculation (1 ns). All simulations were carried out in *NPT* ensemble with the settings described above.

Figure 8 presents the obtained time dependences of the autocorrelation function of the linear velocity of acetonitrile molecules.

Figure 9 shows the obtained time dependences of the mean square displacement of acetonitrile molecules. To calculate the diffusion coefficient by formula (7), curves section from 50 to 150 ps were used.
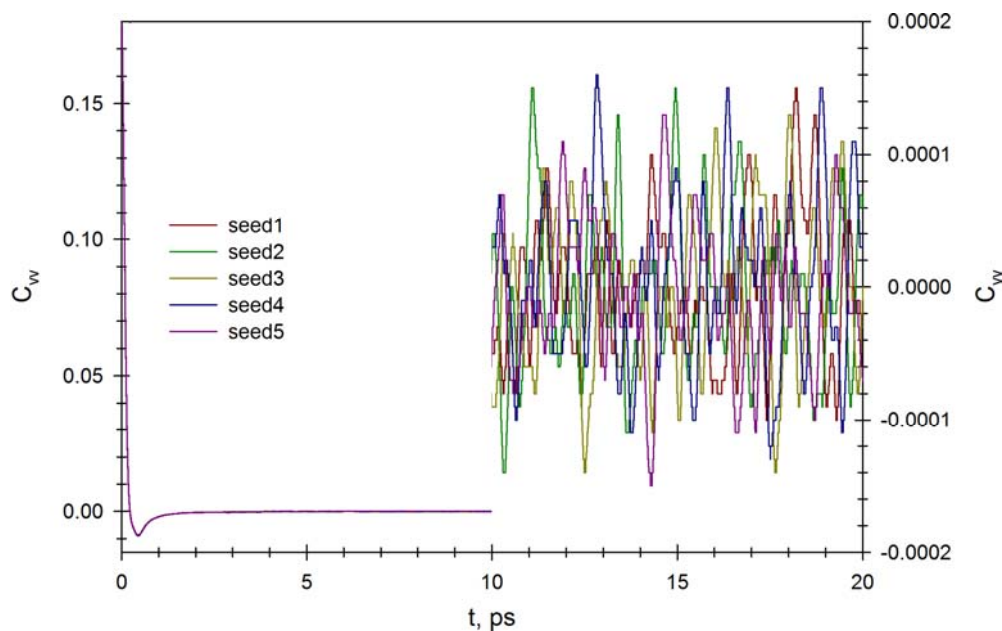
**Figure 8.** Time dependences of the autocorrelation function of the linear velocity of acetonitrile molecules.



**Figure 9.** The obtained time dependences of the mean square displacement of acetonitrile molecules.

The results of calculating the diffusion coefficient of acetonitrile according to the Einstein equation (7) and the Green-Kubo formula (8) are shown in table 6.

**Table 6.** The calculated values of the diffusion coefficient of acetonitrile (500 molecules) by the Einstein equation (7), $D_{msd}$, and the Green-Kubo formula (8), $D_{Cvv}$.

| System number | $D_{msd}$, $10^{-9}$ m$^2$·s$^{-1}$ | $D_{Cvv}$, $10^{-9}$ m$^2$·s$^{-1}$ |
|---|---|---|
| 1 | 3.93 | 3.90 |
| 2 | 3.94 | 3.89 |
| 3 | 3.90 | 3.87 |
| 4 | 3.89 | 3.86 |
| 5 | 3.84 | 3.89 |
| Average value | $3.90 \pm 0.04$ | $3.88 \pm 0.02$ |

46

The obtained average value of the acetonitrile diffusion coefficient $3.89 \cdot 10^{-9}$ $m^2 \cdot s^{-1}$ (table 6) is slightly different from that claimed by the authors $4.03 \cdot 10^{-9}$ $m^2 \cdot s^{-1}$ [46]. The experimental values are in a rather wide range: $4.04 \cdot 10^{-9}$ $m^2 \cdot s^{-1}$ [48], $4.28 \cdot 10^{-9}$ $m^2 \cdot s^{-1}$ [49], $4.31 \cdot 10^{-9}$ $m^2 \cdot s^{-1}$ [50], $4.34 \cdot 10^{-9}$ $m^2 \cdot s^{-1}$ [51], $4.37 \cdot 10^{-9}$ $m^2 \cdot s^{-1}$ [52], $4.85 \cdot 10^{-9}$ $m^2 \cdot s^{-1}$ [53], $4.9 \cdot 10^{-9}$ $m^2 \cdot s^{-1}$ [54], $5.10 \cdot 10^{-9}$ $m^2 \cdot s^{-1}$ [55]. $4.5 \pm 0.3 \cdot 10^{-9}$ $m^2 \cdot s^{-1}$ was considered as the average experimental value of acetonitrile diffusion coefficient. Experimental value in 1.17 (4.5 / 3.89 = 1.17) times higher compared to calculated value, therefore 1.17 was used as correction factor for further calculation of ionic diffusion as it was proposed early at the same circumstances [47].

The procedure of diffusion coefficient calculation for $BF_4^-$ was identical to the solvent's one. The simulated system for this simulations included 1 ion and 500 solvent molecules.

Figure 10 presents the obtained time dependences of the autocorrelation function of the linear velocity of $BF_4^-$.



**Figure 10.** The obtained time dependences of the autocorrelation function of the linear velocity of $BF_4^-$.

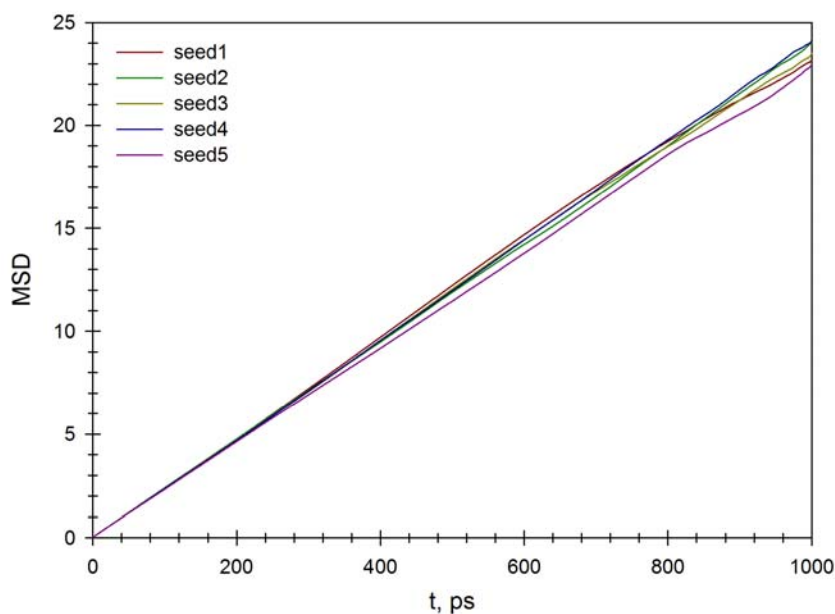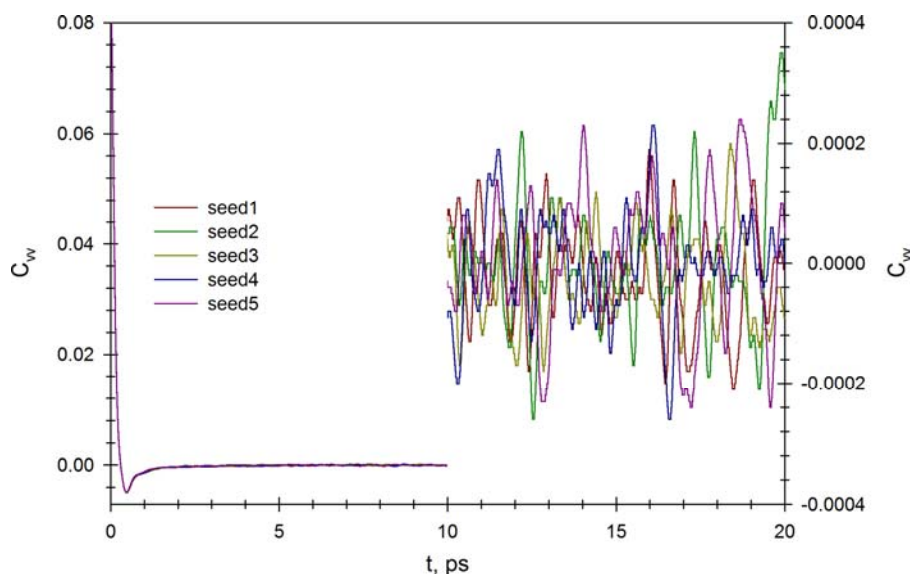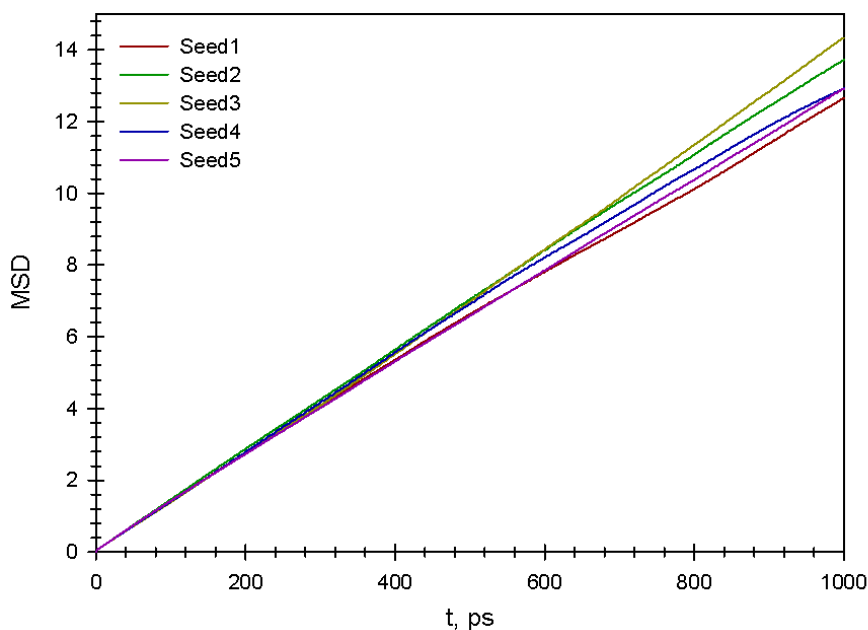Figure 11 shows the obtained time dependences of the mean square displacement of $BF_4^-$.



**Figure 11.** The obtained time dependences of the mean square displacement of the tetrafluoroborate anion

The results of calculating the diffusion coefficient of $BF_4^-$ according to the Einstein equation and the Green-Kubo formula (7) are shown in Table 7.

**Table 7.** The calculated values of the diffusion coefficient of $BF_4^-$

| System number | $D_{msd}$, $10^{-9}$ m$^2$·s$^{-1}$ | $D_{Cvv}$, $10^{-9}$ m$^2$·s$^{-1}$ |
|---|---|---|
| 1 | 2.2646 | 2.31722 |
| 2 | 2.3602 | 2.38136 |
| 3 | 2.2869 | 2.29397 |
| 4 | 2.2812 | 2.30667 |
| 5 | 2.2010 | 2.35999 |
| Average value | $2.28 \pm 0.07$ | $2.33 \pm 0.05$ |

As it follows form the table 7, the average calculated value of $BF_4^-$ diffusion coefficient in infinitely diluted acetonitrile is $2.30 \cdot 10^{-9}$ m$^2$·s$^{-1}$. Taking into account the correction factor of 1.17 for solvent diffusion, the obtained diffusion coefficient of the $BF_4^-$ anion can be estimated as $2.69 \cdot 10^{-9}$ m$^2$·s$^{-1}$.

An experimental value of an ion diffusion coefficient can calculated from the limiting ionic conductivity of an ion by using the Nernst-Einstein equation

$$D_i = \frac{RT}{z_i^2 F^2} \Lambda_{m,i}^0, \tag{9}$$

where $z_i$ is the charge of an ion, $\Lambda_m^0$, is the molar limiting ionic conductivity of an on at infinite dilution.

Taking the limiting ionic conductivity of the $BF_4^-$ anion equal to 107.48 Sm·cm$^2$·mol$^{-1}$ [56], the value of $BF_4^-$ diffusion coefficient was estimated as $2.87 \cdot 10^{-9}$ m$^2$·s$^{-1}$. This means that developed force field of $BF_4^-$ is able to reproduce experimental diffusion coefficient of the anion in AN medium within the relative error of 6.3%.

## Conclusions

Development of new supercapacitors and improving the existing ones requires thorough investigation of processes occurring in an electrolyte solution. Combination of spectral methods with molecular dynamics simulation can become a reliable tool for solving this kind of tasks.

This work is devoted to the development of $BF_4^-$ force field able to reproduce not only the dynamic, but also the spectral properties of the ion in acetonitrile media.

As a thorough literature review of $BF_4^-$ force field models, three models were chosen for further research: Liu/Wu [23-24], ABS [25] and CL&P [26]. Discussed force fields for classical molecular dynamics simulations of the anion in both vacuum and solvent medium. There is no significant difference between $BF_4^-$ spectra in vacuum and solvent medium was revealed, which indicates the prevalence of intra-molecular potentials over inter-molecular potentials in their influence on the vibrational spectrum. Since all discussed force fields are not able to reproduce spectral propertied of the ion with required accuracy, the potential energy surface scanning (PES) of bonds B-F and angles F-B-F were applied by using quantum chemical calculations at the M062X/6-311++G(d,p) level of theory.

Three different techniques of PES generation gave three different sets of intra-molecular parameters. To check these parameters, additional quantum chemical calculations of $BF_4^-$ at the M062X/6-311++G(d,p) level of theory were carried out to evaluate the atomic partial charges and equilibrium geometry. Then, taking into account the Lennard Jones potential parameters from Liu/Wu [23-24] model we have tested new sets of the intramolecular parameters in classical molecular dynamics simulation. Despite all obtained spectra of PES-generated force fields are not able to fully reproduce spectrum of $BF_4^-$, revealed tendencies of the intramolecular potentials influences on specific bands of the vibrational spectrum. The intermolecular parameters obtained from the PES analysis were used as starting point for their next generation. In addition, revealed relationship between the changes of the intramolecular constant values and the shift of the corresponding vibrational frequencies were used as a guide in multidimensional analysis of the intramolecular parameters. This allowed us to develop a new force field for the $BF_4^-$ anion with the best possible spectrum reproduction within the framework of classical molecular dynamics modeling.

The final $BF_4^-$ force field model were developed as a force field model of the electrolyte solution component, therefore reproduction of ionic diffusion properties is as important as reproduction of vibrational spectrum. For this purpose, the difference between diffusion coefficient of Koverga acetonitrile [46] and experimental value was calculated, and further this information were took during the validation of $BF_4^-$ diffusion. The relative error of the final $BF_4^-$ force field diffusion coefficient is 6.3%.

## Acknowledgements

## References

1. González A., Goikolea E., Barrena J. A., Mysyk R. Review on supercapacitors: Technologies and materials. *Renew. Sustain. Energy Rev.* **2016,** *58* 1189-1206.
2. Zhong C., Deng Y., Hu W., Qiao J., Zhang L., Zhang J. A review of electrolyte materials and compositions for electrochemical supercapacitors. *Chem. Soc. Rev.* **2015,** *44* (21), 7484-7539.
3. Dahl K., Sando G., Fox D., Sutto T., Owrutsky J. Vibrational spectroscopy and dynamics of small anions in ionic liquid solutions. *J. Chem. Phys.* **2005,** *123* 084504.
4. Zhang B., Yuan Z., li X., Ren X., Nian H., Shen Y., Yun Q. Ion-molecule interaction in solutions of lithium tetrafluoroborate in propylene carbonate: An ftir vibrational spectroscopic study. *In. J. Electrochem. Sc.* **2013,** *8* 12735-12740.
5. Jow T. R., Xu K., Borodin O., Ue M. *Electrolytes for lithium and lithium-ion batteries*. Springer: New York, NY, 2014; Vol. 58, p 476.
6. Paschoal V. H., Faria L. F. O., Ribeiro M. C. C. Vibrational spectroscopy of ionic liquids. *Chem. Rev.* **2017,** *117* (10), 7053-7112.
7. Ueno S., Tanimura Y., Ten-no S. Molecular dynamics simulation for infrared spectroscopy with intramolecular forces from electronic properties of on-the-fly quantum chemical calculations. *Int. J. Quantum Chem.* **2013,** *113* (3), 330-335.
8. Xu R. J., Blasiak B., Cho M., Layfield J. P., Londergan C. H. A direct, quantitative connection between molecular dynamics simulations and vibrational probe line shapes. *J. Phys. Chem. Lett.* **2018,** *9* (10), 2560-2567.
9. Choi E., Yethiraj A. Conformational properties of a polymer in an ionic liquid: Computer simulations and integral equation theory of a coarse-grained model. *J. Phys. Chem. B* **2015,** *119* (29), 9091-9097.
10. Li B., Ma K., Wang Y.-L., Turesson M., Woodward C. E., Forsman J. Fused coarse-grained model of aromatic ionic liquids and their behaviour at electrodes. *Phys. Chem. Chem. Phys.* **2016,** *18* (11), 8165-8173.
11. Mehta N. A., Levin D. A. Molecular dynamics electrospray simulations of coarse-grained ethylammonium nitrate (ean) and 1-ethyl-3-methylimidazolium tetrafluoroborate (EMIM-$BF_4$). *Aerospace* **2018,** *5* (1).
12. Son C. Y., McDaniel J. G., Schmidt J. R., Cui Q., Yethiraj A. First-principles united atom force field for the ionic liquid Bmim$^+$$BF_4^-$: An alternative to charge scaling. *J. Phys. Chem. B* **2016,** *120* (14), 3560-3568.
13. Tetiana C., Oleg K., Yaroslav K. Microstructure and dynamics of single charged ions in propylene carbonate. *Kharkov Univ. Bull. Chem. Ser.* **2013,** *0* (22), 25-38.
14. Vovchynskyi I. S., Kolesnik Y. V., Filatov Y. I., Kalugin O. N. Molecular modelling on solutions of 1-1′-spirobipirrolidinium tetrafluoroborate in acetonitrile. *J. Mol. Liq.* **2017,** *235* 60-67.
15. Sambasivarao S. V., Acevedo O. Development of opls-aa force field parameters for 68 unique ionic liquids. *J. Chem. Theory Comput.* **2009,** *5* (4), 1038-1050.

16. Doherty B., Zhong X., Gathiaka S., Li B., Acevedo O. Revisiting OPLS force field parameters for ionic liquid simulations. *J. Chem. Theory Comput.* **2017,** *13* (12), 6131-6145.

17. Feng G., Huang J., Sumpter B. G., Meunier V., Qiao R. Structure and dynamics of electrical double layers in organic electrolytes. *Phys. Chem. Chem. Phys.* **2010,** *12* (20), 5468-5479.

18. Kanzaki R., Mitsugi T., Fukuda S., Fujii K., Takeuchi M., Soejima Y., Takamuku T., Yamaguchi T., Umebayashi Y., Ishiguro S.-i. Ion–ion interaction in room temperature ionic liquid 1-ethyl-3-methylimidazolium tetrafluoroborate studied by large angle x-ray scattering experiment and molecular dynamics simulations. *J. Mol. Liq.* **2009,** *147* (1), 77-82.

19. Shim Y., Kim H. J. Nanoporous carbon supercapacitors in an ionic liquid: A computer simulation study. *ACS Nano* **2010,** *4* (4), 2345-2355.

20. Shim Y., Jung Y., Kim H. J. Graphene-based supercapacitors: A computer simulation study. *J. Phys. Chem. B* **2011,** *115* (47), 23574-23583.

21. Yang P.-Y., Ju S.-P., Hsieh H.-S., Lin J.-S. The diffusion behavior and capacitance of tetraethylammonium/tetrafluoroborate ions in acetonitrile with different molar concentrations: A molecular dynamics study. *RSC Adv.* **2017,** *7* (87), 55044-55050.

22. Zhang Q.-Y., Xie P., Wang X., Yu X.-W., Shi Z.-Q., Zhao S.-H. Thermodynamic and transport properties of spiro-(1,1')-bipyrrolidinium tetrafluoroborate and acetonitrile mixtures: A molecular dynamics study. *Chin. Phys. B* **2016,** *25* (6), 066102.

23. Liu Z., Huang S., Wang W. A refined force field for molecular simulation of imidazolium-based ionic liquids. *J. Phys. Chem. B* **2004,** *108* (34), 12978-12989.

24. Wu X., Liu Z., Huang S., Wang W. Molecular dynamics simulation of room-temperature ionic liquid mixture of [Bmim][BF$_4$] and acetonitrile by a refined force field. *Phys. Chem. Chem. Phys.* **2005,** *7* (14), 2771-2779.

25. de Andrade J., Böes E. S., Stassen H. Computational study of room temperature molten salts composed by 1-alkyl-3-methylimidazolium cationsforce-field proposal and validation. *J. Phys. Chem. B* **2002,** *106* (51), 13344-13351.

26. Canongia Lopes J. N., Pádua A. A. H. Molecular force field for ionic liquids iii: Imidazolium, pyridinium, and phosphonium cations; chloride, bromide, and dicyanamide anions. *J. Phys. Chem. B* **2006,** *110* (39), 19586-19592.

27. Frisch M. J., Trucks G. W., Schlegel H. B., Scuseria G. E., Robb M. A., Cheeseman J. R., Scalmani G., Barone V., Petersson G. A., Nakatsuji H., Li X., Caricato M., Marenich A. V., Bloino J., Janesko B. G., Gomperts R., Mennucci B., Hratchian H. P., Ortiz J. V., Izmaylov A. F., Sonnenberg J. L., Williams, Ding F., Lipparini F., Egidi F., Goings J., Peng B., Petrone A., Henderson T., Ranasinghe D., Zakrzewski V. G., Gao J., Rega N., Zheng G., Liang W., Hada M., Ehara M., Toyota K., Fukuda R., Hasegawa J., Ishida M., Nakajima T., Honda Y., Kitao O., Nakai H., Vreven T., Throssell K., Montgomery Jr. J. A., Peralta J. E., Ogliaro F., Bearpark M. J., Heyd J. J., Brothers E. N., Kudin K. N., Staroverov V. N., Keith T. A., Kobayashi R., Normand J., Raghavachari K., Rendell A. P., Burant J. C., Iyengar S. S., Tomasi J., Cossi M., Millam J. M., Klene M., Adamo C., Cammi R., Ochterski J. W., Martin R. L., Morokuma K., Farkas O., Foresman J. B., Fox D. J. *Gaussian 16 rev. C.01*, Wallingford, CT, 2016.

28. Breneman C. M., Wiberg K. B. Determining atom-centered monopoles from molecular electrostatic potentials. The need for high sampling density in formamide conformational analysis. *J. Comput. Chem.* **1990,** *11* (3), 361-373.

29. Cornell W. D., Cieplak P., Bayly C. I., Gould I. R., Merz K. M., Ferguson D. M., Spellmeyer D. C., Fox T., Caldwell J. W., Kollman P. A. A second generation force

field for the simulation of proteins, nucleic acids, and organic molecules. *J. Am. Chem. Soc.* **1995,** *117* (19), 5179-5197.

30. Mayo S. L., Olafson B. D., Goddard W. A. Dreiding: A generic force field for molecular simulations. *J. Phys. Chem.* **1990,** *94* (26), 8897-8909.

31. Schmidt M. W., Baldridge K. K., Boatz J. A., Elbert S. T., Gordon M. S., Jensen J. H., Koseki S., Matsunaga N., Nguyen K. A., Su S., Windus T. L., Dupuis M., Montgomery Jr J. A. General atomic and molecular electronic structure system. *J. Comput. Chem.* **1993,** *14* (11), 1347-1363.

32. Xue H., Twamley B., Shreeve J. n. M. The first 1-alkyl-3-perfluoroalkyl-4,5-dimethyl-1,2,4-triazolium salts. *J. Org. Chem.* **2004,** *69* (4), 1397-1400.

33. Jorgensen W. L., Maxwell D. S., Tirado-Rives J. Development and testing of the opls all-atom force field on conformational energetics and properties of organic liquids. *J. Am. Chem. Soc.* **1996,** *118* (45), 11225-11236.

34. Pádua A. A. H., Costa Gomes M. F., Canongia Lopes J. N. A. Molecular solutes in ionic liquids: A structural perspective. *Acc. Chem. Res.* **2007,** *40* (11), 1087-1096.

35. Pensado A. S., Gomes M. F. C., Lopes J. N. C., Malfreyt P., Pádua A. A. H. Effect of alkyl chain length and hydroxyl group functionalization on the surface properties of imidazolium ionic liquids. *Phys. Chem. Chem. Phys.* **2011,** *13* (30), 13518-13526.

36. Shimizu K., Pensado A., Malfreyt P., Pádua A. A. H., Canongia Lopes J. N. 2d or not 2d: Structural and charge ordering at the solid-liquid interface of the 1-(2-hydroxyethyl)-3-methylimidazolium tetrafluoroborate ionic liquid. *Faraday Discuss.* **2012,** *154* (0), 155-169.

37. Canongia Lopes J. N., Deschamps J., Pádua A. A. H. Modeling ionic liquids using a systematic all-atom force field. *J. Phys. Chem. B* **2004,** *108* (6), 2038-2047.

38. Canongia Lopes J. N., Pádua A. A. H. Molecular force field for ionic liquids composed of triflate or bistriflylimide anions. *J. Phys. Chem. B* **2004,** *108* (43), 16893-16898.

39. Shimizu K., Almantariotis D., Gomes M. F. C., Pádua A. A. H., Canongia Lopes J. N. Molecular force field for ionic liquids v: Hydroxyethylimidazolium, dimethoxy-2-methylimidazolium, and fluoroalkylimidazolium cations and bis(fluorosulfonyl)amide, perfluoroalkanesulfonylamide, and fluoroalkylfluorophosphate anions. *J. Phys. Chem. B* **2010,** *114* (10), 3592-3600.

40. Smith W., Yong C. W., Rodger P. M. DL_POLY: Application to molecular simulation. *Mol. Simulat.* **2002,** *28* (5), 385-471.

41. Lindahl E., Hess B., van der Spoel D. Gromacs 3.0: A package for molecular simulation and trajectory analysis. *J. Mol. Model.* **2001,** *7* (8), 306-317.

42. Pronk S., Páll S., Schulz R., Larsson P., Bjelkmar P., Apostolov R., Shirts M. R., Smith J. C., Kasson P. M., van der Spoel D., Hess B., Lindahl E. Gromacs 4.5: A high-throughput and highly parallel open source molecular simulation toolkit. *Bioinformatics* **2013,** *29* (7), 845-854.

43. Van Der Spoel D., Lindahl E., Hess B., Groenhof G., Mark A. E., Berendsen H. J. C. GROMACS: Fast, flexible, and free. *J. Comput. Chem.* **2005,** *26* (16), 1701-1718.

44. Bussi G., Donadio D., Parrinello M. Canonical sampling through velocity rescaling. *J. Chem. Phys.* **2007,** *126* (1), 014101.

45. Berendsen H. J. C., Postma J. P. M., van Gunsteren W. F., DiNola A., Haak J. R. Molecular dynamics with coupling to an external bath. *J. Chem. Phys.* **1984,** *81* (8), 3684-3690.

46. Koverga V. A., Korsun O. M., Kalugin O. N., Marekha B. A., Idrissi A. A new potential model for acetonitrile: Insight into the local structure organization. *J. Mol. Liq.* **2017,** *233* 251-261.

47. Agieienko V. N., Kolesnik Y. V., Kalugin O. N. Structure, solvation, and dynamics of $Mg^{2+}$, $Ca^{2+}$, $Sr^{2+}$, and $Ba^{2+}$ complexes with 3-hydroxyflavone and perchlorate anion in acetonitrile medium: A molecular dynamics simulation study. *J. Chem. Phys.* **2014,** *140* (19), 194501.

48. Kovacs H., Kowalewski J., Maliniak A., Stilbs P. Multinuclear relaxation and nmr self-diffusion study of the molecular dynamics in acetonitrile-chloroform liquid mixtures. *J. Phys. Chem.* **1989,** *93* (2), 962-969.

49. Kunz W., Calmettes P., Bellissent-Funel M. C. Dynamics of liquid acetonitrile at high frequencies. *J. Chem. Phys.* **1993,** *99* (3), 2079-2082.

50. Hurle R. L., Woolf L. A. Self-diffusion in liquid acetonitrile under pressure. *J. Chem. Soc. Faraday Trans.* **1982,** *78* (7), 2233-2238.

51. Hawlicka E., Grabowski R. Solvation of ions in acetonitrile-methanol solutions of sodium iodide. *Ber. Bunsenges. Phys. Chern.* **1990,** *94* (4), 486-489.

52. Holz M., Mao X. a., Seiferling D., Sacco A. Experimental study of dynamic isotope effects in molecular liquids: Detection of translationrotation coupling. *J. Chem. Phys.* **1996,** *104* (2), 669-679.

53. Liang M., Zhang X.-X., Kaintz A., Ernsting N. P., Maroncelli M. Solvation dynamics in a prototypical ionic liquid + dipolar aprotic liquid mixture: 1-butyl-3-methylimidazolium tetrafluoroborate + acetonitrile. *J. Phys. Chem. B* **2014,** *118* (5), 1340-1352.

54. Marcus Y. The properties of solvents. **1998.**

55. Marekha B. A., Kalugin O. N., Bria M., Buchner R., Idrissi A. Translational diffusion in mixtures of imidazolium ils with polar aprotic molecular solvents. *J. Phys. Chem. B* **2014,** *118* (20), 5509-5517.

56. Bešter-Rogač M., Stoppa A., Buchner R. Ion association of imidazolium ionic liquids in acetonitrile. *J. Phys. Chem. B* **2014,** *118* (5), 1426-1435.

И.С. Вовчинский, О.Н. Калугин. Силовое поле аниона тетрафторобората для молекулярно-динамического моделирования: новый подход.

Харьковский национальный университет имени В.Н. Каразина, химический факультет, кафедра неорганической химии, пл. Свободы, 4, Харьков, 61022, Украина

Разработка новых устройств накопления электрической энергии, включая суперконденсаторы, а также оптимизация существующих, требуют не только новых электролитов, но и глубокого и полного понимания процессов, происходящих в растворах электролитов. Спектральные методы и классическое молекулярно-динамическое моделирование (МДМ) завоевали репутацию надежного инструмента для решения таких задач. Отправной точкой любого МДМ является выбор или разработка силовых полей для всех моделируемых частиц. Сочетание методов колебательной спектроскопии и молекулярной динамики может обеспечить глубокое понимание структуры и динамики ионной подсистемы. В связи с этим к воспроизведение колебательных спектров должно быть включено в требования к силовым полям наиболее распространенных компонентов электролита.

Многие из современных суперконденсаторов основаны на органических электролитах, состоящих из неводных апротонных растворителей, таких как ацетонитрил, пропиленкарбонат, γ-бутиролактон и соли четвертичного аммония с тетрафторборатом и гексафторфосфатом в качестве анионов.

Целью настоящей работы является разработка нового силового поля для тетрафторборат-аниона ($BF_4^-$), способного воспроизводить не только поступательную диффузию в среде ацетонитрила, но и спектральные свойства этого иона в конденсированной фазе. Поскольку найденные в литературе силовые поля $BF_4^-$ не удовлетворяют этим требованиям, были проведены интенсивные квантово-химические расчеты $BF_4^-$ на уровне теории M06-2X/6-311++G(d,p) для построения поверхности потенциальной энергии. относительно связей B–F и углов F–B–F с последующей оценкой соответствующих констант внутримолекулярных потенциалов. Объединяя полученные силовые константы связи и угла с частичными зарядами на атомах B и F, рассчитанными на том же уровне теории, и литературными значения параметров потенциала Леннарда-Джонса, была создана новая модель силового поля для аниона $BF_4^-$. На основании проведенного МД-

моделирования иона $BF_4^-$ в бесконечно разбавленном растворе в ацетонитриле было доказано, что полученная модель способна воспроизводить как транспортные свойства, так и внутриионные колебания тетрафторборат-аниона.

**Ключевые слова:** анион тетрафтороборага, колебательный спектр, молекулярно-динамическое моделирование, коэффициент диффузии.

І.С. Вовчинський, О.М. Калугін. Силове поле аніону тетрафтороборату для молекулярно-динамічного моделювання: новий підхід.

Харківський національний університет імені В.Н. Каразіна, хімічний факультет, кафедра неорганічної хімії, майдан Свободи, 4, Харків, 61022, Україна

Розробка нових пристроїв накопичення електричної енергії, включаючи суперконденсатори, а також оптимізація існуючих вимагають, не тільки нових електролітів, а й глибокого та повного розуміння процесів, що відбуваються в розчинах електролітів. Спектральні методи і класичне молекулярно-динамічне моделювання (МДМ) завоювали репутацію надійного інструменту для вирішення таких завдань. Відправною точкою будь-якого МДМ є вибір або розробка силових полів для всіх модельованих частинок. Поєднання методів коливальної спектроскопії і молекулярної динаміки може забезпечити глибоке розуміння структури та динаміки іонної підсистеми. У зв'язку з цим до відтворення коливальних спектрів має бути включено в вимоги до силових полях найбільш поширених компонентів електроліту.

Багато хто з сучасних суперконденсаторів засновані на органічних електролітах, що складаються з наведених апротонних розчинників, таких як ацетонітрил, пропіленкарбонат, γ-бутіролактон і солі четвертинного амонію з тетрафторборатом і гексафторфосфатом в якості аніонів.

Метою цієї роботи є розробка нового силового поля для тетрафторборат-аніону ($BF_4^-$), здатного відтворювати не тільки поступальну дифузію в середовищі ацетонітрилу, але і спектральні властивості цього іона в конденсованої фазі. Оскільки знайдені в літературі силові поля $BF_4^-$ не задовольняють цим вимогам, були проведені інтенсивні квантово-хімічні розрахунки $BF_4^-$ на рівні теорії M06-2X/6-311++G(d,p) для побудови поверхні потенційної енергії. щодо зв'язків B–F і кутів F–B–F з подальшою оцінкою відповідних констант внутрішньо молекулярних потенціалів. Об'єднуючи отримані силові константи зв'язку і кута з частковими зарядами на атомах B і F, розрахованими на тому ж рівні теорії, і літературними значення параметрів потенціалу Леннарда-Джонса, була створена нова модель силового поля для аніону BF4-. На підставі проведеного МД-моделювання іона $BF_4^-$ в нескінченно розбавленому розчині в ацетонітрилі було доведено, що отримана модель здатна відтворювати як транспортні властивості, так і внутрийонні коливання тетрафторборат-аніону.

**Ключові слова:** аніон тетрафтороборату, коливальний спектр, молекулярно-динамічне моделювання, коефіцієнт дифузії.

УДК 004.94 + 54-145.4 + 544.034.1 + 544.272 + 544.623

# МЕЖЧАСТИЧНЫЕ ВЗАИМОДЕЙСТВИЯ И ДИНАМИКА В РАСТВОРАХ BmimBF₄ И LiBF₄ В ПРОПИЛЕНКАРБОНАТЕ: МД МОДЕЛИРОВАНИЕ

**Д.С. Дударев [a], Е.О. Логачёва [b], Я.В. Колесник [c], О.Н. Калугин [d]**

*\* Харьковский национальный университет имени В.Н. Каразина, химический факультет, пл. Свободы, 4, Харьков, 61022, Украина*

a) ✉ dimadudariev@gmail.com    https://orcid.org/0000-0002-2556-8036
b) ✉ ekaterinalogatcheva@gmail.com    https://orcid.org/0000-0001-7826-8320
c) ✉ ykolesnik@karazin.ua    https://orcid.org/0000-0002-9569-4556
d) ✉ onkalugin@gmail.com    https://orcid.org/0000-0003-3273-9259

Ионные жидкости приобрели огромную популярность в последние десятилетия благодаря комплексу уникальных свойств. Несмотря на широкое использование смесей ионных жидкостей с апротонными диполярными растворителями в электрохимии, актуальным остаётся прогнозирование их макроскопических, в первую очередь транспортных, свойств исходя из микроскопической картины всей совокупности межчастичных взаимодействий в таких системах. Метод молекулярно-динамического моделирования (МДМ) является одним из наиболее мощных инструментов решения подобного рода задач. Однако одной из нерешённых проблем классического МДМ ион-молекулярных систем является корректный учёт эффектов поляризации. В последнее время для её решения было предложено использовать вариацию эффективных зарядов ионов в растворах.

В настоящей работе представлены результаты МДМ структурных и динамических свойств растворов тетрафтороборатов 1-бутил-3-метилимидазолия (BmimBF₄) и лития (LiBF₄) в пропиленкарбонате (PC) при 298.15 К в *NPT* ансамбле с использованием программных пакетов GROMACS и MDNAES.

Показана возможность воспроизведения экспериментальных динамических свойств (коэффициентов диффузии катионов и растворителя, вязкости, а также электропроводности) бинарных систем на основе смесей ионных жидкостей с PC в широком интервале концентраций с учётом эффектов поляризации путём уменьшения парциальных зарядов на атомах ионов.

Структура сольватной оболочки катионов была изучена в рамках функций радиального распределения, распределения координационных чисел, а также наличия водородных связей между органическим катионом и молекулами растворителя. Результаты указывают на более прочную и структурированную сольватную оболочку катиона Li⁺ по сравнению с Bmim⁺, что согласуется с выводами о подвижности этих катионов. Времена переориентации молекул пропиленкарбоната и времена их жизни в рамках первых сольватных оболочек катионов оказались в несколько раз выше для катиона лития.

**Ключевые слова:** тетрафтороборат 1-бутил-3-метилимидазолия, тетрафтороборат лития, пропиленкарбонат, молекулярно-динамическое моделирование, эффекты поляризации, микроструктура, микродинамика, сольватная оболочка.

## Введение

В области электрохимических применений семейство 1-алкил-3-метилимдазолиевых (Rmim⁺) ионных жидкостей (ИЖ) с различными анионами (PF₆⁻, BF₄⁻, CF₃SO₃⁻ и т.д.) выглядит перспективным кандидатом для основных компонентов различных электрохимических устройств [1-3]. Среди ключевых факторов, способствующих применению этих ИЖ в электрохимических устройствах, важнейшей является подвижность ионов, которая ограничена присущей ионным жидкостям высокой вязкостью [4,5]. Эта проблема обычно решается смешением ионных жидкостей с низкомолекулярными электрохимически устойчивыми растворителями (ацетонитрил (AN), γ-бутиролактон (γ-BL) и пропиленкарбонат (PC)). Использование смесей ИЖ с молекулярными жидкостями также позволяет существенно снизить стоимость электролитной части электрохимических устройств [4,5].

Именно из-за своих уникальных свойств смеси ионных жидкостей с молекулярными растворителями вызывают интерес исследователей на протяжении уже более чем двух десятков лет. В числе прочих – наличие максимума на кривой зависимости электропроводности от мольной доли ионной жидкости [6-8], что объясняется возникновением специфических ассоциативных взаимодействий в новых растворах [9].

Как известно, методы молекулярного моделирования, в частности – молекулярно-динамического моделирования (МДМ), являются одними из самых мощных методов анализа таких систем [10-16]. В числе прочего, они позволяют исследовать микроскопические характеристики ионной сольватации в них, которые являются труднодоступными для получения в «классических» экспериментах [17-19].

Одной из актуальных проблем МДМ ион-молекулярных систем является учёт эффектов поляризации при моделировании. Эффекты поляризации оказывают довольно существенное влияние на результаты МДМ, например, на коэффициенты диффузии, которые в ряде случаев оказываются заниженными в 5-10 раз по сравнению с экспериментальными данными [20-22]. Одним из возможных решений проблемы является учёт эффектов поляризации посредством корректировки (фактически – снижения) эффективного заряда атомов в частице (ионе). Физическим обоснованием такого подхода являются *ab initio* расчёты, указывающие на значительный перенос заряда между ионами ионных жидкостей [23].

В настоящей работе исследована возможность учёта эффектов поляризации в системах $LiBF_4$ – PC и $BmimBF_4$ – PC в рамках молекулярно-динамического моделирования путём вариации (снижения) парциальных зарядов на атомах соответствующих ионов.

Валидация силовых полей катионов и анионов проведена по совокупности транспортных свойств, как отдельных частиц, так и электролитных систем в целом.

Особое внимание в работе уделено анализу микроструктуры и микродинамики сольватации катионов, во многом определяющих макроскопические, практически важные свойства ион-молекулярных систем.

### Детали молекулярно-динамического моделирования

Выбранные для изучения системы «ИЖ + растворитель» состоят из катионов 1-бутил-3-метилимидазолия ($Bmim^+$), тетрафтороборат анионов ($BF_4^-$) и молекул растворителя – пропиленкарбоната (PC). Для сравнения также была изучена аналогичная бинарная система с заменой большого многоатомного катиона на одноатомный катион лития, $LiBF_4$-PC.

Для получения реалистичных динамических свойств и учёта эффектов поляризации использовались модели силовых полей с уже сниженными нецелочисленными зарядами на катионах и анионе [23]. Для $Li^+$ была использована модель [24] с вариацией заряда на катионе. Для растворителя использовалась полноатомная нежёсткая и неполяризуемая модель силового поля [25].

Строение катиона и растворителя с обозначениями атомов приведено на рисунке 1.
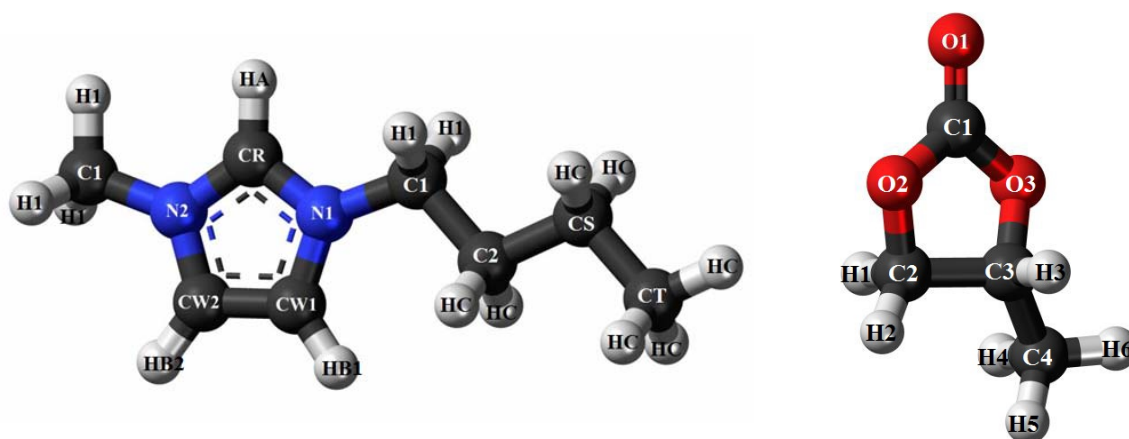


**Рисунок 1.** Обозначения атомов катиона $Bmim^+$ и PC.

Потенциалы внутримолекулярных взаимодействий были представлены суммой потенциалов связей ($r$), валентных ($\theta$) и двугранных углов ($\varphi$) [23,24]

$$U_{intra} = \sum_{ij}^{bonds} \frac{K_{r,ij}}{2} \left( r_{ij} - r_{0,ij} \right)^2 + \sum_{ijk}^{angle} \frac{K_{\theta,ijk}}{2} \left( \theta_{ijk} - \theta_{0,ijk} \right)^2 + \sum_{ijkl}^{dihed} \sum_{n=1}^{5} A_n \cos^{n-1} \left( \varphi_{ijkl} \right). \tag{1}$$

В формуле (1) $K_{r,ij}$ и $K_{\theta,ijk}$ - силовые константы, а индекс «0» соответствует равновесным значениям валентных связей и углов. Двугранный угол $\varphi$ выбирали таким образом, чтобы он равнялся 180° для транс- и 0° для цис-конфигураций.

Потенциальная энергия межмолекулярных взаимодействий вычислялась как сумма потенциалов Леннард-Джонса и кулоновского. Последний вычисляли по методу Particle mesh Ewald (PME) в GROMACS [26] и по методу реактивного поля в MDNAES [27]

$$U_{inter} = \sum_i \sum_{j \neq 1} \left( 4\varepsilon_{ij} \left[ \left( \frac{\sigma_{ij}}{r_{ij}} \right)^{12} - \left( \frac{\sigma_{ij}}{r_{ij}} \right)^6 \right] + \frac{1}{4\pi\varepsilon_0} \frac{q_i q_j}{r_{ij}} \right). \qquad (2)$$

Параметры межмолекулярных взаимодействий для катионов и BF$_4^-$ представлены в таблице 1.

**Таблица 1.** Параметры моделей силовых полей ионов. Колонки «заряд (±0.79)» и «заряд (±1)» указывают на различные использованные заряды для ионов (первые – из источника [23], вторые – пересчитанные нами согласно методике [28] с целью воспроизведения моделей потенциальных полей с целочисленными зарядами для сравнения).

| Атом | Масса, а.е.м. | $\sigma$, нм | $\varepsilon$, кДж/моль | Заряд (±0.79) | Заряд (±1) |
|---|---|---|---|---|---|
| Bmim$^+$ | | | | | |
| CR | 12.0112 | 0.355 | 0.29288 | -0.010 | -0.013 |
| N | 14.0067 | 0.325 | 0.71128 | 0.140 | 0.184 |
| CW | 12.0112 | 0.355 | 0.29288 | -0.110 | -0.144 |
| HA | 1.00797 | 0.170 | 0.04184 | 0.180 | 0.236 |
| HB | 1.00797 | 0.200 | 0.12552 | 0.170 | 0.223 |
| CT | 12.0112 | 0.350 | 0.27614 | -0.294 | -0.294 |
| C1 | 12.0112 | 0.350 | 0.27614 | -0.250 | -0.250 |
| C2 | 12.0112 | 0.350 | 0.27614 | -0.076 | -0.076 |
| CS | 12.0112 | 0.350 | 0.27614 | -0.196 | -0.196 |
| H1 | 1.00797 | 0.250 | 0.12552 | 0.120 | 0.120 |
| HC | 1.00797 | 0.250 | 0.12552 | 0.098 | 0.098 |
| Li$^+$ | | | | | |
| Li | 6.94 | 0.202590 | 0.0765672 | 0.79 | 1 |
| BF$_4^-$ | | | | | |
| B | 10.8110 | 0.368 | 0.25104 | 1.01 | 1.28 |
| F | 18.9984 | 0.280 | 0.08368 | -0.45 | -0.57 |

Моделирование проводили с использованием программного пакета GROMACS [26] и MDNAES [27]. Для всех этапов и систем использовался термостат *V-rescale* с временем релаксации 10 пс и баростат Берендсена с временем релаксации 1000 пс. Временной шаг моделирования – 0.5 фс, температура – 298.15 К, ансамбль – *NPT*, форма ячейки – кубическая.

Были проанализированы следующие системы: бесконечно разбавленные растворы катионов Bmim$^+$, Li$^+$ и аниона BF$_4$ (1 молекула иона + 499 молекул PC), смеси пропиленкарбоната с ионной жидкостью различного мольного состава (таблица 2).

**Таблица 2.** Состав моделируемых систем

| Мольная доля ИЖ | $N(\text{kat}^+) = N(\text{BF}_4^-)$ | $N(\text{PC})$ |
|---|---|---|
| 0.01 | 5 | 495 |
| 0.05 | 25 | 475 |
| 0.2 | 100 | 400 |
| 0.5 | 250 | 250 |
| 0.75 | 375 | 125 |

МДМ проводили в четыре этапа: уравновешивание, валидация моделей ионов (воспроизведение экспериментальных данных отобранными моделями потенциальных полей по определённым критериям), расчёт структурных свойств и микродинамических свойств сольватных оболочек катионов.

Для уравновешивания всех моделируемых систем проводили моделирование длительностью 1 нс. О достижении состояния термодинамического равновесия судили по отсутствию временного дрейфа полной энергии систем.

Правильность выбора потенциальных моделей ионов подтверждали по воспроизведению динамических свойств бесконечно разбавленных систем. Время моделирования для бесконечно разбавленных систем составило 25 нс, для систем конечной концентрации – 10 нс.

На третьем этапе МДМ изучали структурные свойства: функции радиального распределения (ФРР), водородные связи и распределение координационных чисел (КЧ) в сольватных оболочках катионов. Анализ производился при помощи программного пакета TRAVIS [29]. Для изучения структурных свойств проводилось моделирование бесконечно разбавленных систем с катионами $Bmim^+$ или $Li^+$ на протяжении 1 нс.

Изучение динамики молекул растворителя в сольватной оболочке катионов в бесконечно разбавленных системах проводили в программном пакете MDNAES [27]. Время моделирования составило 10 нс.

Коэффициент трансляционной самодиффузии рассчитывали из среднеквадратического смещения по методу наименьших квадратов

$$\lim_{t \to \infty} \left\langle \left| \mathbf{r}_i(t) - \mathbf{r}_i(0) \right|^2 \right\rangle = 6Dt . \tag{3}$$

Вязкость ($\eta$) и электропроводность ($\sigma$) находили по формулам Грина-Кубо [9,27,30,31]:

$$\eta = \frac{1}{Vk_BT} \int_0^\infty d\tau \left\langle \mathbf{P}^{\alpha\beta}(0)\mathbf{P}^{\alpha\beta}(\tau) \right\rangle, \quad \alpha, \beta = x, y, z , \tag{4}$$

$$\sigma = \frac{1}{3Vk_BT} \int_0^\infty \left\langle j(0)j(t) \right\rangle dt , \tag{5}$$

$$j = \sum_i q_i v_i , \tag{6}$$

где $\mathbf{P}^{\alpha,\beta}$, $j$, $V$ – недиагональные элементы тензора напряжения, мгновенный ток системы и объём системы, соответственно.

Оценку динамики молекул растворителя в сольватной оболочке катионов производили в терминах автокорреляционных функций дипольного момента $C_\mu(t)$ и времени жизни молекул в сольватной оболочке $C_{rt}(t)$ (ур. 7,8) [27]:

$$C_\mu(t) = \left\langle \frac{\boldsymbol{\mu}(0)\boldsymbol{\mu}(t)}{|\boldsymbol{\mu}(0)||\boldsymbol{\mu}(t)|} \right\rangle, \tag{7}$$

$$C_{rt}(t) = \frac{\left\langle \sum_i p(0)p(t) \right\rangle}{n}, \tag{8}$$

а также соответствующих характеристических времён, аппроксимируя АКФ $C_\mu(t)$ и $C_{rt}(t)$ моноэкспоненциальной зависимостью.

$$C(t) = \exp\left(-\frac{t}{\tau}\right). \tag{9}$$

### Валидация моделей потенциальных полей катионов

Как уже упоминалось ранее, для катионов и аниона в [23] предложено использовать нецелочисленные заряды. Решено было сравнить такие системы с традиционными с целыми зарядами по величине коэффициента диффузии для бесконечно разбавленных растворов (255 PC + 1 $Bmim^+/Li^+/BF_4^-$). Результаты представлены в таблице 3.

Экспериментальные величины коэффициента диффузии находили из предельной молярной электропроводности по уравнению Нернста-Эйнштейна:

$$D_i = \frac{RT}{z_i^2 F^2} \Lambda_i^0 . \tag{10}$$

**Таблица 3.** Коэффициенты диффузии ионов в бесконечно разбавленных растворах в PC для моделей ионов с разными зарядами

| Ион | Заряд | $D \cdot 10^{10}$, м$^2$/с | Эксперимент* |
|---|---|---|---|
| Bmim$^+$ | +1 | 2.3±0.6 | 3.8 |
| | +0.79 | 3.1±0.5 | |
| Li$^+$ | +1 | 0.8±0.4 | 2.2 |
| | +0.79 | 2.2±0.6 | |
| BF$_4^-$ | -1 | 3.7±0.8 | 5.0 |
| | -0.79 | 5.3±0.5 | |

\* Значения коэффициентов самодиффузии найдены по экспериментальным значениям предельной ионной проводимости [32].

Результаты моделирования указывают, что зарядовые модели со значением ±0.79 лучше воспроизводят экспериментальные данные по динамическим свойствам. Соответственно, подобный учёт методов поляризации может улучшить воспроизведение динамических свойств ионов в бесконечно разбавленных системах. Для проверки подобного подхода в смесях молекулярных растворителей с ионными жидкостями было решено также использовать эти модели с модифицированными зарядами на ионах.

На рис. 2 представлены результаты МД моделирования коэффициентов самодиффузии ионов и молекул растворителя, а также вязкости и электропроводности растворов в зависимости от состава бинарных систем ионная подсистема – пропиленкарбонат в сравнении с экспериментальными данными.

Стоит упомянуть, что в отличие от ионных жидкостей с органическим катионом, LiBF$_4$ растворяется в PC ограниченно. Установлено [33], что насыщенный раствор имеет мольную долю около 0.40, поэтому расчёты проводились только для систем с χ = 0.01, 0.05, 0.20.

Как видно из рис. 2, полученные по результатам МД моделирования транспортные характеристики достаточно хорошо согласуются с экспериментальными данными. Отдельно стоит отметить воспроизведение наличия и положения максимума на кривой зависимости электропроводности от мольной доли ИЖ для обоих типов катионов.

Из анализа рис. 2 можно заключить, что для растворов LiBF$_4$ характерны меньшие величины коэффициента диффузии и электропроводности, большие значения вязкости и более резкое изменение всех величин при изменении концентрации в сравнении с BmimBF$_4$. Эта закономерность наблюдается даже с учётом ограниченных экспериментальных данных по LiBF$_4$ в PC и меньшему количеству рассчитанных для него точек на кривых. Меньший коэффициент диффузии в системе со сферическим катионом является следствием меньшей подвижности молекул в системе. На этот же факт указывает и различие в вязкости – большая вязкость для систем с литием является следствием сниженной подвижности, что вызвано особенностями сольватации катиона Li$^+$ по сравнению с Bmim$^+$.

### Результаты и обсуждение

*Микроструктура сольватных оболочек катионов.* Для бесконечно разбавленной системы Bmim$^+$ в PC были получены ФРР для пар H--O1 (атом водорода имидазольного кольца – атом кислорода карбонильной группы), на которых можно проследить локализацию молекул растворителя вокруг катиона (рис. 3(а)). Видно, что наибольшая локализация молекул растворителя (причиной которой является образование водородных связей) происходит вокруг атомов водорода имидазольного кольца. Также наблюдается незначительная локализация вокруг атомов водорода метильной группы. При этом для первых можно выделить довольно чёткий радиус первой сольватной оболочки (ПСО) ~0.46 нм. На рис. 3(б) построен аналогичный график ФРР в системе с катионом лития Li$^+$--O (три кислорода пропиленкарбоната). На нём явно для пары Li$^+$--O1 наблюдается очень выраженный первый максимум с радиусом ПСО ~0.31 нм.

Из сравнения ФРР для катионов Bmim$^+$ и Li$^+$ (рис. 3) можно сделать вывод о том, что для второго характерна более сильная сольватация молекул PC. Для подтверждения этого были получены распределения координационных чисел (КЧ) в сольватных оболочках катионов в бесконечно разбавленных растворах (рис. 4). Вновь для Li$^+$ наблюдается сольватация с преимущественным КЧ 5, тогда как для Bmim$^+$ возможно большее количество вариантов одновре-

менного присутствия молекул РС с преимущественным КЧ 3, что наряду с данными ФРР указывает на менее сильную сольватацию молекул растворителя вокруг органического несимметричного катиона.
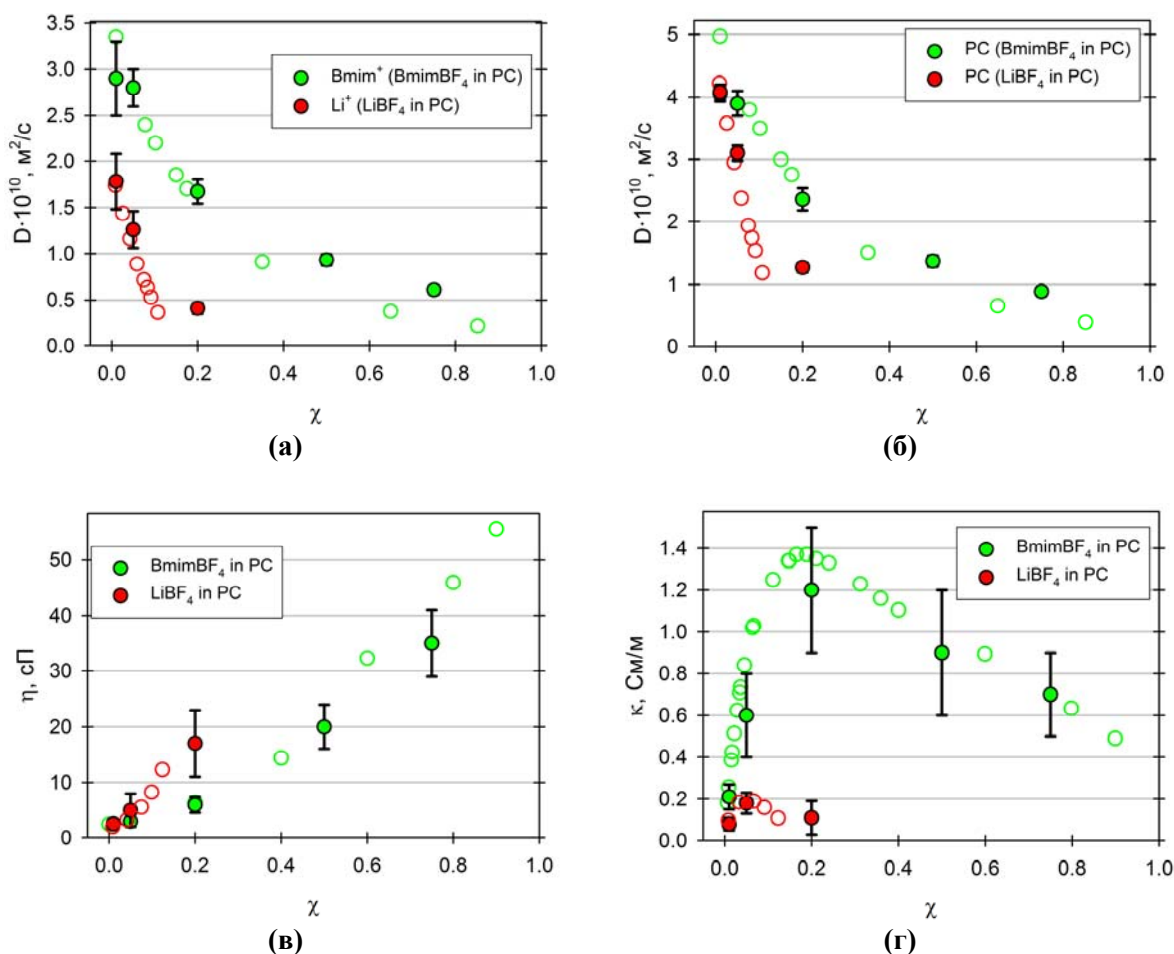


**(а)**



**(б)**



**(в)**



**(г)**

**Рисунок 2.** Зависимость коэффициента диффузии $Bmim^+$ и $Li^+$ **(а)**, РС **(б)**, вязкости **(в)** и электропроводности системы **(г)** от мольной доли ИЖ. Пустые метки соответствуют экспериментальным данным [32-36].
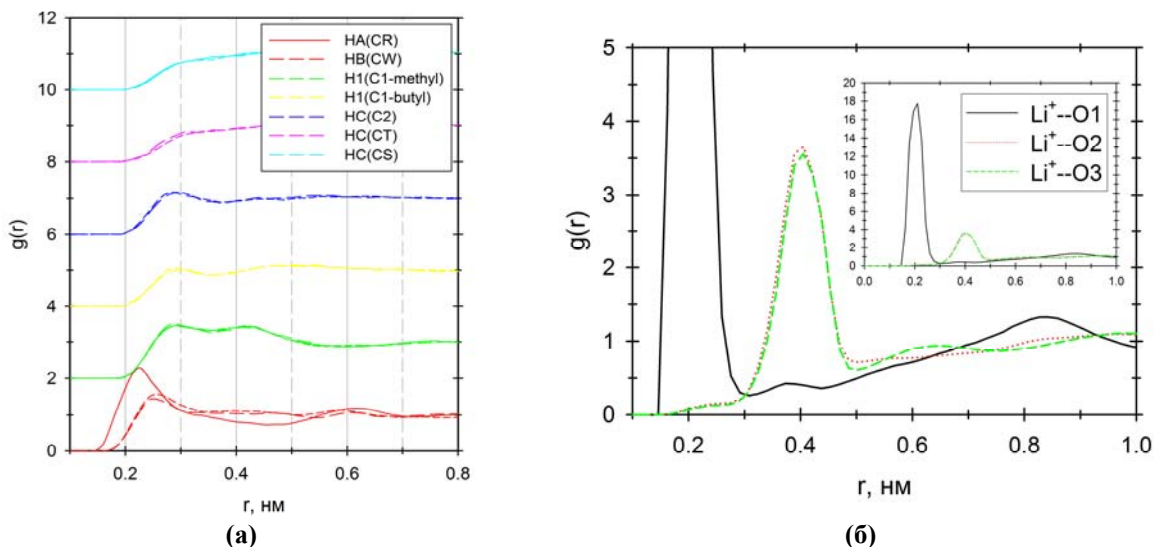


**(а)**



**(б)**

**Рисунок 3.** ФРР для пар H--O1 ($Bmim^+$ в РС) **(а)** и Li--O ($Li^+$ в РС) **(б)**.

Анализ наличия слабых водородных связей между всеми атомами водорода катиона Bmim[+] и атомом кислорода O1 молекул растворителя PC проводили, отобрав критерии для существования слабой водородной связи как H--O< 0.32 нм, C--O< 0.40 нм [37]. Расстояния находили из положения максимума на ФРР для первого соседа по всем искомым парам. Результаты представлены на рисунке 5.

Для удобства упомянутые расстояния на рис. 5 являются максимальными на соответствующих осях абсцисс и ординат. Таким образом, все атомы водорода 1-бутил-3-метилимидазолия образуют слабую водородную связь с кислородами молекул пропиленкарбоната. Самую сильную водородную связь (относительно остальных атомов водорода катиона) образует атом HA(CR), затем примерно равные по силе – HB1(CW1), HB2(CW2) и три атома H1(C1) метильной группы. Такой порядок силы связи следует ожидать, учитывая суммарный положительный заряд для трёх атомов водорода метильной группы (они образуют более сильную водородную связь, чем атомы H1(C1) бутильного радикала), эти же результаты подтверждаются функциями радиального распределения, полученными ранее в данной работе.
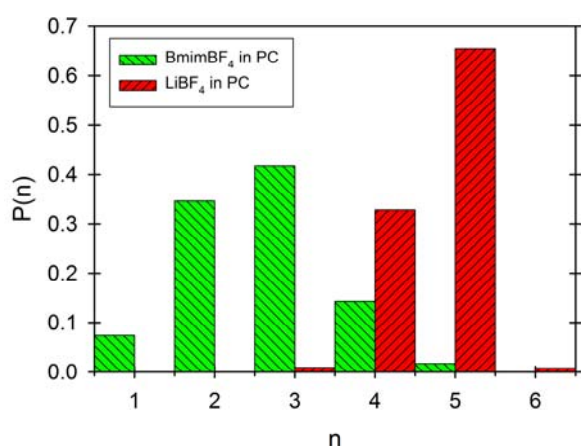


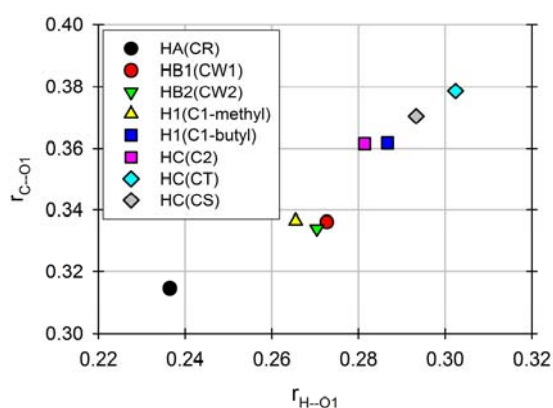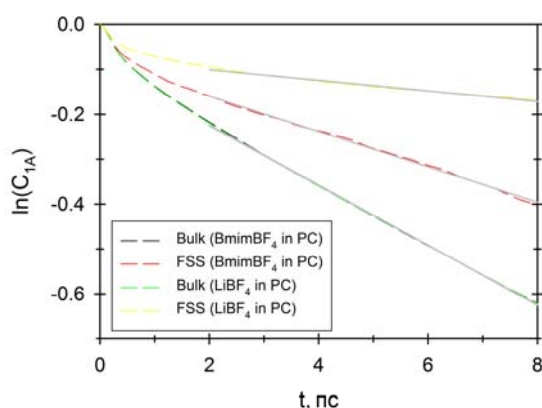**Рисунок 4.** Распределение КЧ в сольватных оболочках катионов

**Рисунок 5.** Зависимость расстояния C--O1 от H--O1 (Bmim[+] в PC)
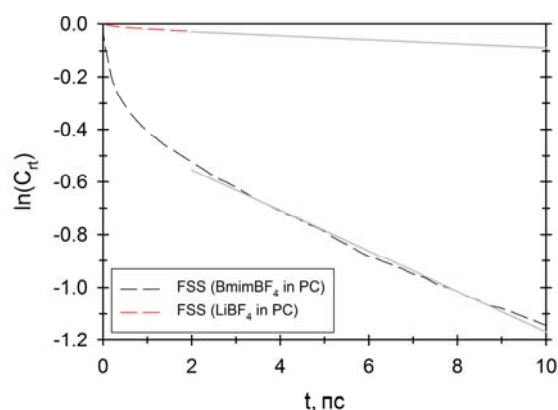


**(а)**          **(б)**

**Рисунок 6.** АКФ направления дипольного момента молекул растворителя **(а)** и времени жизни молекул растворителя в ПСО катионов **(б)**. «Bulk» соответствует объёму растворителя, «FSS» – ПСО катионов.

*Динамика ионной сольватации.* При анализе микродинамики сольватации катионов были найдены времена переориентации молекул растворителя $\tau_\mu$ и их времена жизни в первой сольватной оболочке (ПСО) катионов $\tau_{rt}$ по уравнениям (7-9). Результаты расчётов представлены в таблице 4 и на рис. 6.

**Таблица 4.** Времена переориентации молекул РС и их пребывания в ПСО катионов

| Область | $\tau_\mu$, пс | | $\tau_{rt}$, пс | |
|---|---|---|---|---|
| | Bmim$^+$ | Li$^+$ | Bmim$^+$ | Li$^+$ |
| Объём растворителя | 14.9 | 15.0 | — | — |
| ПСО | 25.4 | 85.3 | 13.0 | 134.5 |

По полученным результатам можно сделать вывод, что катион лития является структурообразующим (время переориентации в рамках ПСО в ~5.5 раз превышает аналогичное в остальном объёме системы) и создаёт более прочную сольватную оболочку в сравнении с органическим катионом.

С другой стороны, для 1-бутил-3-метилимидазолия также характерна положительная сольватация и структурообразование вокруг катиона (время переориентации молекул растворителя почти вдвое больше в ПСО по сравнению с остальным объёмом раствора).

### Выводы

В работе исследована возможность учёта эффектов поляризации в системах LiBF$_4$ – PC и BmimBF$_4$ – PC в рамках молекулярно-динамического моделирования путём вариации (снижения) зарядов атомов катионов и анионов. Это позволило воспроизвести не только экспериментальные коэффициенты диффузии катионов и аниона в бесконечно разбавленных растворах, но и воспроизвести экспериментальные концентрационные зависимости диффузии частиц, вязкости и электропроводности бинарных систем электролит-молекулярный растворитель. Полученные результаты могут служить доказательством того, что предложенный подход может быть использован для МД моделирования аналогичных систем с другими ионными жидкостями, простыми солями и молекулярными растворителями.

Используя аппарат пространственных и временных корреляционных функций, была детально изучена микроструктура и микродинамика сольватных оболочек катионов Bmim$^+$ и Li$^+$ в PC.

Анализ структурных характеристик указывает на образование слабых водородных связей между катионами 1-бутил-3-метилимидазолия и молекулами растворителя. Также обнаружено, что сольватная оболочка Li$^+$ более структурирована и прочна по сравнению с аналогичной для Bmim$^+$. Результаты анализа микродинамики указывают на то, что молекулы PC в первой сольватной оболочке Bmim$^+$ являются более подвижными и обладают меньшим временем удержания по сравнению с оболочкой Li$^+$.

### Благодарность

### Литература / References

1. Hallett J.P., Welton T. Room-Temperature Ionic Liquids: Solvents for Synthesis and Catalysis. *Chem. Rev.* **2011**, *111*, 3508-3576.
2. Torimoto T., Tsuda T., Okazaki K.I., Kuwabata S. New Frontiers in Materials Science Opened by Ionic Liquids. *Adv. Mater.* **2010**, *22*, 1196-1221.
3. Olivier-Bourbigou H., Magna L., Morvan D. Ionic liquids and catalysis: recent progress from knowledge to applications. *Appl. Catal. A* **2010**, *373*, 1-56.
4. MacFarlane D.R., Forsyth M., Howlett P.C., Pringle J.M., Sun J., Annat G., Neil W., Izgorodina E.I. Ionic Liquids in Electrochemical Devices and Processes: Managing Interfacial Electrochemistry. *Acc. Chem. Res.* **2007**, *40*, 1165-1173.
5. MacFarlane D.R., Tachikawa N., Forsyth M., Pringle J.M., Howlett P.C., Elliott G.D., Davis H.J., Watanabe M., Simon P., Angell C. Energy applications of ionic liquids. *Energy Environ. Sci.* **2014**, *7*, 232-250.

6. Nishida T., Tashiro Y., Yamamoto M. Physical and electrochemical properties of 1-alkyl-3-methylimidazolium tetrafluoroborate for electrolyte. *J. Fluor. Chem.* **2003**, *120*, 135-141.

7. Kalugin O.N., Voroshylova I.V., Riabchunova A.V., Lukinova E.V., Chaban V.V. Conductometric Study of Binary Systems Based on Ionic Liquids and Acetonitrile in a wide Concentration Range. *Electrochim. Acta* **2013**, *105*, 188-199.

8. Marcus Y., Hefter G. Ion Pairing. *Chem. Rev.* **2006**, *106*, 4585-4621.

9. Dommert F., Schmidt J., Qiao B., Zhao Y., Klekeler C., Delle Site L., Berger R., Holm C. Comparative Study of Two Classical Force Fields on Statics and Dynamics of [EMIM][BF$_4$] Investigated Via Molecular Dynamics Simulations. *J. Chem. Phys.* **2008**, *129*, 224501.

10. Gkagkasa K., Ponnuchamyb V., Dašićc M., Stankovićc I. Molecular dynamics investigation of a model ionic liquid lubricant for automotive applications. *Tribol. Int.* **2017**, *113*, 83-91.

11. Thomas M., Sancho Sanz I., Holloczki O., Kirchner B. Ab initio molecular dynamics simulations of ionic liquids. In *NIC Symposium 2016*, Julich, Germany, Feb 11-12, 2016; Binder K., Muller M., Kremer M., Schnurpfeil A., Eds.; Forschungszentrum Jülich GmbH, Zentralbibliothek, pp 117-124.

12. Yan T., Burnham C.J., Del Pópolo M.G., Voth G.A. Molecular Dynamics Simulation of Ionic Liquids: The Effect of Electronic Polarizability. *J. Phys. Chem. B* **2004**, *108* (32), 11877-11881.

13. Batista M.L.S., Coutinho J.A.P., Gomes J.R.B. Prediction of Ionic Liquids Properties through Molecular Dynamics Simulations *Curr. Phys. Chem.* **2014**, *4* (2), 151-172.

14. Fatemi S.M., Foroutan M. Recent findings about ionic liquids mixtures obtained by molecular dynamics simulation *J. Nanostructure Chem.* **2015**, *5* (3), 243-253.

15. Docampo-Álvarez B., Gómez-González V., Montes-Campos H., Otero-Mato J.M., Méndez-Morales T., Cabeza O., Gallego L.J., Lynden-Bell R.M., Ivaništšev V.B., Fedorovʹ M.V., Varela L.M. Molecular dynamics simulation of the behaviour of water in nano-confined ionic liquid–water mixtures. *J. Phys.: Condens. Matter* **2016**, *28*, 464001.

16. Dasari S., Mallik B.S. Biosolvation Nature of Ionic Liquids: Molecular Dynamics Simulation of Methylated Nucleobases in Hydrated 1-Ethyl-3-methylimidazolium Acetate. *ACS Omega* **2018**, *3* (7), 8344-8354.

17. Pratik D., Jindal K.S. Recent advances in molecular simulations of ionic liquid–ionic liquid mixtures. *COGSC* **2019**, *18*, 90-97.

18. Gómez-González V., Docampo-Álvarez B., Otero-Mato J.M., Cabeza O., Gallego L.J,, Varela L.M. Molecular dynamics simulations of the structure of mixtures of protic ionic liquids and monovalent and divalent salts at the electrochemical interface. *Phys. Chem. Chem. Phys.* **2018**, *20*, 12767-12776.

19. Bedrov D., Piquemal J.-P., Borodin O., MacKerell A.D., Roux B., Schröder C. Molecular Dynamics Simulations of Ionic Liquids and Electrolytes Using Polarizable Force Fields. *Chem. Rev.* **2019**, *119*, 7940-7995.

20. Bhargava B.L., Balasubramanian S. Refined Potential Model for Atomistic Simulations of Ionic Liquid [Bmim][PF$_6$]. *J. Chem. Phys.* **2007**, *127*, 114510.

21. Köddermann T., Paschek D., Ludwig R. Molecular Dynamic Simulations of Ionic Liquids: A Reliable Description of Structure, Thermodynamics and Dynamics. *Chemphyschem* **2007**, *8*, 2464-2470.

22. Cadena C., Zhao Q., Snurr R.Q., Maginn E.J. Molecular Modeling and Experimental Studies of the Thermodynamic and Transport Properties of Pyridinium-Based Ionic Liquids. *J. Phys. Chem. B* **2006**, *110*, 2821-2832.

23. Mondal A., Balasubramanian S.J. Quantitative prediction of physical properties of imidazolium based room temperature ionic liquids through determination of condensed phase site charges: a refined force field. *Phys. Chem.* **2014**, *118*, 3409-3422.

24. Chernozhuk T.V., Kalugin O.N., Kolesnik Ya.V. Microstructure and dynamics of single charged ions in propylene carbonate. *Kharkov Univ. Bull. Chem. Ser.* **2013**, *22* (45), 25-38.

25. Koverga V.A., Voroshylova I.V., Smortsova Y., Miannay F.A., Cordeiro N., Idrissi A., Kalugin O.N. Local structure and hydrogen bonding in liquid γ-butyrolactone and propylene carbonate: A molecular dynamics simulation. *J. Mol. Liq.* **2019**, *287*, 110912.

26. Abraham M.J., Murtola T., Schulz R., Pall S., Smith J.C., Hess B., Lindahl E. GROMACS: High Performance Molecular Simulations Through Multi-Level Parallelism from Laptops to Supercomputers. *SoftwareX* **2015**, *1-2*, 19-25.

27. Kalugin O.N., Kolesnik Ya.V. MDNAES: the program set for computer simulation of ion-molecular systems by using molecular dynamics method. *Kharkov Univ. Bull. Chem. Ser.* **1999**, *4* (27), 58-79.

28. Koverga V., Kalugin O.N., Miannay F.A., Smortsova Y., Goloviznina K., Marekha B., Jedlovszky P., Idrissi A. The local structure in the BmimPF$_6$/acetonitrile mixture: the charge distribution effect. *Phys. Chem. Chem. Phys.* **2018**, *20*, 21890-21902.

29. Brehm M., Kirchner B. TRAVIS - a free analyzer and visualizer for Monte Carlo and molecular dynamics. *J. Chem. Inf. Model.* **2011**, *51* (8), 2007-2023.

30. Hess B. Determining the shear viscosity of model liquids from molecular dynamics simulations. *J. Chem. Phys.* **2002**, *116*, 209-217.

31. Hansen J.P., McDonald I.R. Statistical mechanics of dense ionized matter. IV. Density and charge fluctuations in a simple molten salt. *Phys. Rev. A* **1975**, *11*, 2111-2123.

32. Ryabchunova A.V., Gavryukova E.O., Kirichenko A.A., Kalugin O.N. Electrical conductivity of solutions of imidazolium ionic liquids in propylene carbonate over a wide range of concentrations. In *Modern problems of electrochemistry: education, science, production: a collection of scientific works*, Proceedings of the VII Ukrainian Congress of Electrochemistry, Kharkiv, Ukraine, Sep 21-25, 2015; Omelchuk A.O., Sahnenko M.D., Eds.; Kharkiv: NTU "KhPI", 2015, pp 155-156.

33. Varlamova T.M., Yurina E.S. Lithium perchlorate (tetrafluoroborate)-diethyl carbonate-propylene carbonate electrolyte systems. *Russ. J. Phys. Chem.* **2006**, *80*, 1265-1268.

34. Marekha B.A., Kalugin O.N., Bria M., Buchner R., Idrissi A. Translational Diffusion in Mixtures of Imidazolium ILs with Polar Aprotic Molecular Solvents. *J. Phys. Chem. B* **2014**, *118*, 5509-5517.

35. Phuoc H.L., Tran A.T., Walczyk D.J., Miller A.M., Yu L. Conductivity, viscosity, and thermodynamic properties of propylene carbonate solutions in ionic liquids. *J Mol. Liq.* **2017**, *246*, 215-220.

36. Richardson P.M., Voice A.M., Ward I.M. Pulsed-Field Gradient NMR Self Diffusion and Ionic Conductivity Measurements for Liquid Electrolytes Containing LiBF$_4$ and Propylene Carbonate. *Electrochim. Acta* **2014**, *130*, 606-618.

37. Grabowski S.J. Weak to Strong Hydrogen Bonds. In *Hydrogen Bonding - New Insights*. Dordrecht: Springer, 2006; pp 149-192.

Д.С. Дударєв, К.О. Логачова, Я.В. Колесник, О.М. Калугін. Міжчастинкові взаємодії та динаміка у розчинах BmimBF$_4$ і LiBF$_4$ у пропіленкарбонаті: МД моделювання.

Харківський національний університет імені В.Н. Каразіна, хімічний факультет, кафедра неорганічної хімії, майдан Свободи, 4, Харків, 61022, Україна

Іонні рідини набули великої популярності в останні десятиліття завдяки комплексу унікальних властивостей. Попри широке використання сумішей іонних рідин з апротонними диполярними розчинниками в електрохімії, актуальним залишається прогнозування їх макроскопічних, в першу чергу транспортних, властивостей виходячи з мікроскопічної картини всієї сукупності міжчастинкових взаємодій у таких системах. Метод молекулярно-динамічного моделювання (МДМ) є одним з найбільш потужних інструментів вирішення подібного роду завдань. Однак, однією з невирішених проблем класичного МДМ іон-молекулярних систем є коректне урахування ефектів поляризації. Останнім часом для її вирішення було запропоновано використовувати варіацію ефективних зарядів іонів в розчинах.

У даній роботі представлені результати МДМ структурних і динамічних властивостей розчинів 1-бутил-3-метилімідазолій (BmimBF$_4$) та літій (LiBF$_4$) тетрафтороборатів в пропіленкарбонаті (PC) при 298.15 К в *NPT* ансамблі з використанням програмних пакетів GROMACS і MDNAES.

Показана можливість відтворення експериментальних динамічних властивостей (коефіцієнтів дифузії катіонів і розчинника, в'язкості, а також електричної провідності) бінарних систем на основі сумішей

іонних рідин з PC в широкому інтервалі концентрацій з урахуванням ефектів поляризації шляхом зменшення парціальних зарядів на атомах іонів.

Структура сольватної оболонки катіонів була вивчена в рамках функцій радіального розподілу, розподілу координаційних чисел, а також наявності водневих зв'язків між органічним катіоном і молекулами розчинника. Результати вказують на більш міцну і структуровану сольватну оболонку катіона Li$^+$ в порівнянні з Bmim$^+$, що узгоджується з висновками про рухливості цих катіонів. Часи переорієнтації молекул пропіленкарбонату і часи їхнього життя в перших сольватних оболонках катіонів виявилися в кілька разів вищими для літій катіону.

**Ключові слова:** 1-бутил-3-метилімідазолій тетрафтороборат, літій тетрафтороборат, пропіленкарбонат, молекулярно-динамічне моделювання, ефекти поляризації, мікроструктура, мікродинаміка, сольватна оболонка.

D.S. Dudariev, K.O. Logacheva, Ya.V. Kolesnik, O.N. Kalugin. Interparticle interactions and dynamics in BmimBF$_4$ and LiBF$_4$ solutions in propylene carbonate: MD simulation.

V.N. Karazin Kharkiv National University, School of Chemistry, Inorganic chemistry department, 4 Svobody sqr., 61022 Kharkiv, Ukraine

Ionic liquids have gained immense popularity in recent decades due to a combination of unique properties. Despite the widespread use of ionic liquids mixtures with aprotic dipolar solvents in electrochemistry, it remains relevant to predict their macroscopic, primarily transport, properties based on the microscopic picture of the entire set of interparticle interactions in such systems. The method of molecular dynamics simulation (MDS) is one of the most powerful tools for solving problems of this kind. However, one of the unsolved problems of the classical MDS of ion-molecular systems is the correct accounting of polarization effects. Recently it was proposed to use a variation of the effective ion charges in solutions to solve this task.

This paper presents the results of the MDS structural and dynamic properties of 1-butyl-3-methylimidazolium (BmimBF$_4$) and lithium (LiBF$_4$) tetrafluoroborates solutions in propylene carbonate (PC) at 298.15 K in *NPT* ensemble using GROMACS and MDNAES software packages.

The possibility of reproducing the experimental dynamic properties (diffusion coefficients of cations and solvent, viscosity, and electrical conductivity) of binary systems based on mixtures of ionic liquids with PC in a wide concentration range was shown. Polarization effects were taken into account by reducing the partial charges of the ion atoms.

The structure of the solvation shell of cations was studied within the framework of radial distribution functions, distribution of coordination numbers and the presence of hydrogen bonds between the organic cation and solvent molecules. The results point to stronger and more structured solvation shell of the Li$^+$ cation compared to Bmim$^+$, which is consistent with the conclusions about the mobility of these cations. The reorientation times of propylene carbonate molecules and their lifetimes in the framework of the first solvation shells of the cations are several times higher for the lithium cation.

**Keywords:** 1-butyl-3-methylimidazolium tetrafluoroborate, lithium tetrafluoroborate, propylene carbonate, molecular dynamics simulation, polarization effects, microstructure, microdynamics, solvation shell.

УДК 544.354 + 54-43 + 544.777 + 544.773.422

# AQUEOUS SOLUTION OF POLY (HEXAMETHYLENE GUANIDINE HYDROCHLORIDE) AND POLY (DIETHYLENAMINE GUANIDINE HYDROCHLORIDE) AS STUDIED WITH ACID-BASE INDICATORS

## A.Yu. Kharchenko [a,*], M.A. Romakh [b, *], K.V. Yanova, [c, †]
## M.N. Tereshchuk [d], N.O. Mchedlov-Petrossyan [e, *]

[*] *V.N. Karazin Kharkiv National University, School of Chemistry, 4 Svobody sqr., 61022 Kharkiv, Ukraine*
[†] *Ukrainian State University of Chemical Technology, 8 Gagarin av., 49005 Dnipro, Ukraine*

a) ✉ anastasiia_kharchenko@ukr.net    https://orcid.org/0000-0001-5675-5611
b) ✉ masha1997romah@gmail.com    https://orcid.org/0000-0003-0457-1129
c) ✉ yanovakarolina@gmail.com    https://orcid.org/0000-0001-5041-1121
d) ✉ latiniys229@gmail.com    https://orcid.org/0000-0003-4458-1831
e) ✉ mchedlov@karazin.ua    https://orcid.org/0000-0001-6853-8411

In this paper, the properties of cationic polyelectrolytes as tools for governing the protolytic equilibrium of acid-base indicators in water were examined. For this purpose, water-soluble and pH-dependent poly (hexamethylene guanidine hydrochloride), PHMG, and poly (diethylenamine guanidine hydrochloride), PDEG, were studied. As molecular probes, a set of anionic indicator dyes were used; the key parameter is the so-called apparent ionization constant, $K_a^{app}$. The electrokinetic potential of the above polycationic species in the acidic pH region is substantially positive. As a rule, the polyelectrolytes display marked influence on the absorption spectra and state of the acid-base equilibrium of the anionic dyes at pH < 7, especially in the case of PHMG. Both effects resemble those known for the same dyes in aqueous solutions of cationic surfactants but are less expressed. Normally, the acid-base equilibria were studied at polyelectrolyte : dye ratio of 150 : 1, at ionic strength 0.05 M, and 25 °C. The decrease in the $pK_a^{app}$ ($\equiv -\log K_a^{app}$) value on going from water to the PHMG solution is most expressed for bromocresol green ($HB^- \rightleftharpoons B^{2-} + H^+$): $pK_{a,2}^{app} - pK_{a,2}^{w} = -1.93$. For bromophenol blue, bromocresol purple, and sulfonefluorescein, the shift of the equilibrium is less expressed. Some kinds of specific interactions with the polyelectrolytes were revealed for methyl orange and bromophenol blue. Also, the dependence of $pK_a^{app}$ on logarithm of ionic strength allows estimating the degree of counterion binding by the polycation: $\beta = 0.4 \pm 0.1$.

**Keywords:** polycation, indicator dye, apparent ionization constant, poly (hexamethylene guanidine hydrochloride), poly (diethylenamine guanidine hydrochloride), sulfonefluorescein, methyl orange, sulfonephthaleins.

## Introduction

This paper is aimed to study the influence of cationic polyelectrolytes on the protolytic equilibrium of acid-base indicators in water. Solutions of cationic polyelectrolytes, particularly poly (hexamethylene guanidine hydrochloride) (PHMG), possess antibacterial properties, so the investigation of surface characteristics of colloidal particles (e.g., the $\zeta$-potential) is necessary for studying interactions polyion–bacterium [1]. Cationic polyelectrolytes are used for synthesis of polymer subunit vaccines, for example, polyoxidonium medicine [2]. Also, the cationic polyelectrolytes are applied as flocculants for dyeing wastewater treatment [3-5]. For instance, recently, Jia et al. reported the synthesis of a series of new hydrophobic cationic poly(dimethyldiallylammonium chloride)s and showed the efficiency of the removal of water-soluble dyes in dyeing wastewater using two anionic dyes Reactive Scarlet 3BS and Reactive Black M [3]. It was shown that the composition of a complex of a cationic unit of poly(dimethyldiallylammonium chloride)s with a dye depends on the structure of polyelectrolyte and the polyelectrolyte : dye (P : D) ratio varies from 1 to 4.

On the other hand, indicator dyes were used for the determination of polyelectrolytes concentration [6]. The application of association processes between organic reagents (dyes, e.g., xanthenes) and cationic polyelectrolytes for determination of the later were scrutinized by Chmilenko et al. [7,8]. These investigations were aimed to detect as low as possible polyelectrolyte concentrations, so the P : D ratio was about 1 in these studies. Under such conditions, the influence of polyions on the acid-base equilibria of dyes in solution may somewhat differ from that at high concentrations of the polye-

lectrolytes. Higher P : D ratio, normally 100 : 1, was used by us earlier when studying interactions between indicator dyes and an anionic polyelectrolyte poly (sodium 4-styrenesulfonate) [9].

Therefore, it is important to study the changes of protolytic properties of dyes when their concentration is much lower than that of a cationic polyelectrolyte. This allows ruling out the interaction between dye molecules fixed at the polyion, known as metachromasy.

So, our aim was to determine the acidic strength of common anionic indicator dyes in aqueous solutions of cationic electrolytes, with high P : D values. As a key parameter, the so-called apparent ionization constant, $K_a^{app}$, was chosen. The present study was devoted to aqueous solutions of poly (hexamethylene guanidine hydrochloride), PHMG, and poly (diethylenamine guanidine hydrochloride), PDEG. The structures of PHMG and PDEG are shown in Figure 1. Owing to the presence of secondary amino groups such polyelectrolytes are pH-dependent [8].
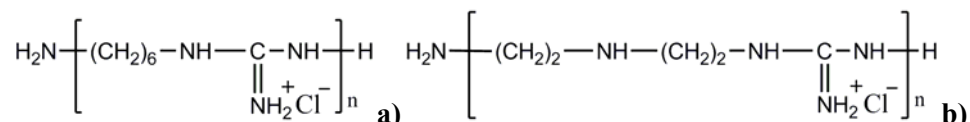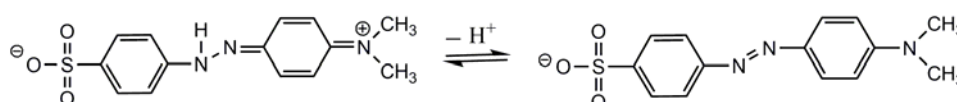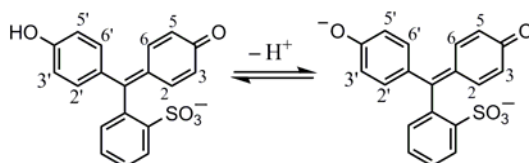


**Figure 1.** Structural formulae of poly (hexamethylene guanidine hydrochloride) (PHMG) (**a**) and poly (diethylenamine guanidine hydrochloride) (PDEG) (**b**).

As indicator dyes, methyl orange, sulfonefluorescein, and three sulfonephthalein dyes were used. The protolytic properties of these anionic dyes in micellar solution are well documented. In our previous work, we obtained the $pK_a^{app}$ ($\equiv -\log K_a^{app}$) values of dyes in $5 \times 10^{-4}$ M solution of di-$n$-tetradecyldimethylammonium bromide and 0.01 M solution of cetyltrimethylammonium bromide [10,11]. The medium effects, i.e., the differences between the so-called apparent $pK_a^{app}$ values and the thermodynamic values in water, $pK_a^w$, vary from –1.1 to –1.8 $pK_a$ units in the above systems [10,11]. Similar medium effect were observed earlier for bromothymol blue in aqueous solutions of poly [(vinylbenzyl)trimethylammonium chloride] by Baumgartner et al. [12].

The ionization of the zwitter-ion of methyl orange, $HB^{\pm}$, corresponds to the charge type ±/–. The second step of sulfonephthaleins ionization occurs according to the charge type –/= (bromophenol blue, bromocresol green, bromocresol purple). Also, sulfonefluorescein was used as a dye which ionizes by two steps (±/– and –/=). The equilibria of the dyes are shown in Schemes 1–3. Analogously to the systems "cationic dye – polyanion", these anionic dyes are bound to polycations primarily due to electrostatic interactions [4,9,13–15].



**Scheme 1.** The ionization of methyl orange.



**Scheme 2.** The ionization of sulfonephthalein dyes: 3,3',5,5'- tetrabromo- (bromophenol blue); 2,2'-dimethyl-3,3',5,5'-tetrabromo- (bromocresol green); 3,3'-dimethyl-5,5'-dibromosulfonephthalein (bromocresol purple).
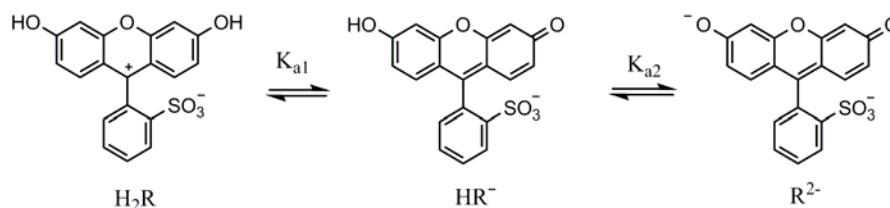


**Scheme 3.** The ionization of sulfonefluorescein.

## Experimental section

**Materials.** The cationic polyelectrolytes poly (hexamethylene guanidine hydrochloride) (PHMG) and poly (diethylenamine guanidine hydrochloride) (PDEG) were synthesized in Ukrainian State University of Chemical Technology, Dnipro; the synthesis is described in publications [16] and [17], respectively. These substances were prepared initially as 25 wt % aqueous solution. The molecular mass of PGMG is $10 \times 10^3$ g mol$^{-1}$ while PDEG is characterized by some less molecular mass of $8 \times 10^3$ g mol$^{-1}$. The stock solutions of PHMG and PDEG with the concentrations, which as a rule didn't exceed 0.10 M, were prepared by weighting. They appeared to be slightly alkaline. The weighted sample of the stock polyelectrolyte solution was diluted with pure water, stirred, and used as a stock solution. The working solutions were prepared by further dilution. Hereafter, the concentrations of polyelectrolytes are expresses in monomer mol dm$^{-3}$ (monomol dm$^{-3}$ or M). The pH values of the diluted polyelectrolyte solutions in water without buffer additives were somewhat enhanced as compared with the air-saturated water. For example, in 0.00132 M PHMG pH = 7.23 and in 0.0145 M PDEG pH = 8.33. Poly (sodium 4-styrenesulfonate), molecular mass of $70 \times 10^3$ g mol$^{-1}$, was purchased from Sigma-Aldrich as a powder. The polyelectrolyte was used as received; its solutions were prepared as described previously [9]. The anionic surfactant sodium $n$-dodecylsulfate was used as received from Vekton (Russia). Hydrochloric, acetic, and phosphoric acids, and borax used for preparation of working solutions were of analytical grade. The aqueous solution of NaOH was prepared using the saturated stock solution of alkali using CO$_2$-free water and kept protected from the atmosphere. The ionic strength, $I$, of the acetate buffer mixtures used for determination of the ionization constants did not exceed 0.01 M. The total $I$ value of the bulk (aqueous) phase was maintained by appropriate NaCl addition. The samples of the dyes neutral red, bromophenol blue, bromocresol green, bromocresol purple, methyl orange, and sulfonefluorescein were already used in our previous studies [9-11,18,19].

**Methods.** The apparent ionization constants of indicator dyes were determined via a standard procedure [9–12, 18, 19]. Absorption spectra were measured with Hitachi U-2000 spectrophotometer against pure water as blanks, at 25°C. The pH values were created by buffer solutions. The pH determinations were performed by using R 37-01 potentiometer and pH-121 pH-meter (Russia) with an ESL-43-07 glass electrode (Gomel, Belarus) in a cell with liquid junction (3.0 M KCl). An Ag|AgCl electrode was used as a reference electrode. The cell was calibrated with standard buffer solutions: pH 9.18, 6.86, 4.01, and 1.68 at 25°C.

The ionization of an indicator acid in solution can be described by the below equation:

$$\text{HB}^z \; \rightleftharpoons \; \text{B}^{z-1} + \text{H}^+, \; K_a \tag{1}$$

Therefore, the apparent ionization constant, $K_a^{\text{app}}$, should be expressed as:

$$\text{p}K_a^{\text{app}} = \text{pH}_\text{w} + \log \frac{\left[\text{HB}^z\right]_t}{\left[\text{B}^{z-1}\right]_t} = \text{pH}_\text{w} + \log \frac{A_\text{B} - A}{A - A_\text{HB}} \tag{2}$$

The brackets denote equilibrium concentrations. The acid-base couple HB$^z$/B$^{z-1}$ is (partly) associated with polycations; pH$_\text{w}$ is the pH value of the continuous (aqueous) phase; $A$ is the absorbance at the current pH$_\text{w}$ value, $A_\text{B}$ and $A_\text{HB}$ are absorbances under conditions of complete transformation of the indicator into the corresponding form. The subscript $t$ (total) denotes that the concentration is expressed in moles per dm$^3$ of the whole solution.

The precise dye concentrations were ascertained by spectrophotometric method using the previously known molar absorptivity values. The dye concentrations in working solutions were about $1 \times 10^{-5}$ M. Similarly to anionic polyelectrolyte solutions, cationic polyelectrolyte solutions results in metachromasy of some dyes [20]. So, it is necessary to control the polyelectrolyte : dye concentration ratio, P : D, for all chosen dyes.

The polyelectrolyte particle size distribution and zeta-potentials, $\zeta$, were determined via dynamic light scattering, DLS, using Zetasizer Nano ZS Malvern Instruments apparatus. The equilibration time of each probe was 120 s, the number of size measurements of each probe was 10 ns, and every measurement consisted of 12 to 30 runs (automatic choice). In the case of zeta-potential, the number of measurements was 5, the number of runs was chosen automatically (up to 100 runs). Distilled water wasn't filtrated. For assign the viscosity value, the "solvent builder", was used. This program, which is introduced in the Zetasizer soft, allows calculating the viscosity of the dispersant at NaCl additions.

## Results and discussion

**DLS characterization of polyelectrolyte solutions.** The dependence of $\zeta$-potential of PHMG on pH values was already reported by Wojciechowski and Klodzinska [1]. We measured this parameter of PHMG at pH 2. A mean value of $+21\pm9$ mV was evaluated. However, the $\zeta$ value changed from 8.7 to 39.8 mV, and some precipitation was observed during the measurements. Probably, electrocoagulation is the main reason of this disturbing phenomenon, but in any case a substantial positive charge of the macromolecular species is firmly proved. The same is true for PDEG. A particles' size of 1–2 nanometers was roughly estimated, which is in agreement with the above mentioned molecular mass.

*Methyl orange.* First of all, methyl orange as indicator dye was used because of its relatively simple structure and well-known solvatochromic properties [21]. As it was shown in our previous paper devoted to aqueous solutions of an anionic polyelectrolyte [9], the appropriate conditions for the determination of apparent ionization constants of dyes are reached in semi-diluted polyelectrolyte solutions. Hereafter, we define the polyelectrolyte : dye concentration ratio as P : D. In general, at P : D = 100 – 1000, one can reach condition similar to those in surfactant micelles, when a dye molecule interacts only with cationic sites of polyelectrolyte and is not influenced by another dye molecule. These conclusions should be correct for methyl orange too. For example, Vleugels et al. [20] carried out a detailed investigation of the interaction between methyl orange and polycations. They have investigated the influence of molecular structure of the cations, composition (i.e., P : D ratio), pH, and ionic strength on association between methyl orange and polycations. It was shown that in solutions of poly (diallyldimethylamine hydrochloride), a pH-independent quaternary ammonium salt with molecular mass of $107\times10^3$ g mol$^{-1}$, the metachromatic band of dye aggregates appeared in acetate buffer (pH = 4.0, $I$ = 0.01 M) at P : D $\approx$ 0.2–1.0.

In our study in unbuffered systems with pH $\approx$ 7.0 and $I \to 0$, the methyl orange aggregate band about 350 nm appeared in PDEG solutions even at P : D = 100. This type of aggregates is well documented in the literature [20, 21]. However, under these conditions no distinct bands were observed in the case of PHMG (Figure 2).
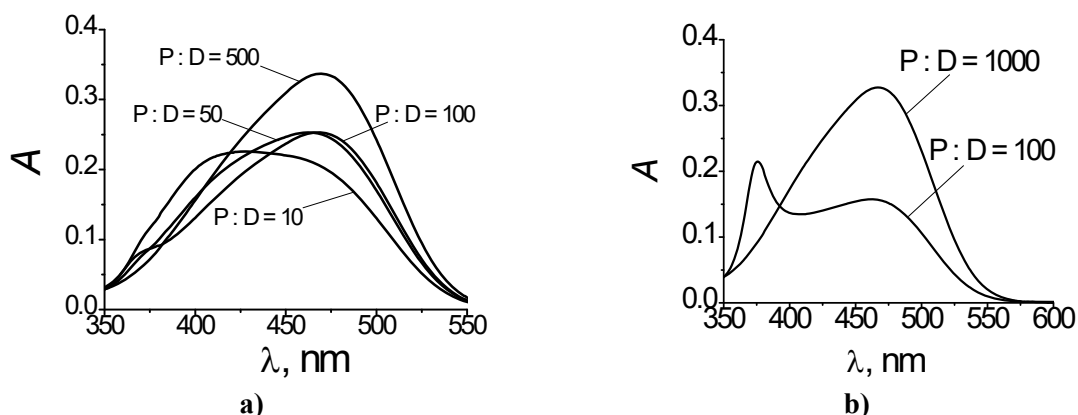


**Figure 2.** Absorption spectra of methyl orange in PHMG (**a**) and PDEG (**b**) solutions at different P : D values, $c$ (dye) = $1.45\times10^{-5}$ M.

The $pK_a^{app}$ values of methyl orange were determined under conditions that allowed to avoid dye aggregation. Therefore, the experiments for PHMG and PDEG were made at the P : D ratio of 500 and 1000, respectively. The pH-dependence of absorption spectra is depicted in Figure 3.

The $pK_a^{app}$ values in colloidal solution of PHMG and PDEG are $2.91\pm0.03$ and $3.19\pm0.05$, respectively. They are lower as compared with the themodynamic value in water: $pK_a^w$ = $3.42\pm0.02$ [22]; 3.45 [23], but the decrease in micellar solutions of cationic surfactants and in corresponding microemulsions is much more expressed: the $pK_a^{app}$ values in such systems are below unity [22, 24]. Though methyl orange is a solvatochromic indicator, no significant shifts of absorption maximum was observed. While in a cationic surfactant-based microemulsion, $\lambda_{max}$ moved from 462–463 nm to 420 nm [24], in PHMG and PDEG solutions $\lambda_{max}$ = 469 nm and 466.5 nm, respectively at pH $\approx$ 7.0,

$I \to 0$. Hence, these small shifts are bathochromic, which is not typical for the anionic form of methyl orange on going from water to organic microenvironments.
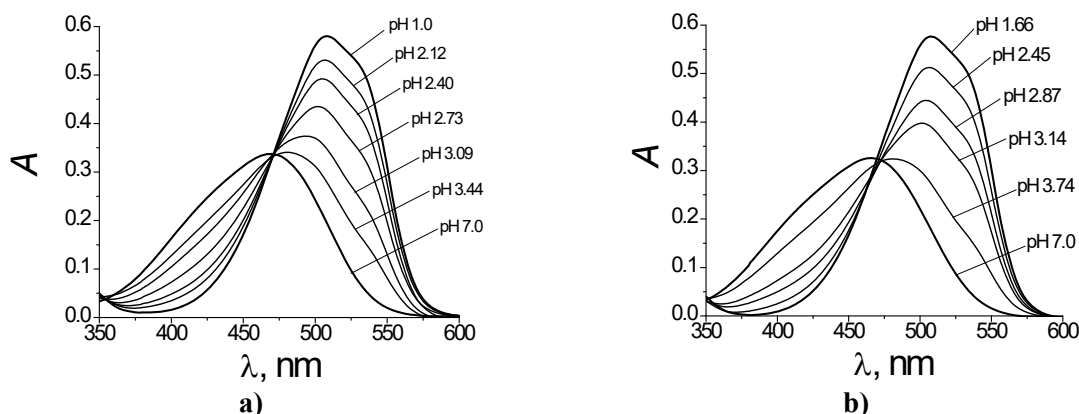


**Figure 3.** Absorption spectra of methyl orange in PHMG solutions at P : D = 500 (**a**) and in PDEG solutions at P : D = 1000 (**b**) at different pH; HCl solutions, $I = 0.05$ M (HCl + NaCl), $c$ (dye) $= 1.45 \times 10^{-5}$ M.

Relatively small medium effects, i.e., the $pK_a^{app}$ shifts, for methyl orange in PHMG and PDEG solutions can result from charge type "zwitter-ion $\to$ anion". Also, the incomplete binding of the zwitter-ion by the macromolecule should not be ruled out because the $\lambda_{max}$ values in the polyelectrolyte solutions are ca. the same as in water.

*Sulfonefluorescein.* In order to examine the influence of the charge type of an acid-base indicator couple on the medium effects ($pK_a^{app}$ shifts) in cationic polyelectrolyte solutions we used the dye sulfonefluorescein. In this case (Scheme 3), the two-step ionization occurs from the zwitter-ion to the anion and then to the dianion. The absorption spectra of sulfonefluorescein at different pH and $I = 0.05$ M are presented in Figure 4. The ratio P : D = 100 was chosen for the absorption spectra analysis of sulfonefluorescein in PHMG solutions. As sulfonefluorescein is not a metachromatic dye, such P : D ratio is enough for observation of isolated dye molecules in polyelectrolyte microenvironment. Two distinct isosbestic points were observed that opens the possibility to determine the indices of the apparent ionization constants: $pK_{a1}^{app} = 3.00\pm0.08$ and $pK_{a2}^{app} = 5.77\pm0.09$. In water, $pK_a^w = 3.10$ and $pK_a^w = 6.76$ [18]. Thus, the medium effect in the case of the ionization of the anion ($-0.99$ $pK_a$ units) is much more expressed than in the case of the zwitter-ion $\to$ anion equilibrium ($-0.1$ $pK_a$ units). Here, as in the case of methyl orange, the degree of binding of zwitter-ionic form is unclear. By contrast, the association of anionic dye species with the polycation is more probable.
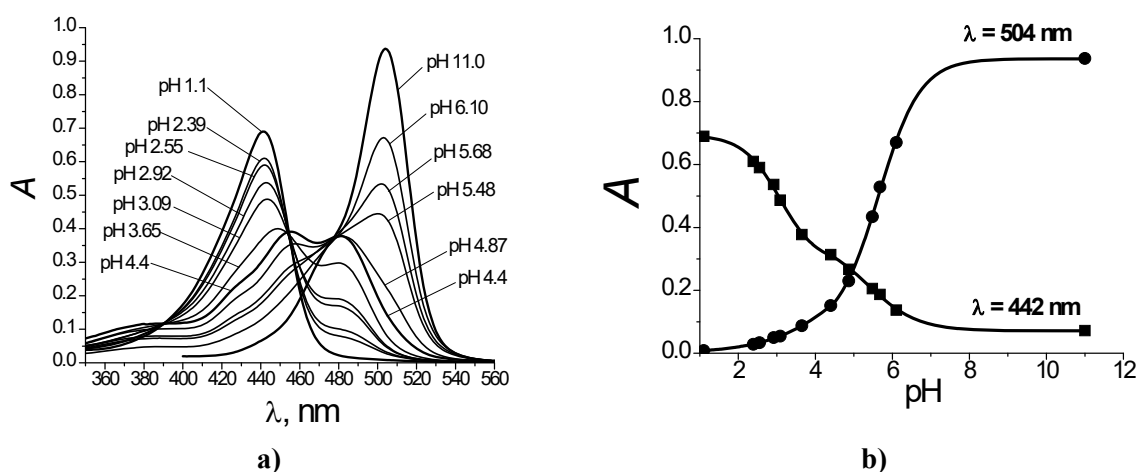


**Figure 4.** The absorption spectra of sulfonefluorescein in PHMG solution at P : D = 100 at different pH (the HCl solutions, acetate and phosphate buffer were used), $I = 0.05$ M, $c$ (dye) $= 1.39 \times 10^{-5}$ M (**a**); the dependence of absorption of sulfonefluorescein in PHMG solution on pH, P : D = 100, $I = 0.05$ M (**b**).

The $pK_{a2}^{app}$ values of the dye in $5 \times 10^{-4}$ M solution of di-*n*-tetradecyldimethylammonium bromide, $I = 0.01$ M [10] and 0.01 M solution of cetyltrimethylammonium bromide, $I = 0.05$ M [11] are 4.91 and 5.73, respectively. Again, the medium effects in PHMG solutions are less expressed than in micellar solutions of cationic surfactants.

Thus, the influence of PHMG on protolytic equilibria of dyes is much more expressed in the case of the charge type –/=. Therefore, sulfonephthalein dyes (Scheme 2) were used for further investigations.

***Sulfonephthaleins.*** A pronounced metachromatic effect was observed for bromophenol blue in solutions of PHMG and PDEG (Figure 5). At low P : D ratio, the dye aggregates manifest themselves in significant changes of absorption spectra. Moreover, in PHMG solution at P : D = 1 a fine-dispersed sediment appears due to association of dye molecules with polyelectrolyte cationic sites.
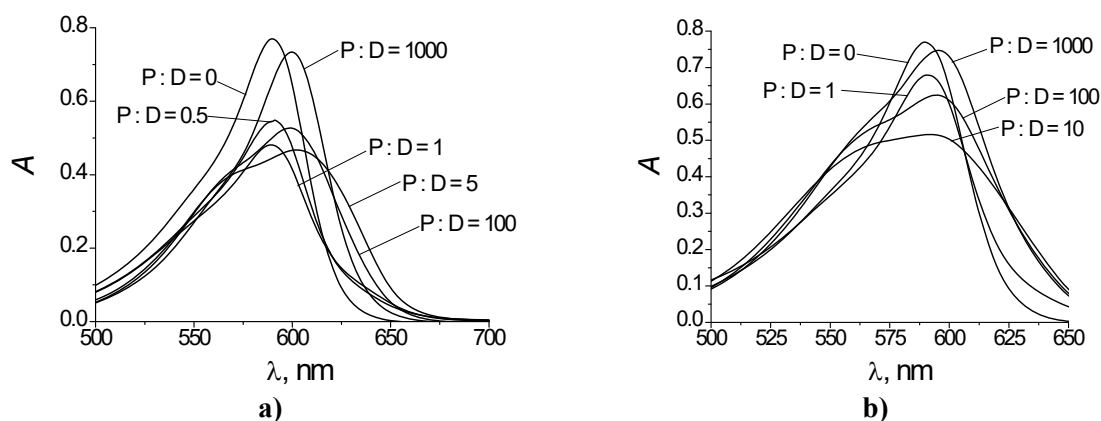


**Figure 5.** The absorption spectra of bromophenol blue in PHMG (**a**) and PDEG (**b**) solution at different P : D values, $c$ (dye) $= 1 \times 10^{-5}$ M, pH $\approx 11.0$, $I \rightarrow 0$.

Correspondingly, the determination of $pK_a^{app}$ values of bromophenol blue was complicated by the abovementioned coagulation processes. In Figure 6, the absorption spectra of bromophenol blue solutions are shown at different pH and P : D = 100 and 1000. In the case of PDEG at higher pH values, pH 12, the dye is displaced from pseudophase due to deprotonation of the polycations and disappearance of its positive charge [8].
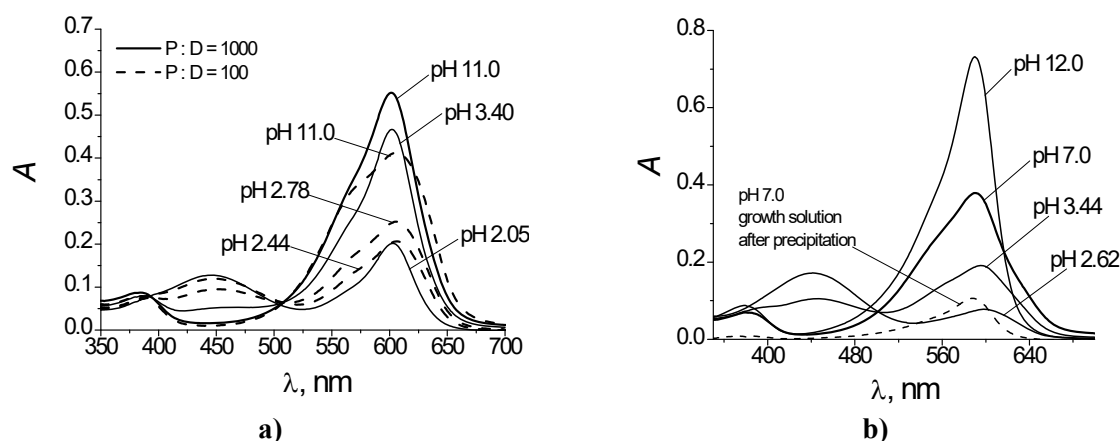


**Figure 6.** The absorption spectra of bromophenol blue in PHMG solution at P : D = 100 and 1000 at different pH (the HCl solutions were used) (**a**), and in PDEG solution at P : D = 100 at different pH (the HCl solutions were used) (**b**), $I = 0.05$ M, $c$ (dye) $= 1.0 \times 10^{-5}$ M.

At low P : D values, bromocresol purple also forms aggregates, but at P : D = 150 it is possible to obtain the $pK_a^{app}$ value in PHMG solutions (Table 1). On the other hand, the polyelectrolyte PDEG cannot bind the dye molecules probably due to deprotonation of the polycation within the pH range

that corresponds to the protolytic equilibrium of bromocresol purple ($pK_a^w = 6.30$). This statement is confirmed by significant dependence of $pK_a^{app}$ values on pH ($pK_a^{app} = 5.98 - 6.33$). The $pK_a^{app}$ value increases along with the pH rise. The highest medium effect is observed for bromocresol green, $pK_a^{app} - pK_a^w = -1.93$. However, in this case the $pK_a^{app}$ value is also influenced by pH: $pK_a^{app}$ changes from 2.74 to 3.18 at pH 2.39 to 3.95. This may be a result of structural changes of the macromolecule. The absorption spectra are represented in Figures 7 and 8.

It may be concluded that the cationic polyelectrolytes under study in this work influence the protolytic equilibria of dyes similarly to micelles of cationic surfactants.

**Table 1.** The indices of the apparent ionization constants of the dyes in PHMG solutions at P : D = 150 and $I = 0.05$ M.

| Indicator dye | $pK_a^w$ | $pK_a^{app}$ | $pK_a^{app} - pK_a^w$ |
|---|---|---|---|
| Methyl orange, $pK_{a,1}$ | 3.44 | $2.91 \pm 0.03$ [a] | −0.53 |
| Sulfonefluorescein, $pK_{a,1}$ | 3.10 | $3.00 \pm 0.08$ [b] | −0.10 |
| Sulfonefluorescein, $pK_{a,2}$ | 6.76 | $5.77 \pm 0.09$ [b] | −0.99 |
| Bromocresol purple, $pK_{a,2}$ | 6.30 | $4.88 \pm 0.08$ [c] | −1.42 |
| Bromophenol blue, $pK_{a,2}$ | 4.20 | $\approx 2.5$ [d] | $\approx$ −1.7 |
| Bromocresol green, $pK_{a,2}$ | 4.90 | $2.97 \pm 0.18$ | −1.93 |

[a] In PDEG solutions, $pK_a^{app} = 3.19 \pm 0.05$; [b] P : D = 100; [c] in PDEG solutions, $pK_a^{app} = 6.19 \pm 0.16$; [d] in PDEG solutions, $pK_a^{app} \approx 3.3$.
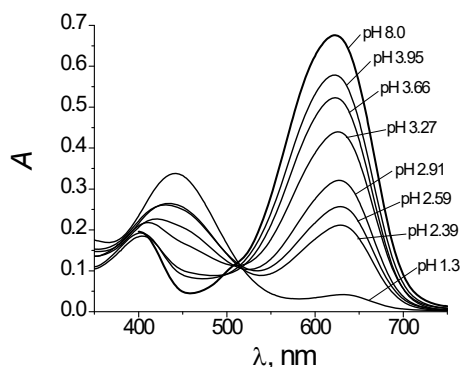


**Figure 7.** The absorption spectra of bromocresol green in PHMG solutions at different pH values (the HCl solutions were used) at P : D = 150 and $I = 0.05$ M, $c$ (dye) $= 1.7 \times 10^{-5}$ M.



a)  b)

**Figure 8.** The absorption spectra of bromocresol purple in PHMG solutions at different pH values (acetate and phosphate buffer were used) at P : D = 140 and $I = 0.05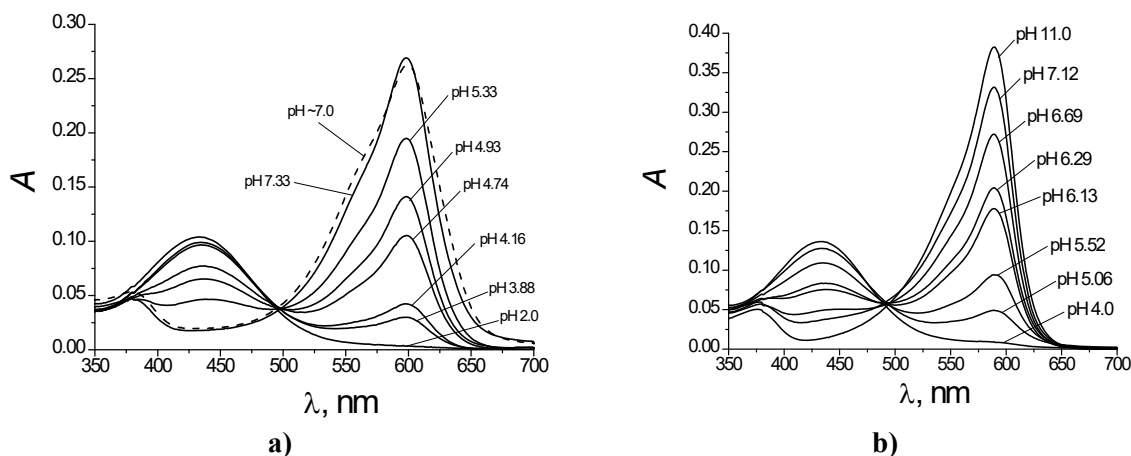$ M, $c$ (dye) $= 9 \times 10^{-6}$ M (**a**); the absorption spectra of bromocresol purple in PDEG solutions at different pH values (acetate and phosphate buffer were used) at P : D = 150 and $I = 0.05$ M, $c$ (dye) $= 9 \times 10^{-6}$ M (**b**).

***Dependence of*** $pK_a^{app}$ ***on ionic strength of PHMG solution.*** We have also examined the influence of the ionic strength maintained by NaCl on the acid-base equilibrium in these systems. As an example, the ionization of sulfonefluorescein was chosen because of less expressed tendency to precipitation in the presence of the polyelectrolytes under study. The absorption spectra of the dye at different pHs are exemplified in Figures 9, 10. It should be noted that at higher ionic strength, the isosbestic point that corresponds to the anion to dianion transition is somewhat fuzzy. As a probable reason the structural changes of the macromolecule in the acidic pH region may be assumed.
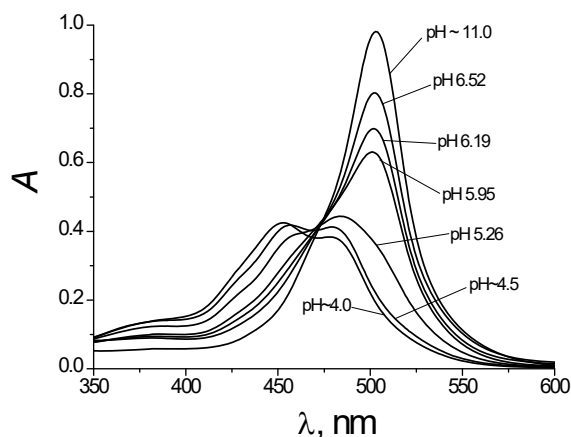
 

**Figure 9.** The absorption spectra of sulfonefluorescein in PHMG solution at P : D = 100 at different pH (acetate and phosphate buffer were used), $I = 0.10$ M, $c$ (dye) $= 1.35 \times 10^{-5}$ M.
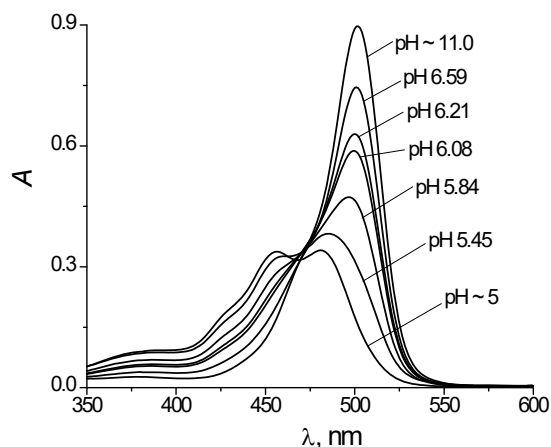
**Figure 10.** The absorption spectra of sulfonefluorescein in PHMG solution at P : D = 100 at different pH (acetate and phosphate buffer were used), $I = 0.20$ M, $c$ (dye) $= 1.35 \times 10^{-5}$ M.

Assuming that the degree of binding of the dye anions by the PHMG stays unaffected during the $I$ (NaCl + buffer mixture) variation and following the relations derived for ionic surfactants [18, 19], the slope of the $pK_a^{app}$ vs $\log I$ may be considered as the degree of counterions binding, $\beta$. Here, Cl$^-$ should be considered as counterion.



$$pK_a^{app} = (6.30 \pm 0.05) + (0.39 \pm 0.07) \log I, \; R^2 = 0.989$$

**Figure 11**. Dependence of $pK_a^{app}$ on logarithm of ionic strength; sulfonefluorescein in the PHMG – NaCl system.

This $\beta$ value is lower than that estimated with the help of the same dye for the cetyltrinethylammonium bromide – Br$^-$ system (0.76±0.02) [11]. The $\beta$ value for the poly (sodium 4-styrenesulfonate) – Na$^+$ system determined using a set of cationic 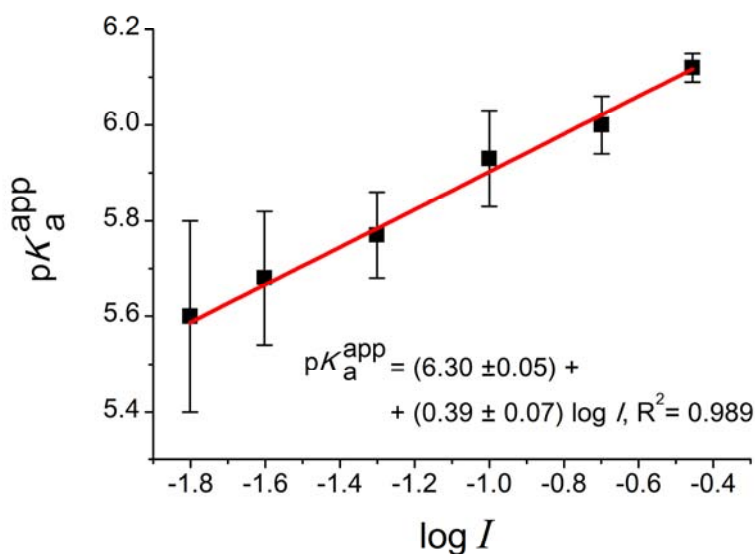dyes varies within the range of 0.58–0.72 [9]. For cationic polyelectrolytes, ion exchange constants of different counterions are available [25, 26]. They give evidence for relatively low affinity of the Cl$^-$ ions to the cationic polyions.

*Interaction of PHMG with an anionic polyelectrolyte.* In addition to the above results we examined the interaction between a cationic polyelectrolyte and an anionic one. As cationic component, PHMG was chosen, whereas the previously studied poly (sodium 4-styrenesulfonate) [9] was used as a macroscopic counterion. Mixing these compounds predictably resulted in mutual coagulation. Next, the addition of sodium *n*-dodecylsulfate (0.02 M) caused peptization: the colloidal system was restored (Figure 12a).
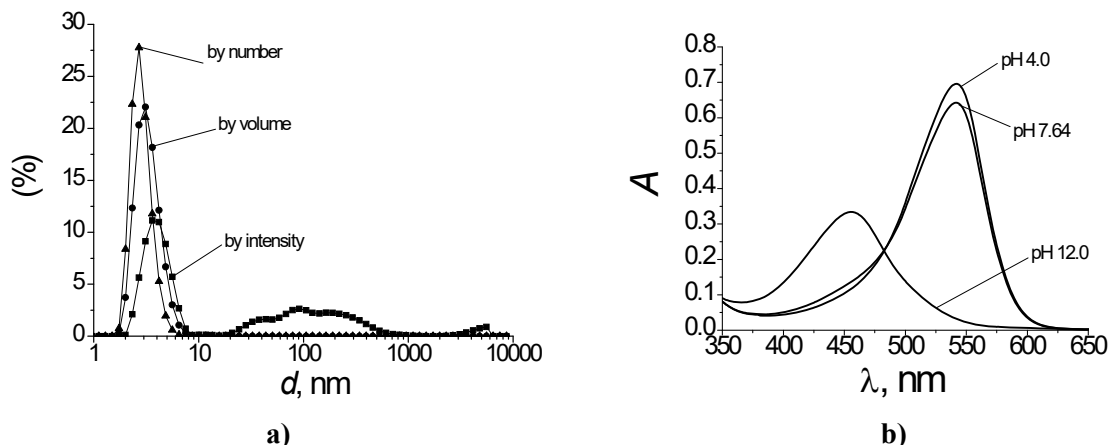


**a)**             **b)**

**Figure 12.** The size distribution of particles in system poly (sodium 4-styrenesulfonate) – PHMG – sodium *n*-dodecylsulfate, the analytical concentration was $c$ (poly (sodium 4-styrenesulfonate)) = 0.0047 M, $c$ (PHMG) = 0.005 M, $c$ (sodium *n*-dodecylsulfate) = 0.02 M (**a**), the absorption spectra of neutral red in system poly (sodium 4-styrenesulfonate) – PHMG – sodium *n*-dodecylsulfate at $I$ = 0.05 M, poly (sodium 4-styrenesulfonate) : D ~ 150, $c$ (poly (sodium 4-styrenesulfonate)) = $c$ (PHMG) = 0.005 M, $c$ (sodium *n*-dodecylsulfate) = 0.02 M (**b**).

In Figure 12b, the absorption spectra of anionic dye neutral red are shown. The p$K_a^{app}$ value of neutral red in the restored mixed colloid system was found of about 8.70 that semi-quantitatively agrees with that one in micellar solution of sodium *n*-dodecylsulfate, 9.21 [27]. Hence, the charge of thus obtained colloidal species is certainly negative, which explains the driving force of the peptization phenomenon.

## Conclusions

1. The cationic polyelectrolytes examined in this paper exhibit strong interaction with anionic dyes. Besides the well-known metachromatic effect, the macromolecules display an expressed shift of the protolytic equilibria of indicators towards the acidic region.
2. The quantitative processing of the data at appropriate polyelectrolyte : dye ratio allows determining the apparent ionization constants of the indicators. Their values resemble the corresponding effect of micelles of cationic surfactants.
3. The dependence of p$K_a^{app}$ vs. logarithm of ionic strength in the PHMG – NaCl system was treated analogously to the corresponding salt effects in micelles of ionic surfactants. This allowed estimating the degree of counterion Cl$^-$ binding by the polycation as $\beta = 0.4 \pm 0.1$.
4. Interaction between PHMG and poly (sodium 4-styrenesulfonate) results in a kind of mutual coagulation. The deposit thus formed is dissolved by adding sodium *n*-dodecylsulfate. This procedure leads to appearance of negatively charged colloidal species.

**References**

1. Wojciechowski K., Klodzinska E. Zeta potential study of biodegradable antimicrobial polymers. *Colloids and Surfaces A: Physicochemical and Engineering Aspects.* **2015,** *483* (Supplement C), 204-208.
2. Kabanov V.A. From synthetic polyelectrolytes to polymer-subunit vaccines. *Pure and Applied Chemistry.* **2004,** *76* (9), 1659-1677.
3. Jia Q., Song C., Li H., Zhang Z., Liu H., Yu Y., Wang T. Synthesis of strongly cationic hydrophobic polyquaternium flocculants to enhance removal of water-soluble dyes in wastewater. *Research on Chemical Intermediates.* **2017,** *43* (5), 3395-3413.
4. Li Q., Yue Q.-Y., Sun H.-J., Su Y., Gao B.-Y. A comparative study on the properties, mechanisms and process designs for the adsorption of non-ionic or anionic dyes onto cationic-polymer/bentonite. *Journal of Environmental Management.* **2010,** *91* (7), 1601-1611.
5. Szyguła A., Guibal E., Palacín M.A., Ruiz M., Sastre A.M. Removal of an anionic dye (Acid Blue 92) by coagulation–flocculation using chitosan. *Journal of Environmental Management.* **2009,** *90* (10), 2979-2986.
6. Masadome T. Determination of cationic polyelectrolytes using a photometric titration with crystal violet as a color indicator. *Talanta.* **2003,** *59* (4), 659-666.
7. Chmilenko T.S., Ivanitsa L.A., Chmilenko F.A. Substituent and environment influence on analytical properties of associates of xanthene dyes with polyhexamethyleneguanidine chloride. *Bulletin of Dnipropetrovsk National University.* **2014,** *21* (20), 10.
8. Chmilenko T.S., Chmilenko F.A. *Analytical chemistry of polyelectrolytes* (in Russian). Dnipropetrovsk University Press: **2012**.
9. Kharchenko A.Y., Moskaeva O.G., Klochaniuk O.R., Marfunin M.O., Mchedlov-Petrossyan N.O. Effect of poly (sodium 4-styrenesulfonate) on the ionization constants of acid-base indicator dyes in aqueous solutions. *Colloids and Surfaces A: Physicochemical and Engineering Aspects.* **2017,** *527*, 132-144.
10. Mchedlov-Petrossyan, N.O., Kamneva N.N., Kharchenko A.Y., Shekhovtsov S.V., Marinin A.I., Kryshtal A.P. The influence of the micellar pseudophase of the double-chained cationic surfactant di-*n*-tetradecyldimethylammonium bromide on the absorption spectra and protolytic equilibrium of indicator dyes. *Colloids and Surfaces A: Physicochemical and Engineering Aspects.* **2015,** *476*, 57-67.
11. Kamneva N.N., Kharchenko A.Y., Bykova O.S., Sundenko A.V., Mchedlov-Petrossyan N.O. The influence of 1-butanol and electrolytic background on the properties of CTAB micelles as examined using a set of indicator dyes. *Journal of Molecular Liquids.* **2014,** *199*, 376-384.
12. Baumgartner E., Fernandez-Prini R., Turyn D. Change of apparent acidity constant of indicators in polyelectrolyte solutions. *Journal of the Chemical Society, Faraday Transactions 1: Physical Chemistry in Condensed Phases.* **1974,** *70*, 1518-1526.
13. Medjahed K., Tennouga L., Mansri A., Chetouani A., Hammouti B., Desbrières J. Interaction between poly(4-vinylpyridine-graft-bromodecane) and textile blue basic dye by spectrophotometric study. *Research on Chemical Intermediates.* **2013,** *39* (7), 3199-3208.
14. Egawa Y., Hayashida R., Anzai J.-i. Multilayered Assemblies Composed of Brilliant Yellow and Poly(allylamine) for an Optical pH Sensor. *Analytical Sciences.* **2006,** *22* (8), 1117-1119.
15. Shen J.-J., Ren L.-L., Zhuang Y.-Y. Interaction between anionic dyes and cationic flocculant P(AM-DMC) in synthetic solutions. *Journal of Hazardous Materials.* **2006,** *136* (3), 809-815.
16. Yanova K.V., Kutyanina V.S., Solovyev V.M. A study of methods of synthesis of poly (hexamethylene guanidine hydrochloride). *Voprosy Khimii I Khimicheskoi Tekhnologii.* **2000**, No.1, 281–284.
17. Yanova K.V., Kutyanina V.S., Solovyev V.M. A study of methods of synthesis of poly (diethylenamine guanidine hydrochloride). *Voprosy Khimii I Khimicheskoi Tekhnologii.* **2000**, No.4, 72–74.
18. Mchedlov-Petrossyan N.O. Protolytic equilibrium in lyophilic nanosized dispersions: Differentiating influence of the pseudophase and salt effects. *Pure and Applied Chemistry.* **2008,** *80* (7), 1459-1510.
19. Mchedlov-Petrossyan N.O., Vodolazkaya N.A., Kamneva N.N. Acid-base equilibrium in aqueous micellar solutions of surfactants. In *Micelles: Structural Biochemistry, Formation*

*and Functions & Usage*, Bradburn, D.; Bittinger, J., Eds. Nova Science Publishers: N. Y., 2013; pp. 1-71.

20. Vleugels L.F.W., Domańska I., Voets I.K., Tuinier R. On the driving forces for complexation of methyl orange with polycations. *Journal of Colloid and Interface Science.* **2017,** *491*, 141-150.

21. Quadrifoglio F., Crescenzi V. The interaction of methyl orange and other azo-dyes with polyelectrolytes and with colloidal electrolytes in dilute aqueous solution. *Journal of Colloid and Interface Science.* **1971,** *35* (3), 447-459.

22. Drummond C.J., Grieser F., Healy T.W. Acid-base equilibria in aqueous micellar solutions. Part 4.-Azo indicators. *Journal of the Chemical Society, Faraday Transactions 1: Physical Chemistry in Condensed Phases.* **1989,** *85* (3), 561-578.

23. Boily J.-F., Seward T.M. On the Dissociation of Methyl Orange: Spectrophotometric Investigation in Aqueous Solutions from 10 to 90 ° C and Theoretical Evidence for Intramolecular Dihydrogen Bonding. *Journal of Solution Chemistry.* **2005,** *34* (12), 1387-1406.

24. Nikiforova E.M., Bryleva E.Yu., Mchedlov-Petrosyan N.O. The distribution of the anion and zwitterion forms of methyl orange between the disperse microemulsion pseudophase and continuous water phase. *Russian J. Phys. Chem. A.* **2008**, *82*(9), 1434-1437.

25. Plaisance M., Ter-Minassian-Ssaraga L. Spread Insoluble Cationic Polysoap Monolayers II. Specific Effect of Counterion Binding on Surface Density Pressure and Potential at Collapse Point. *Journal of Colloid and Interface Science.* **1977**, *59*(1), 113-122.

26. Itaya T., Ochiai H. Counterion Binding to Poly (allylammonium) Cation. *Journal of Polymer Science: Part B: Polymer Physics*. **1992**, *30*, 587-590.

27. Kharchenko A.Yu., Kamneva N.N., Mchedlov-Petrossyan N.O. The properties and composition of the SDS – 1-butanol mixed micelles as determined via acid-base indicators. *Colloids Surf. A.* **2016**, *507*, 243-254.

А.Ю. Харченко*, М.А. Ромах*, К.В. Янова†, М.Н. Терещук†, Н.О. Мчедлов-Петросян*. Водные растворы поли (гексаметилен гуанидин гидрохлорида) и поли (диэтиленамино-гуанидин гидрохлорида): исследование при помощи кислотно-основных индикаторов.

* Харьковский национальный университет имени В.Н. Каразина, химический факультет, пл. Свободы, 4, Харьков, 61022, Украина

† Украинский государственный химико-технологический университет, проспект Гагарина, 8, Днепр, 49000, Украина

В настоящей статье исследованы свойства катионных полиэлектролитов как средства управления протолитическими равновесиями кислотно-основных индикаторов в воде. С этой целью изучены водорастворимые pH-зависимые поли (гексаметилен гуанидин гидрохлорид), ПГМГ, и поли (диэтиламин гуанидин гидрохлорид), ПДЕГ. В качестве молекулярных зондов использован набор анионных индикаторных красителей, при этом ключевым параметром являются так называемые кажущиеся константы ионизации, $K_a^{app}$. Электрокинетический потенциал обоих катионных макромолекул в кислой области pH существенно положительный. Как правило, исследованные полиэлектролиты оказывают заметное влияние на спектры поглощения и положение кислотно-основных равновесий анионных красителей при pH < 7, особенно выраженное в случае ПГМГ. Оба упомянутых эффекта напоминают таковые для этих же красителей в растворах катионных ПАВ, но менее выражены. Кислотно-основные равновесия исследовались главным образом при соотношении полиэлектролит : краситель = 150 : 1, при ионной силе 0.05 М и 25 $^o$С. Снижение значения $pK_a^{app}$ ($\equiv -\log K_a^{app}$) при переходе от воды к растворам ПГМГ наиболее значителен для бромкрезолового зелёного ($HB^- \rightleftharpoons B^{2-} + H^+$): $pK_{a,2}^{app} - pK_{a,2}^{w} = -1.93$. Для бромфенолового синего, бромкрезолового пурпурного и сульфофлуоресцеина соответствующий сдвиг менее выражен. Обнаружены также некоторые специфические взаимодействия метилоранжа и бромфенолового синего с полиэлектролитами. Кроме того, зависимость $pK_a^{app}$ от логарифма ионной силы позволяет оценить степень связывания противоионов поликатионом: $\beta = 0.4 \pm 0.1$.

**Ключевые слова:** поликатион, индикаторный краситель, кажущаяся константа ионизации, поли (гексаметилен гуанидин гидрохлорид), поли (диэтиламин гуанидин гидрохлорид), сульфофлуоресцеин, метилоранж, сульфофталеины.

А.Ю. Харченко*, М.О. Ромах*, К.В. Янова†, М.М. Терещук†, М.О. Мчедлов-Петросян*. Водні розчини полі (гексаметилен гуанідін гідрохлориду) та полі (диетиленаміно-гуанідін гідрохлориду: дослідження за допомогою кислотно-основних індикаторів.

* Харківський національний університет імені В. Н. Каразіна, хімічний факультет, пл. Свободи, 4, Харків, 61022, Україна

† Український державний хіміко-технологічний університет, проспект Гагаріна, 8, Дніпро, 49000, Україна

В цій статті досліджено властивості катіонних поліелектролітів як засобів керування протолітичними рівновагами кислотно-основних індикаторів у воді. З цією метою вивчено водорозчинні pH-залежні полі (гексаметилен гуанідін гідрохлорид), ПГМГ, та полі (діетиламін гуанідін гідрохлорид), ПДЕГ. Як молекулярні зонди використано набір аніонних індикаторних барвників, причому ключовим параметром є так звані уявні константи іонізації, $K_a^{app}$. Електрокінетичний потенціал обох макромолекул в кислій області pH суттєво позитивний. Як правило, досліджені поліелектроліти помітно впливають на спектри поглинання та стан кислотно-основних рівноваг барвників при pH < 7, особливо в разі ПГМГ. Обидва зазначені ефекти нагадують такі що спостерігалися для цих самих барвників у розчинах катіонних ПАР, але не настільки виражені. Кислотно-основні рівноваги досліджувалися здебільшого при співвідношенні поліелектроліт : барвник = 150 : 1, при іонній силі 0,05 М і 25 °C. Зниження значення $pK_a^{app}$ ($\equiv -\log K_a^{app}$) при переході від води до розчинів ПГМГ найбільш значне для бромкрезолового зеленого ($HB^- \rightleftharpoons B^{2-} + H^+$): $pK_{a,2}^{app} - pK_{a,2}^{w} = -1.93$. Для бромфенолового синього, бромкрезолового пурпурного та сульфофлуоресцеїна відповідний зсув менш виражений. Виявлено також деякі специфічні взаємодії метилоранжу та бромфенолового синього з поліелектролітами. Крім того, залежність $pK_a^{app}$ від логарифму іонної сили дозволяє оцінити ступінь зв'язування протиіонів полікатіоном: $\beta = 0.4 \pm 0.1$.

**Ключові слова:** полікатіон, індикаторний барвник, уявна константа іонізації, полі (гексаметилен гуанідин гідрохлорид), полі (диетиленаміно-гуанідін гідрохлорид), сульфофлуоресцеїн, метилоранж, сульфофталеїни.

УДК 546.26+544.77.03+544.77.051.1

# BEHAVIOR OF FULLERENE C$_{70}$ IN BINARY ORGANIC SOLVENT MIXTURES AS STUDIED USING UV-VIS SPECTRA AND DYNAMIC LIGHT SCATTERING

## N.A. Marfunin [a], N.O. Mchedlov-Petrossyan [b]

*V.N. Karazin Kharkiv National University, School of Chemistry, 4 Svoboda sqr., 61022 Kharkiv, Ukraine*

a) ✉ marfunin.n.a@gmail.com          ⓘ https://orcid.org/0000-0001-9886-3186
b) ✉ mchedlov@karazin.ua             ⓘ https://orcid.org/0000-0001-6853-8411

In this paper, the formation of colloidal species of fullerene C$_{70}$ in organic solvents was studied. The examining of the UV-visible spectra was accompanied by particle size analysis using dynamic light scattering, DLS. Stock solutions of C$_{70}$ in non-polar toluene and *n*-hexane were diluted with polar solvents acetonitrile and methanol. The appearance of colloidal species with a size within the range of ≈50–500 nm is accompanied by alterations of the absorption spectra.

In the toluene–acetonitrile and toluene–methanol binary mixed solvents at 25 $^{\circ}$C, the absorption spectra of C$_{70}$ (5×10$^{-6}$ M) tend to retain the features of the spectrum in neat aromatic solvent even if the C$_{70}$ molecules are gathered into colloidal aggregates. Earlier such phenomenon was observed for C$_{60}$ in benzene–acetonitrile and toluene–methanol solvent systems. This gives support to the idea of rather stable primary solvate shells formed by aromatic molecules around the fullerene molecules. The behavior of C$_{70}$ in toluene mixtures with methanol was compared with the earlier reported results from this laboratory for the C$_{60}$ fullerene in the same solvent system.

The study of *n*-hexane–methanol mixtures was performed at elevated temperature because of limited miscibility of these solvents at 25 $^{\circ}$C. Accordingly, the C$_{70}$–toluene–methanol system was also examined at 40 $^{\circ}$C. A small but distinctly noticeable difference was revealed. Whereas in the case of the last-named system, the absorption spectrum typical for molecular form of C$_{70}$ is still observable when colloidal species are already present in the solution, the turning-point between molecules and colloids as determined by both UV-visible spectra and DLS coincides for the *n*-hexane–methanol binary mixed solvent. Hence, the solvation shells formed by the aliphatic solvent around C$_{70}$ are less stable as compared with those formed by toluene.

Finally, the absorption spectra of C$_{70}$ in the mixed solvents toluene–*n*-hexane were analyzed. These data give some support to the assumption of preferable solvation of the C$_{70}$ molecules by the aromatic co-solvent.

**Keywords:** fullerene C$_{70}$, toluene, *n*-hexane, acetonitrile, methanol, molecular solutions, organosol, UV-visible absorption spectra, dynamic light scattering, particle size.

## State of the Arts

Behavior of fullerenes C$_{60}$ and C$_{70}$ in solvents of different nature was a matter of numerous studies during last decades [1–8]. In nonpolar solvents, these compounds probably exist in molecular form, especially if equilibrium methods are used for the preparation of the solutions [7–9]. Now it is of common knowledge that addition of polar solvents results in formation of (nanosized) colloidal species.

Let us consider state of the arts. As early as 1993, Sun and Bunker revealed that the absorption and emission spectra of C$_{70}$ in toluene change dramatically at adding acetonitrile and ascribed this phenomenon to fullerene aggregation [10]. This study was continued by the authors [11,12]. Next was a detailed study by Ghosh et al. [13], who used dynamic light scattering, DLS, spectrophotometry, steady state emission spectra, fluorescence polarization, and fluorescence lifetimes for C$_{70}$ in toluene–acetonitrile solvent system and in other binary mixed solvents: benzene–acetonitrile (methanol, hexane), benzonitrile–acetonitrile (hexane), and *o*-dichlorobenzene – acetonitrile.

Rudalevige et al. [14] confirmed the formation of C$_{60}$ and C$_{70}$ aggregates in mixtures of benzene or toluene with acetonitrile using static and dynamic light scattering, as well as photoluminescence.

Alargova et al. examined the behavior of C$_{60}$ and C$_{70}$ transferred to acetonitrile from different nonpolar solvents [15]. In all the above studies, fullerenes in acetonitrile form aggregates, or nanosized colloidal particles.

A more detailed consideration of the problem is presented in a review paper [8]. Note that fullerenes readily form crystal solvates with many solvents in the solid state [4,8]. Some nitrogen-containing

solvents, e.g., *N*-methylpyrrolidine-2-one, exhibit specific interactions with fullerenes [16,17], and such systems should be considered separately.

Naturally, when studying fullerenes in a mixed solvent it is important to estimate the critical composition (if any) of the transformation of molecular solution to a colloidal system. Nath et al. examined mixtures of nonpolar solvents with polar ones via spectrophotometry and revealed that in the case of $C_{60}$ such a critical composition corresponds to the relative permittivity of $\varepsilon_r \geq 13$ [18], whereas for $C_{70}$ this threshold corresponds to much higher polarity, $\varepsilon_r \approx 27$–$31$ [19].

A study in our laboratory showed that the critical composition depends on the fullerene concentration, at least for the $C_{60}$–toluene–methanol system [20]. On going from $4 \times 10^{-7}$ M to $4 \times 10^{-5}$ M $C_{60}$, the threshold changes from 67.5 to 55.0–57.5 vol. % $CH_3OH$ [20]. Basing on both DLS and spectrophotometry, some other regularity concerning the above system were also discussed in this paper [20]. In another publication [21], the peculiarities of $C_{60}$ behavior in benzene–acetonitrile systems were reported.

Though fullerene solutions in such solvents as *n*-hexane should be considered as true ones, i.e., molecular, some examples of oversaturated solutions with $C_{60}$ colloidal species about 200 nm have been reported [22]. On the other hand, Ginzburg et al. [23–27] disclosed unusual properties of $C_{60}$ and $C_{70}$ in aromatic solvents (benzene, toluene, xylenes) using ebullioscopy, X-ray diffraction patterns, and some other methods: the fullerene molecules are surrounded by shells of hundreds aromatic solvent molecules. This allows considering such molecular solutions as a kind of periodic colloidal systems, or colloidal crystals [10].

This paper is aimed to elucidate some features of $C_{70}$ solutions in mixed toluene- and *n*-hexane-based solvent systems and to make some conclusions concerning the state of fullerenes in polar–nonpolar binary mixed solvents.

## Experimental

The $C_{70}$ sample (NeoTechProduct., 99 %+) was used as received. After storing a weight amount of $C_{70}$ in toluene or *n*-hexane about two weeks, the solution was filtered using the 0.22 $\mu$m pore sized PTFE filters. The solubility of $C_{70}$ in these two solvents is (1.27; 1.67; 1.8)$\times 10^{-3}$ M and $1.5 \times 10^{-5}$ M, respectively [8]. In the case of toluene, the amount of $C_{70}$ was substantially below the solubility limit, and after filtration practically no substance was left on the filter. Thus, the concentration was calculated assuming complete dissolution. In the case of *n*-hexane, a marked quantity of the fullerene was collected on the filter, and therefore in this case the concentration of the stock solution was determined using the reported value of the molar absorptivity [28]. All solutions were stored in the dark. Toluene, *n*-hexane, acetonitrile, and methanol were purified and dehydrated via standard procedures. The absorption spectra were run using the Hitachi U-2000 spectrophotometer against solvent blanks. A Zetasizer Nano ZS apparatus (Malvern Instruments) was used for analyzing the particle size distribution via DLS. Sun and Bunker [11] demonstrated the dependence of spectroscopic results in the procedure of solution preparation in the $C_{70}$–toluene–$CH_3CN$ system. We used the following method. An aliquot of toluene was placed into a flask, a polar component was added and the solution was mixed. In such way the solution was almost made up to the mark. Then, a small volume of the stock solution of $C_{70}$ was added and after mixing the measurements were done. This procedure allowed avoiding the appearance of a broad and unstable in time absorption band about 700 nm observed by Sun and Bunker [11]. In the case of the *n*-hexane–methanol system, the $C_{70}$ solution in *n*-hexane was mixed with the required volume of methanol; both solutions were preliminary heated and all solvent parameters necessary for processing the DLS data were used for 40 °C. Normally, the colloidal particles are formed just after preparation of the solutions, contrary to the case of toluene–*N*-methylpyrrolidine-2-one system [16], and as a rule were stable within several h. The solvent composition was expressed as volume percent if not otherwise specified.

## Results and Discussion

*Toluene–acetonitrile system, 25 °C*
As it was mentioned in the overview, this is currently the most studied system. Our results confirm the published data. In Figure 1, the absorption spectra are presented. In pure toluene, the absorption maxima are as follows: $\lambda_{max} = 315$; 334; 365; 383; and 473 nm.

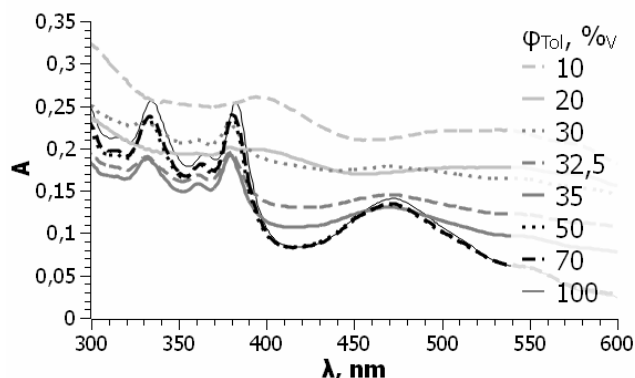**Figure 1.** Selected absorption spectra of $C_{70}$ ($5 \times 10^{-6}$ M) in the toluene–acetonitrile solvent system at 25 $^{\circ}$C.

A gradual decreasing in the intensity at 382 nm takes place along with the increase in the first $CH_3CN$ fraction. Up to 50 % of toluene, positions of the maxima alter but slightly; a hypsochromic shift of ca. 1–2 nm was observed. Further rise of the acetonitrile content cause dramatic changes of the spectra, especially within the range of 500–600 nm (see the spectrum at 30 % toluene). The absorption maxima became fuzzy, the integral intensity strongly increases. Such absorption is an evidence of aggregation of fullerene molecules. Under such conditions, a contribution of light scattering cannot be ruled out. Our spectral data resemble in outline those reported by others [10,13,19].

As a turning-point, the toluene content of 32.5 to 35 % should be considered. At 32.5 %, the $\lambda_{max}$ values of $C_{70}$ somewhat differ from those in pure toluene: 315; 333; 361; 380; and 470 nm, but some features of molecular spectrum, e.g., the band with $\lambda_{max}$ around 380 nm, are still observed. In Figure 2 (left), the dependences of the absorbance at 470 nm and 600 nm on the solvent composition are depicted. Abrupt changes occur within the range of 30–36 % toluene. The $A_{600}$ symbol means the absorption at 600 nm. $H_{470}$ denotes the additional intensity of absorption after subtracting the "basic line". The latter is drawn from absorption at 540 nm to 425 nm in pure toluene.

In Figure 2 (right), the dependence of particle size is presented. It can be firmly stated that the aggregation of the $C_{70}$ molecules occurs at toluene content around 40 %. This corresponds to a decrease in the fluorescence quantum yield and integral absorption intensity [11]. Hence, the absorption spectrum retains the main features that are typical for the molecular fullerene, while the particle size is over 200 nm. As a plausible reason, we may assume that the fullerene molecules hold their initial aromatic solvation shell even when colloidal species are formed. At higher content of acetonitrile, the $C_7H_8$ molecules are probably replaced by $CH_3CN$. As an alternative explanation, the presence of single molecules solvated with toluene may be assumed. Than their absence in the DLS picture should be explained by overlapping their signal by strong scattering of colloidal species. Sun and Bunker, however, consider such assumption as improbable basing on the fluorescence and fluorescence excitation spectra [11].
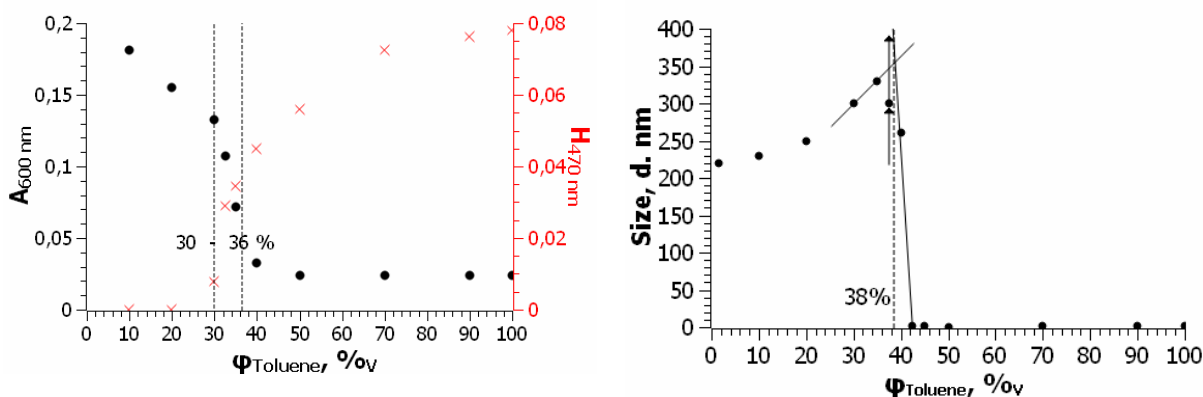


**Figure 2.** Alterations of the electronic absorption spectra of $C_{70}$ (left; optical path length 1.00 cm) and the particle size distribution (by intensity, right) in toluene–acetonitrile solvent system, fullerene concentration $5 \times 10^{-6}$ M; 25 $^{\circ}$C. The size at 37.5 % toluene increases over time.

Particle size distribution is typified in Figure 3. The results for 30 % toluene agree with those published by Ghosh et al. for $6 \times 10^{-6}$ M $C_{70}$; see Fig. 4C in ref. [13]. Note, that in acetonitrile-reach mixed solvents, the size of colloidal species is substantially smaller as compared with those just after the turning-point (Figure 2, right and Figure 3), like in the $C_{60}$–toluene–methanol system [20].
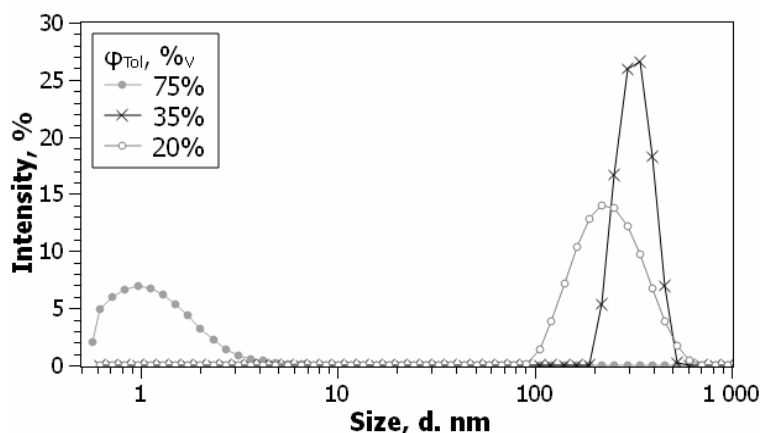


**Figure 3.** Examples of particle size distribution (by intensity) $C_{70}$ ($5 \times 10^{-6}$ M) in the toluene–acetonitrile solvent system at 25 $^{\circ}$C.

In the previous studies on $C_{60}$ in this laboratory, similar regularities were observed. In a benzene–acetonitrile mixed solvent, the absorption band with $\lambda_{max}$ = 335 nm at 50 % benzene is close to that in pure benzene (only the intensity drops by ca. 20 %), while the colloidal species with the size of 100-200 nm are registered via DLS; the data refer to $C_{60}$ concentration of $4 \times 10^{-5}$ M [29]. The data obtained for $C_{60}$ in the toluene–methanol system are of the same type [20]. In 50 % toluene solution, the band maximum, 336 nm, is the same as in toluene, whereas the intensity is ca. 18 % lower than in the entire aromatic solvent, though large colloidal species are already present in the solution (fullerene concentration $6.8 \times 10^{-6}$ M; 25 $^{\circ}$C). Even at 30 % toluene, a band with the same $\lambda_{max}$ is observed, though of much lower intensity [20].

Nath et al. established the threshold content of the polar solvent where the aggregation begins by examining the absorption spectra of $C_{60}$ within the range of 450–650 nm [18, 19]. As it was already stated in the pioneering work by Sun and Bunker for $C_{70}$ in toluene–acetonitrile mixed solvent [10] and confirmed by us for $C_{60}$ in toluene–methanol system [20], such threshold depends to some extent on the fullerene concentration. Though Sun and Bunker preferred to use for the aggregates under discussion the term "cluster" and expected the $C_{70}$ solution at 70 % acetonitrile quite different from a conventional colloidal solution [10], both results reported by Ghosh [13] and our data (Figure 2, right) indicate the presence of colloidal species at the corresponding concentrations of the fullerene.* The lower the fullerene concentration is, the higher content of a polar solvent is necessary to reach the aggregation. This is quite understandable because of poor solubility of fullerenes in polar solvent.

More interesting is another observation made by Sun and Bunker: under conditions of extreme dilution, down to $8 \times 10^{-8}$ M, the absorption spectrum in 70 % $CH_3CN$ is close to the spectrum in neat toluene. In this connection, Sun and Bunker stated "The result indicates that the formation of the new species involves more than one $C_{70}$ molecule" [10]. As these authors have not used the DLS method, we made the corresponding measurements. Even at somewhat higher $C_{70}$ concentration of $1.2 \times 10^{-7}$ M, only species of about 1 nm (like shown in Figure 3) were found in 70 % acetonitrile.

Concluding, at least the first stages of the fullerene aggregation occur in the systems under study with retaining some part of the primary aromatic shell as follows from matching the UV-vis and DLS data. Also, the lower the toluene content is, the smaller is the size of the colloidal species. In extreemely diluted $C_{70}$, the aggregates are undetectable via the DLS method even in 70 % of acetonitrile.

---

* *The coagulation of such aggregates by electrolytes [29] additionally confirms their typically colloidal nature.*

*Toluene–methanol system, 25 °C*

Now let us compare the above data with those previously reported for $C_{60}$ in the same solvent system [20]. In the last-named study, a DLS investigation of $C_{60}$ within the whole range of toluene–methanol binary mixed solvent was performed at three concentrations of the fullerene, $4\times10^{-7}$, $4\times10^{-6}$, and $4\times10^{-5}$ M. In brief, the conclusions are as follows:

(i) At $4\times10^{-7}$ M $C_{60}$ the aggregates appear at 67.5 vol % methanol, whereas in $4\times10^{-5}$ M solution, it already occur at 55.0–57.5 vol % of alcohol. Similar tendency was observed for $C_{70}$ in the toluene–acetonitrile system by Sun and Bunker [11].

(ii) Normally, the higher the fullerene concentration is, the larger are the aggregates at the same composition of the mixed solvent. For $C_{70}$ in toluene–acetonitrile system, similar tendency was reported by Ghosh et al., see ref. [13], Fig. 4B,C.

(iii) The dependence of the size of the aggregates on the methanol content is in line with the Volmer's rule [30]: the less soluble is the compound in the given solvent, the smaller particles are formed. For example, at $4\times10^{-7}$ M $C_{60}$ in 99; 95; and 70 vol. % methanol, the particle size is around 200; 260-320; and 470–500 nm, respectively. The polydispersity index, PDI, increases in the same direction. As an alternative (or additional) explanation, the participation of toluene in the aggregates may be proposed. Because fullerenes readily form solvates containing hundreds of toluene molecules [27], they may aggregate not as "bare" $C_{60}$ molecules, but rather as solvates, at least at high toluene content in the mixed solvent.

(iv) The results obtained at $C_{60}$ concentration of $4\times10^{-6}$ M are closer rather to those for $4\times10^{-7}$ M $C_{60}$, than for $4\times10^{-5}$ M.

Note, that at $6.8\times10^{-6}$ M $C_{60}$ a band at 336 nm, typical for the monomeric species, was observed not only at 70 %, but even at 80 % of methanol, where the 300 nm-sized colloidal species predominate.

Going back to the solutions of $C_{70}$ examined in the present study, we can argue that the picture is quite similar. Even at 35 % of toluene, the spectrum is similar to that in pure toluene except intensity increase at wavelength over 400 nm (Figure 4).
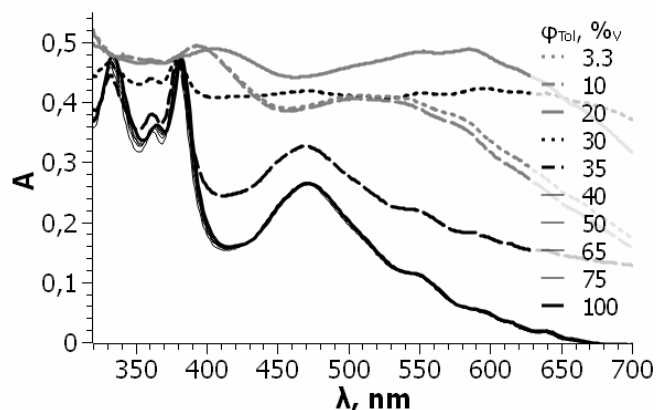


**Figure 4.** Selected absorption spectra of $C_{70}$ ($5\times10^{-6}$ M) in the toluene–methanol solvent system at 25 °C, normalized at absorption at 382 nm.

At the same time, at such composition of the solvent colloidal species already appear (Figure 5, fullerene concentration $5\times10^{-6}$ M). As in the previous case, the size of the colloidal particles rises (here: up to 480 nm) and then decreases along with decrease in the content of toluene.

The peculiarity of this system consists in the appearance of small amounts of 100–200 nm-sized particles even at 40, 50, 60 % toluene, however, only in the distribution by intensity. They are absent in other types of distributions, but they are observed repeatedly and their percentage in the above mixed solvents is 15, 11, and 3%, respectively. In the $C_{60}$–toluene–methanol system, small amounts of such particles were observed even at 5 % of methanol [20].

Further increase in the methanol fraction results in formation of colloidal species, which are observable also in distributions by volume and particle number.
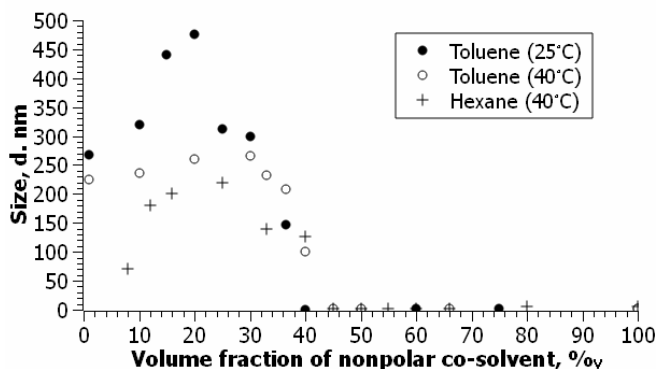
**Figure 5.** Alterations of the particle size distribution (by intensity) in toluene–methanol and *n*-hexane–methanol solvent systems; 25 °C.

### Toluene–methanol system, 40 °C

The reason for studying this system at an enhanced temperature was further comparing with the *n*-hexane–methanol system, which tends to stratify below 40 °C [31]. The spectra are presented in Figure 6, particle sizes are given above in Figure 5.
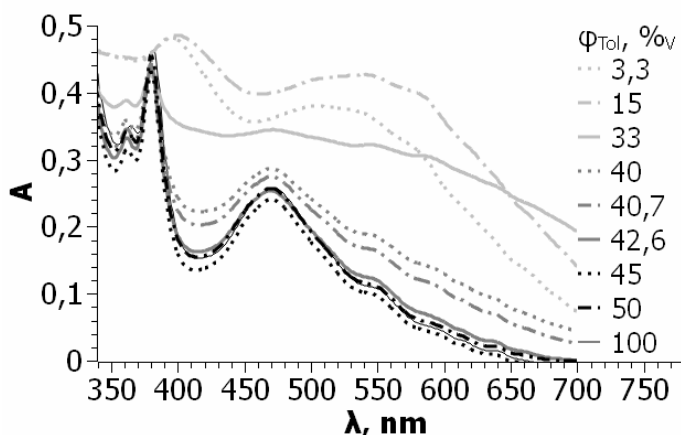


**Figure 6.** Selected absorption spectra of $C_{70}$ ($5 \times 10^{-6}$ M) in the toluene–methanol solvent system at 40 °C, normalized at absorption at 382 nm.
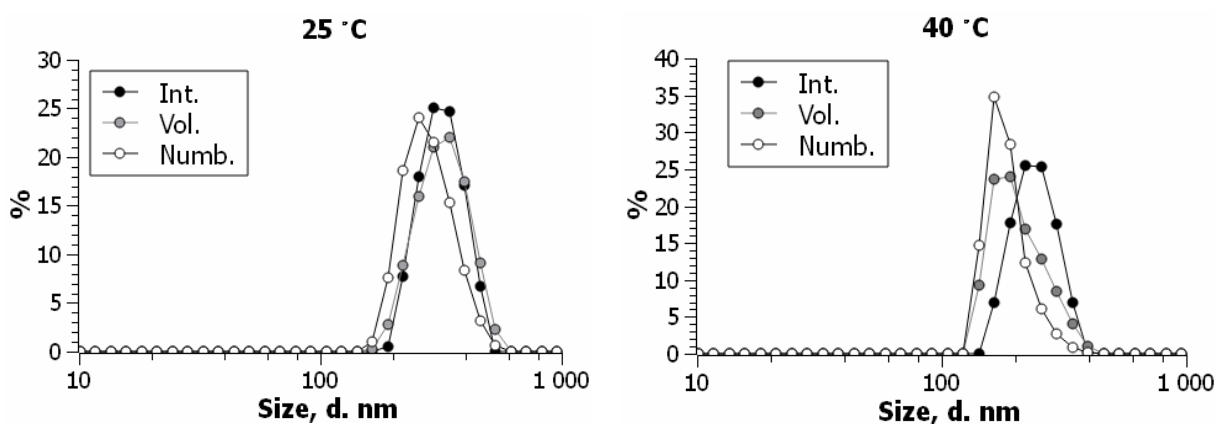


**Figure 7.** The particle size distribution by intensity, volume, and number for $C_{70}$ ($5 \times 10^{-6}$ M) in the toluene–methanol binary solvent, 10 vol. % of toluene at 25 °C.

The morphology of the absorption curve retains in outline down to 42.6 % toluene, despite some intensity decrease in the short wavelength portion. Along with further decrease in the content of toluene, a flattering of the spectral curve and substantial rise of the integral absorption takes place. The

peak about 380 nm is observable even at 30 % toluene. This band undergoes a slight hypsochromic 3-4 nm shift as compared with the band in entire toluene.

In the DLS patterns, the turning-point corresponds to 40 % toluene (Figure 5). Again, as at 25 ºC, at 45 and 50 % toluene, 25–75 nm-sized particles were observed only in the distribution by intensity (35 and 20 %, respectively). The particles size in the undoubtedly colloidal region is maximal at 30 % toluene, and then decreases (Figure 5). Normally, at the elevated temperature the colloidal species are smaller than at 25 ºC, whereas other regularities typical for fullerenes in toluene(or benzene)–polar solvent mixed solvents are fulfilled.

In Figure 7, the particle size distributions of $C_{70}$ at 25 and 40 ºC are exemplified for toluene content of 10 %. In these conditions we are talking about typical organosols.

### n-Hexane–methanol system, 40 ºC

The absorption spectra are presented in Figure 8, and the alterations of size are already given in Figure 5.
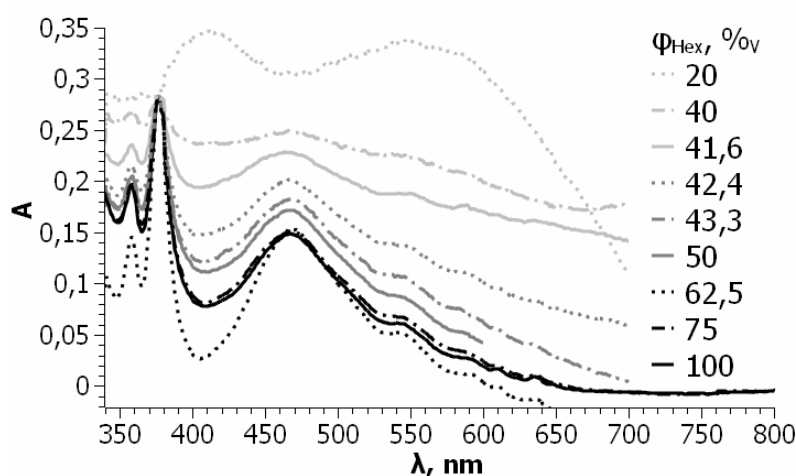


**Figure 8.** Absorption spectra of $C_{70}$ in the *n*-hexane–methanol solvent system at 40 ºC, normalized at absorption at 377 nm.

In this system, the *n*-hexane was introduced in form of a portion of the stock fullerene solution. Therefore, the concentration of $C_{70}$ in the working solutions was inconstant. For example, at *n*-hexane content of 100; 66.7; 50; 25; 15; and 10 %, the $C_{70}$ concentrations in the working solutions were (10.0; 6.67; 5.0; 2.5; 1.5; and 1.0) $\times 10^{-6}$ M.

In Figure 5 it is clearly seen that the turning-point is at 40 % *n*-hexane. At 55–45 % *n*-hexane some 50–100 nm-sized particles are observed only by intensity, but rather distinct (30–60%) and repeatable. At the content of the hydrocarbon < 40%, big particles are fixed in all types of distribution. Here, a decrease in size at high concentrations of methanol is also evident, as in the toluene-containing systems (Figure 5). However, it should be taken into account that the fullerene concentration is very low in this range.

The character of the electronic absorption spectra at 42.4–41.6 % of $C_6H_{14}$ retains the features of that in entire *n*-hexane, though some alterations in the long wavelength portion are evident (Figure 8). At 40 % *n*-hexane, the spectrum changes cardinally.

Hence, whereas in the case of the last-named system, the absorption spectrum typical for molecular form of $C_{70}$ is still observable when colloidal species are already present in the solution, the turning-point between molecules and colloids as determined by both UV-visible spectra and DLS coincides for the *n*-hexane–methanol binary mixed solvent. Hence, the solvation shells formed by the aliphatic solvent around $C_{70}$ are less stable as compared with those formed by toluene.

### Toluene–n-hexane system, 25 ºC

Finally, the absorption spectra of $C_{70}$ in toluene–*n*-hexane system were studied. Normalized UV-visible spectra are presented in Figure 9. In this special case, the procedure was as follows. Two

volumes of solvents were mixed, e.g. 75 vol.% *n*-hexane means that 7.5 mL of this solvent (containing $C_{70}$) were mixed with 2.5 mL of toluene, etc.
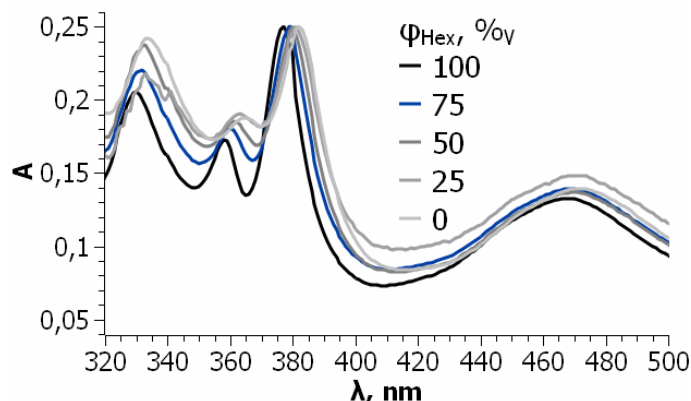


**Figure 9.** Selected normalized absorption spectra of $C_{70}$ in the toluene–*n*-hexane solvent system; fullerene concentrations: (10.0; 7.5; 5.0; 2.5; and 57,5)$\times 10^{-6}$ M, respectively.

Though both co-solvents belong to nonpolar ones, these spectral data allow to shed some light upon the solvation character. The gradual bathochromic shift on going from *n*-hexane to toluene and the absence of an isosbestic point allows expecting that the replacement of aliphatic molecules by aromatic ones occurs little by little. The shifts are relatively small. Indeed, Ghosh et al. mentioned that the color of $C_{70}$ in benzene–*n*-hexane solutions does not display color change [13].

In the system of interest, the shifts from 376.5 to 382.0 and from 358.1 to 364.5 nm equal to 5.5 and 6.4 nm, respectively (Table 1). But even this modest solvatochromic effect discloses a tendency to preferred solvation of $C_{70}$ molecules by toluene. Indeed, the average values of $\lambda_{max}$ are 379.3 and 361.3 nm, respectively. In both vol % and molar fraction scales, these values correspond to somewhat lower content of toluene. The same conclusion can be made using wave numbers instead of wavelengths. Thus, despite the proximity of the absorption peaks in both solvent, an evidence of better solvation by toluene molecules is obtained.

**Table 1.** Positions of two characteristic absorption maxima in the $C_{70}$ UV-spectra in the toluene–*n*-hexane system, 25 $^\circ$C

| Toluene, volume % | Toluene, molar fraction | Absorption maxima, nm | |
|---|---|---|---|
| 100 | 1.00 | 382.0 | 364.5 |
| 75 | 0.787 | 381.0 | 363.3 |
| 50 | 0.552 | 380.0 | 362.0 |
| 37 | 0.420 | 379.5 | 361.5 |
| 25 | 0.291 | 379.2 | 362.8 |
| 17 | 0.201 | 379.0 | 361.0 |
| 10 | 0.120 | 378.0 | 359.4 |
| 5 | 0.061 | 377.0 | 358.6 |
| 0 | 0 | 376.5 | 358.1 |

## Conclusions

1. Formation of colloidal species of $C_{70}$ in toluene–acetonitrile, toluene–methanol, and *n*-hexane–methanol binary solvent mixtures is detected by both UV-visible spectroscopy and dynamic light scattering methods. In all the examined systems, some turning-point from molecular solution to organosol can be fixed by both methods.

2. Whereas for the *n*-hexane–methanol system at 40 $^\circ$C the turning point as estimated by UV-visible spectra and DLS measurements agree, in the toluene–acetonitrile (at 25 $^\circ$C) and in toluene–methanol systems (at 25 and 40 $^\circ$C) the absorption spectra retain some distinct features of molecular absorption even when colloidal aggregates are firmly detected in the solution. This agrees with our previous data for $C_{60}$ in benzene–acetonitrile and toluene–methanol

solvent systems. It may be explained by high affinity of aromatic molecules to the fullerenes: some $C_{70}$ (and $C_{60}$) molecules form aggregates keeping their aromatic solvation shells.

3. UV spectra of $C_{70}$ in the toluene–$n$-hexane binary mixtures confirm a better expressed affinity of toluene to the all-carbon molecule. Better solvation of $C_{70}$ with the aromatic toluene as compared with the aliphatic $n$-hexane is in line with the solubility of the fullerene in these two solvents, $1.6 \times 10^{-3}$ and $1.5 \times 10^{-5}$ M, respectively.

4. Organosols of $C_{70}$ obey some rules, like previously observed for $C_{60}$ in similar systems. High content of the polar solvent, high temperature, and low fullerene concentration favor formation of smaller colloidal particles.

## References

1. Ruoff R.S., Tse D.S., Malhotra R., Lorents D.C. Solubility of $C_{60}$ in a variety of solvents. *J. Phys. Chem.* **1993**, *97*(13), 3379-3383.

2. Marcus Y. Solubilities of buckminsterfullerene and sulfur hexafluoride in various solvents. *J. Phys. Chem.* **1997**, *101*(42) 8617-8623.

3. Beck M.T. Solubility and molecular state of $C_{60}$ and $C_{70}$ solvents and solvent mixtures. *Pure Appl. Chem.* **1998**, *70*(10), 1881-1887.

4. Marcus Y., Smith A.L., Korobov M.V., Mirakyan A. L., Avramenko N. V., Stukalin E.B. Solubility of $C_{60}$ fullerene. *J. Phys. Chem.B* **2001,** *105*(13), 2499-2506.

5. Kinchin A.N., Kolker A.M., Islamova N.I. Correlations between the thermodynamic parameters of solution of fullerene $C_{60}$ and the properties of nonaqueous solvents. (in Russian). Zhurn. Fiz. Khim. **2002**, *76*(10), 1772-1776.

6. Semenov K.N., Charykov N.A., KeskinovV.A., Piartman A.K., Blokhin A.A., Kopyrin A.A. Solubility of light fullerenes in organic solvents. *J. Chem. Eng. Data.* **2010**, *55*(1), 13-36.

7. Avdeev M.V., Aksenov V.L., Tropin T.V. Models of cluster formation in solutions of fullerenes. *Russ. J. Phys. Chem. A* **2010**, *84*(8), 1273-1283.

8. Mchedlov-Petrossyan N.O. Fullerenes in Liquid Media: An Unsettling Intrusion into the Solution Chemistry. *Chem. Rev.* **2013,** *113*(7), 5149-5193.

9. Aksenov V.L., Avdeev M.V., Tropin T.V., Priezzhev V.B., Schmelzer J.W.P. Cluster growth and dissolution of fullerenes in non-polar solvents. *J. Mol. Liquids.* **2006**, *127*, 142-144.

10. Sun Y.-P., Bunker C.E. $C_{70}$ in solvent mixtures. *Nature*, **1993**, *365*, 398.

11. Sun Y.-P., Bunker C.E. Formation and Properties of $C_{70}$ Solidlike Species in Room-Temperature Solutions. *Chem. Mater*. **1994**, *6*(5), 578-580.

12. Sun Y.-P., Ma B., Bunker C.E., Liu B. All-Carbon Polymers (Polyfullerenes) from Photochemical Reactions of Fullerene Clusters in Room-Temperature Solvent Mixtures. *J. Am. Chem. Soc.* **1995**, *117*(51), 12705-12711.

13. Ghosh H.N., Sapre A.V., Mittal J.P. Aggregation of $C_{70}$ in Solvent Mixtures. *J. Phys. Chem.* **1996**, *100*(22), 9439-9443.

14. Rudalevige T., Francis A.H., Zand R. Spectroscopic studies of fullerene aggregates. *J. Phys. Chem. A.* **1998**, *102*(48), 9797-9802.

15. Alargova R.G., Deguchi S., Tsujii K. Stable Colloidal Dispersions of Fullerenes in Polar Organic Solvents. *J. Am. Chem. Soc.* **2001,** *123*(43), 10460-10467.

16. Alfe M. Alfe, B. Apicella, R. Barbella, A. Bruno, A. Ciajolo. Aggregation and interactions of $C_{60}$ and $C_{70}$ fullerenes in neat *N*-methylpyrrolidinone and in *N*-methylpyrrolidinone/toluene mixtures. *Chem. Phys. Lett.* **2005**, *405*, 193-197.

17. Nagorna T.V., Kuzmenko M.O., Kyzyma O.A., Chudoba D., Nagornyi A.V., Tropin T.V., Garamus V.M., Jazdzewska M., Bulavin L.A. Structural reorganization of fullerene $C_{70}$ in N-methyl-2-pyrrolidone / toluene mixtures. *J. Mol. Liquids.* **2018**, *272*, 948-952.

18. Nath S., Pal H., Nath A.V.S., Pal H., Sapre A.V. Effect of solvent polarity on the aggregation of $C_{60.}$ *Chem. Phys. Lett.* **2000**, *327*, 143-148.

19. Nath S., Pal H., Sapre A.V., Effect of solvent polarity on the aggregation of fullerenes: a comparison between $C_{60}$ and $C_{70}$. *Chem. Phys. Lett.* **2002**, *360*, 422-428.

20. Mchedlov-Petrossyan N.O., Kamneva N.N., Al-Shuuchi Y.T.M., Marynin A.I., Shekhovtsov S.V. The peculiar behavior of fullerene $C_{60}$ in mixtures of 'good' and polar solvents: Colloidal

particles in the toluene–methanol mixtures and some other systems. *Colloids Surfaces A*. **2016**, *509*, 631-637.

21. Mchedlov-Petrossyan N.O., Kamneva N.N., Al-Shuuchi Y.T.M., Marynin A.I., Zozulia O.S. Formation and ageing of the fullerene C$_{60}$ colloids in polar organic solvents. *J. Mol. Liquids*. **2017**, *235*, 98-103.

22. Chamberlain T.W., Popov A.M., Knizhnik A.A., Samoilov G.E., Khlobystov A.N. The role of molecular clusters in the filling of carbon nanotubes. *ACS NANO* **2010**, *4*(9), 5203-5210.

23. Ginzburg B.M., Tuĭchiev Sh. Variations in the structure of aromatic solvents under the influence of dissolved fullerene C$_{70}$. *Crystallogr. Rep*. **2008**, *53*(4), 645-650.

24. Ginzburg B.M., Tuĭchiev Sh., Shukhiev S. Permittivity of Low_Concentration C60 Fullerene Solutions in *p_Xylene*. *Tech. Phys. Lett*. **2009**, *35*(6), 491-493.

25. Ginzburg, B. M.; Tuĭchiev, Sh.; Tabarov, S. Kh. Effect of C$_{60}$ Fullerene on the Boiling Point of Its Solutions in Some Aromatic Solvents*Russ. J. Appl. Chem*. **2009**, *82*(3), 387–390.

26. Ginzburg B.M., Tuichiev Sh., Yakimanskii A.V. Supramolecular Benzene Structure and Its Changes under the Action of Dissolved Fullerenes. *Crystallogr. Rep.* **2011***, 56*(2), 238-241.

27. Ginzburg B.M., Tuichiev Sh., Rashidov D., Sodikov F.H., Tabarov S.H., Shepelevskii A.A. Step-Wise Concentration Influence of Fullerenes C$_{60}$ and C$_{70}$ on the Various Parameters of Condensed Systems. Part 1: The Concept of Step-Wise Behavior and its Manifestation in Fullerene Solutions. *J. Macromol. Sci., Part B: Physics*. **2015**, *54*, 533-543.

28. Cataldo F., Iglesias-Groth S., Hafez Y. On the molar extinction coefficients of the electronic absorption spectra of C$_{60}$ and C$_{70}$ fullerenes radical cation. *Eur. Chem. Bull*. **2013**, *2*(12)*, 1013-1018.

29. Mchedlov-Petrossyan N.O., Kamneva N.N., Al-Shuuchi Y.T.M., Marynin A.I. , Zozulia O.S., Kryshtal A.P., Klochkov V.K., Shekhovtsov S.V. Towards better understanding of C$_{60}$ organosols. *Phys. Chem. Chem. Phys*. **2016**, *18*, 2517-2526.

30. Volmer M. Kinetik der Phasenbildung (Russian translation), Nauka, Moscow, 1986, Ch. 5.

31. Semenov I.A., Sitnikov D.N., Romanovskiy A.A., Ulyanov B.A. Solubility and equuiliria in bimary mixtures of methanol with *n*-pentane, *n*-hexane, and *n*-heptane. (in Russian). *Izvestiya Vusov. Khim. I Khim. Technol*. **2012**, *55*(8), 39-42.

Н.А. Марфунин, Н.О. Мчедлов-Петросян. Поведение фуллерена C$_{70}$ в бинарных смесях органических растворителей, исследованное при помощи электронной спектроскопии и динамического рассеяния света.

Харьковский национальный университет имени В.Н. Каразина, химический факультет, пл. Свободы, 4, Харьков, 61022, Украина

В данной работе было изучено формирование коллоидных частиц фуллерена C$_{70}$ в органических растворителях. Исследование электронных спектров поглощения сопровождалось анализом размера частиц при помощи динамического рассеяния света, ДРС. Исходные растворы C$_{70}$ в неполярных толуоле и *н*-гексане разбавляли полярными растворителями ацетонитрилом и метанолом. Появление коллоидных частиц с размерами в диапазоне ≈50–500 нм сопровождается изменением спектров поглощения. В бинарных смешанных растворителях толуол–ацетонитрил и толуол–метанол при 25 $^{\circ}$C спектры поглощения C$_{70}$ (5×10$^{-6}$ M) проявляют тенденцию сохранять особенности спектра в чистом ароматическом растворителе, даже если молекулы C$_{70}$ присутствуют уже только в агрегатах. Ранее такое явление наблюдалось для C$_{60}$ в системах растворителей бензол–ацетонитрил и толуол–метанол. Это подтверждает предположение о наличии стабильных первичных сольватных оболочек, образованных ароматическими молекулами вокруг молекул фуллерена. Поведение C$_{70}$ в смесях толуола с метанолом сопоставлено с ранее опубликованными результатами этой лаборатории для фуллерена C$_{60}$ в той же системе растворителей.

Исследование смесей *н*-гексан–метанол проводилось при повышенной температуре из-за ограниченной смешиваемости этих растворителей при 25 $^{\circ}$C. Соответственно, система C$_{70}$–толуол–метанол была также исследована при температуре 40 °C. Было обнаружено небольшое, но отчетливо заметное различие в свойствах этих двух систем. В то время как во втором случае типичный для молекулярной формы C$_{70}$ спектр поглощения все еще наблюдается, когда коллоидные частицы уже присутствуют в растворе, точка перехода между молекулами и агрегатами совпадает для бинарного смешанного растворителя *н*-гексан–

метанол как по данным как электронной спектроскопии, так и ДРС. Следовательно, сольватные оболочки, образованные алифатическим растворителем вокруг $C_{70}$, менее стабильны по сравнению с оболочками, образованными толуолом.

Наконец, были проанализированы спектры светопоглощения $C_{70}$ в смешанном растворителе толуол–*н*-гексан. Эти данные говорят в пользу предпочтительной сольватации молекул $C_{70}$ ароматическим компонентом бинарного растворителя.

**Ключевые слова:** фуллерен $C_{70}$, толуол, *н*-гексан, ацетонитрил, метанол, молекулярные растворы, органозоли, электронные спектры поглощения, динамическое рассеяние света, размер частиц.

М.О. Марфунін, М.О. Мчедлов-Петросян. Поведінка фуллерену $C_{70}$ у бінарних сумішах органічних розчинників, вивчена за допомогою електронної спектроскопії та динамічного розсіяння світла.

Харківський національний університет імені В. Н. Каразіна, хімічний факультет, пл. Свободи, 4, Харків, 61022, Україна

У даній роботі було вивчене формування колоїдних частинок фуллерену $C_{70}$ в органічних розчинниках. Вивчення електронних спектрів поглинання супроводжувалося аналізом розміру частинок за допомогою динамічного розсіяння світла, ДРС. Вихідні розчини $C_{70}$ у неполярних толуолі та *н*-гексані розводили полярними розчинниками ацетонітрилом та метанолом. Поява колоїдних часток з розмірами у діапазоні ≈50-500 нм супроводжується зміною спектрів поглинання. У бінарних змішаних розчинниках толуол–ацетонітрил та толол–метанол при 25 °C спектри поглинання $C_{70}$ ($5 \times 10^{-6}$ M) мають тенденцію зберігати особливості спектру у чистому ароматичному розчиннику, навіть якщо молекули $C_{70}$ наявні лише у формі агрегатів. Раніше таке явище спостерігалось для $C_{60}$ у системах розчинників бензол–ацетонітрил і толуол–метанол. Це підтверджує ідею щодо існування стабільних первинних сольватних оболонок, утворених ароматичними молекулами навколо молекул фуллерену. Поведінка $C_{70}$ у сумішах толуолу з метанолом порівнювалас з раніше опублікованими результатами цієї лабораторії для фуллерену $C_{60}$ у тій же системі розчинників.

Вивчення сумішей *н*-гексан–метанол проводилося при підвищеній температурі через обмежену змішуваність цих розчинників при 25 °C. Відповідно, система $C_{70}$–толуол–метанол також була досліджена при 40 °C. Було виявлено невелику, але помітну різницю. В той час як у випадку останньої системи типовий для молекулярної форми $C_{70}$ спектр поглинання все ще спостерігається, коли колоїдні частинки вже присутні у розчині, точка переходу між молекулами та агрегатами співпадає для бінарного змішаного розчинника *н*-гексан–метанол за даними як електронної спектроскопії, так і ДРС. Таким чином, сольватні оболонки, утворені аліфатичним розчинником навколо $C_{70}$, є менш стабільними у порівнянні з оболонками, що утворені толуолом.

Врешті було проаналізовано спектри світлопоглинання $C_{70}$ у змішаному розчиннику толуол–*н*-гексан. Ці дані свідчать на користь переважної сольватації молекул $C_{70}$ ароматичним компонентом бінарного розчинника.

**Ключові слова:** фуллерен $C_{70}$, толуол, *н*-гексан, ацетонітрил, метанол, молекулярні розчини, органозолі, електронні спектри, динамічне розсіяння світла, розмір частинок.

**ЕТИЧНІ НОРМИ ПУБЛІКАЦІЇ НАУКОВИХ РЕЗУЛЬТАТІВ ТА ЇХ ПОРУШЕННЯ**. Редакційна колегія робить все можливе для дотримання етичних норм, прийнятих міжнародним науковим товариством, і для запобігання будь-яких порушень цих норм. Така політика є важливою умовою плідної участі журналу в розвитку цілісної системи знань в галузі хімії та суміжних галузях. Діяльність редакційної колегії значною мірою спирається на рекомендації Комітету з етики наукових публікацій (Committee of Publication Ethics), а також на цінний досвід міжнародних журналів та видавництв. Подання статті на розгляд означає, що вона містить отримані авторами нові нетривіальні наукові результати, які раніше не були опубліковані. Кожну статтю рецензують щонайменше два експерти, які мають усі можливості вільно висловити мотивовані критичні зауваження щодо рівня та ясності представлення матеріалу, його відповідності профілю журналу, новизни та достовірності результатів. Рекомендації рецензентів є основою для прийняття остаточного рішення щодо публікації статті. Якщо статтю прийнято, вона розміщується у відкритому доступі; авторські права зберігаються за авторами. За наявності будь-яких конфліктів інтересів (фінансових, академічних, персональних та інших), учасники процесу рецензування мають сповістити редакційну колегію про це. Всі питання, пов'язані з можливим плагіатом або фальсифікацією результатів ретельно обговорюються редакційною колегією, рівно як спори щодо авторства та доцільність роздроблення результатів на невеличкі статті. Доведені плагіат чи фальсифікація результатів є підставами для безумовного відхилення статті.

**STATEMENT ON THE PUBLICATION ETHICS AND MALPRACTICE**. The Editorial Board has been doing its best to keep the ethical standards adopted by the world scientific community and to prevent the publication malpractice of any kind. This policy is considered to be an imperative condition for the fruitful contribution of the journal in the development of the modern network of knowledge in chemistry and boundary fields. The activity of the Editorial Board in this respect is based, in particular, on the recommendations of the Committee of Publication Ethics and valuable practice of world-leading journals and publishers. The submission of a manuscript implies that it contains new significant scientific results obtained by authors that where never published before. Each paper is peer reviewed by at least two independent experts who are completely free to express their motivated critical comments on the level of the research, its novelty, reliability, readability and relevance to the journal scope. These comments are the background for the final decision about the paper. Once the manuscript is accepted, it becomes the open-access paper, and the copyright remains with authors. All participants of the review process are strongly asked to disclose conflicts of interest of any kind (financial, academic, personal, etc.). Any indication of plagiarism or fraudulent research receives extremely serious attention from the side of the Editorial Board, as well as authorship disputes and groundless subdivision of the results into several small papers. Confirmed plagiarism or fraudulent research entail the categorical rejection of the manuscript.

**ЭТИЧЕСКИЕ НОРМЫ ПУБЛИКАЦИИ НАУЧНЫХ РЕЗУЛЬТАТОВ И ИХ НАРУШЕНИЯ**. Редакционная коллегия делает все возможное для соблюдения этических норм, принятых международным научным сообществом, и для предотвращения любых нарушений этих норм. Такая политика является необходимым условием плодотворного участия журнала в развитии целостной системы знаний в области химии и смежных областях. Эта деятельность редакционной коллегии опирается, в частности, на рекомендации Комитета по этике научных публикаций (Committee of Publication Ethics), а также на ценный опыт авторитетных международных журналов и издательств. Представление статьи на рассмотрение подразумевает, что она содержит полученные авторами новые нетривиальные научные результаты, которые ранее нигде не публиковались. Каждую статью рецензируют минимум два эксперта, которые имеют все возможности свободно высказать мотивированные критические замечания относительно уровня и ясности изложения представленного материала, его соответствия профилю журнала, новизны и достоверности результатов. Рекомендации рецензентов являются основанием для принятия окончательного решения о публикации статьи. Статья, в случае принятия к опубликованию, размещается в открытом доступе; авторские права сохраняются за авторами. При наличии каких-либо конфликтов интересов (финансовых, академических, личных и т.д.) участники процесса рецензирования должны сообщить об этом редколлегии. Любые спорные вопросы, связанные с возможным плагиатом или фальсификацией результатов, внимательно рассматриваются редакционной коллегией, равно как споры об авторстве и целесообразность дробления результатов на небольшие статьи. В случае подтверждения плагиата или фальсификации результатов статья безоговорочно отклоняется.

**ІНФОРМАЦІЯ ДЛЯ АВТОРІВ.** Журнал публікує статті російською, англійською та українською мовами. До публікації приймаються: огляди (за погодженням з редколегією); оригінальні статті, обсяг 6-10 журнальних сторінок; короткі повідомлення, обсяг до 3 журнальних сторінок. Крім звичайного списку літератури, в статті обов'язково повинен бути другий список, всі посилання якого дані латиницею. Правила підготовки цього списку наведені в розділі «Трансliterація» на сайті журналу. Обидва списки повинні бути повністю ідентичні. При рецензуванні статей один з критеріїв - наявність посилань на публікації останніх років. Стаття обов'язково повинна містити резюме російською, українською та англійською мовами. У всіх трьох необхідно вказати назву статті, прізвища авторів і ключові слова. Орієнтовний обсяг резюме - 1800 знаків (без урахування заголовку і ключових слів). Редакція приймає електронний (MS Word) і два роздрукованих (для харків'ян) тексту рукопису. Адреси вказані в розділі «Контакти» на сайті журналу. Супровідний лист до статті, виправленої відповідно до зауважень рецензента, повинен містити відповіді на всі зауваження. Подається електронний і один роздрукований (для харків'ян) варіант. Рукописи, які пройшли рецензування, прийняті до публікації і оформлені відповідно до правил для авторів, приймаються у форматі doc (не docx) електронною поштою (chembull@karazin.ua). Роздрукований варіант не потрібен. Докладніша інформація розміщена на сайті журналу http://chembull.univer.kharkov.ua.

**INFORMATION FOR AUTHORS.** Papers in Ukrainian, Russian and English are published. These may be invited papers; review papers (require preliminary agreement with Editors); regular papers; brief communications. In preparing the manuscript it is mandatory to keep the statement on the publication ethics and malpractice, which can be found on the web-site and in each issue. The article should contain summaries in English, Russian, and Ukrainian. In all three it is necessary to indicate the title of the article, the names of the authors and the keywords. The approximate volume of summary is 1800 characters (excluding the title and key words). The help in translation is provided by request for foreign authors.. Any style of references is acceptable, but all references within the paper must be given in the same style. In addition, the second, transliterated, list of references is required if at least one original reference is given in Cyrillic. See section "Transliteration" of the web-site for details. Please use papers of previous issues as samples when prepare the manuscript. The MS Word format is used. Standard fonts (Times New Roman, Arial, Symbol) are preferable. Figures and diagrams are required in vector formats. Figure captions are given separately. All figures, tables and equations are numbered. Please use MS Equation Editor or MathType to prepare mathematical equations and ISIS Draw to prepare chemical formulas and equations. The decimal point (not coma) is accepted in the journal. Please avoid any kind of formatting when prepare the manuscript. Manuscripts may be submitted to the Editor-in-Chief via e-mai chembull@karazin.ua. For more detailed information see the journal web-site http://chembull.univer.kharkov.ua.

**ИНФОРМАЦИЯ ДЛЯ АВТОРОВ.** Журнал публикует статьи на русском, английском и украинском языках. К публикации принимаются: обзоры (по согласованию с редколлегией); оригинальные статьи, объем 6-10 журнальных страниц; краткие сообщения, объем до 3 журнальных страниц. Помимо обычного списка литературы, в статье обязательно должен быть второй список, все ссылки которого даны латиницей. Правила подготовки этого списка приведены в разделе «Транслитерация» на сайте журнала. Оба списка должны быть полностью идентичны. При рецензировании статей один из критериев - наличие ссылок на публикации последних лет. Статья обязательно должна содержать резюме на русском, украинском и английском языках. Во всех трех необходимо указать название статьи, фамилии авторов и ключевые слова. Ориентировочный объем резюме - 1800 знаков (без учета заглавия и ключевых слов). Редакция принимает электронный (MS Word) и два распечатанных (для харьковчан) текста рукописи. Адреса указаны в разделе «Контакты» на сайте журнала. Сопроводительное письмо к статье, исправленной в соответствии с замечаниями рецензента, должно содержать ответы на все замечания. Подается электронный и один распечатанный (для харьковчан) вариант. Прошедшие рецензирование и принятые к публикации рукописи, оформленные в соответствии с правилами для авторов, принимаются в формате doc (не docx) по электронной почте (chembull@karazin.ua). Распечатанный вариант не требуется. Более подробная информация размещена на сайте журнала http://chembull.univer.kharkov.ua.